UNIVERSITÀ DEGLI STUDI FIRENZE

PhD in Chemical Sciences

CYCLE XXXIV

COORDINATOR Prof. PIERO BAGLIONI

Deposition of soft polymeric capsules on surfaces for prolonged active release

Academic Discipline CHIM/02

Doctoral Candidate	**Supervisors**
Dr. Seymany Kéo-Oudone	Prof. Bonini Massimo
	Dr. Beth Schubert

_____   _____

_____

Coordinator
Prof. Piero Baglioni

_____

Years 2018/2021

ABSTRACT

The work reported in this Thesis deals with the investigation of soft polymeric microcapsules for the delivery of active ingredients to surfaces during washing processes. It is evident that current encapsulation methods involve a great amount of energy and materials to produce perfume carriers contained in home- and beauty-care products. Additionally, the deposition and retention of perfumes on target surfaces remains a challenge in cleaning processes as substrates are subjected to multiple rinses during the washing procedure. Therefore, the development of a new encapsulation technology presenting an improved sustainability profile and able to efficiently deliver perfumes on surfaces would contribute to a more effective use of materials, thus significantly lowering the environmental footprint of consumer goods. The soft microcapsules described in this Thesis exploit the self-assembly properties of Soluplus®, an amphiphilic poly(ethylene glycol)-poly(vinyl acetate)-poly(vinyl caprolactam) (PEG-PVAc-PVCL) graft copolymer, to encapsulate fragrances and deliver them to various target surfaces. The primary focus was to investigate the interactions between the copolymer and three perfume molecules, namely Eucalyptol, Citronellol and Methyl Nonyl Acetaldehyde, in order to correlate the materials' physico-chemical properties with the formation of perfume carriers in water, including microcapsules and polymeric micelles. We then studied how surface chemistry and fragrance properties affect the interactions between different model surfaces and the perfume-loaded microcapsules or polymeric micelles. With the ultimate goal of applying this new encapsulation technology to home- and beauty-care products, we chose to incorporate the soft microcapsules in a prototype laundry formulation, which was used to wash fabrics. We evaluated how the models for deposition of perfumes established on flat model surfaces could be used for real-life applications. These results participate in the expansion of the knowledge on the use of amphiphilic polymers for the targeted delivery of hydrophobic active compounds such as perfumes promoted by microcapsules and/or polymeric micelles.

TABLE OF CONTENTS

PREFACE

The work reported in this Thesis takes part in a research project called Self-Assembled MicroCAPSules (SAMCAPS): Synthesis, Characterization and Eco-friendly Application in Home Care Products. Joining the Center for Colloid and Surface Science (CSGI) and the Procter & Gamble company (P&G), the SAMCAPS project aims at developing soft polymeric microcapsules for the delivery of active ingredients to solid surfaces during washing processes. The reason behind this initiative is the need for new encapsulation methods that present improved sustainability and eco-friendly profiles, all the while being cost-effective for industrial applications in home- and beauty-care products. To achieve this goal, the project has been divided into individual missions assigned to four Ph.D. students: the design of new, biodegradable amphiphilic polymers; the development of novel ways to encapsulate perfumes using the self-assembly properties of amphiphilic polymers; the control of the perfume release from the soft microcapsules systems; and finally, the improvement of the perfumes deposition on various substrates. Reaching these objectives would enable the development of an encapsulation process that saves time, energy and raw materials to create perfume microcapsules, thus generating a more sustainable encapsulation technique. This Ph.D. project has been focused on the last aspect of the SAMCAPS program, namely the targeted delivery of fragrances on solid surfaces promoted by amphiphilic polymers.

Chapter I describes the foundations of this work, including the state of the art and notions required to understand the construction of this project. Chapter II deals with the investigation of the physical chemical interactions between the polymer and different perfumes for the formation of the soft microcapsules. Chapter III describes the studies conducted on the adsorption of fragrance active molecules on model surfaces, assisted by microcapsules and polymeric micelles. Chapter IV shows the exploitation of the developed technology on real-life applications. Finally, Chapter V presents the conclusions and future perspectives.

Experimental details can be found in Appendix I, while physical chemical properties of the studied fragrances are reported in Appendix II.

This Ph.D. project was funded by the Marie Skłodowska-Curie Actions within the Horizon 2020 framework as a European Industrial Doctorate (EID) program. Half of this work was conducted at the Brussels Innovation Center (BIC) of P&G in Belgium while the other half was performed at the CSGI of Florence in Italy.

AFM	Atomic Force Microscopy
APN	Alpha-Pinene
ATR-FTIR	Attenuated Total Reflection Fourier Transform InfraRed Spectroscopy
Au	Gold
BET	Brunauer-Emmett-Teller analysis
BIC	Brussels Innovation Center
CLSM	Confocal Laser Scanning Microscopy
CMC	Critical Micelle Concentration
CRM	Confocal Raman Microscopy
CSGI	Center for Colloid and Surface Science
CTN	Citronellol
DD	Delta-Damascone
DLS	Dynamic Light Scattering
DSC	Differential Scanning Calorimetry
DTES	Dodecyltriethoxysilane
DTG	Differential Thermogravimetry
ECL	Eucalyptol
EID	European Industrial Doctorate
ELS	Electrophoretic Light Scattering
EtOH	Ethanol
GCMS	Gas Chromatography coupled with Mass Spectrometry
GISAXS	Grazing Incidence Small Angle X-Ray Scattering
H_2O_2	Hydrogen peroxide
H_2SO_4	Sulfuric acid
HBN	Habanolide
HS	Headspace
HSP	Hansen Solubility Parameters
IES	Iso-E Super
LMN	Limonene
MA	Methyl Anthranilate
MNA	Methyl Nonyl Acetaldehyde
MPEG	Poly(ethylene glycol) methyl ether
N_2	Nitrogen
P&G	Procter & Gamble
PCEMA	Poly(2-cinnamoyloxyethyl methacrylate)
PEG	Poly(ethylene glycol)
PET	Polyethylene terephthalate or polyester

PGMA	Poly(glycidyl methacrylate)
PI	Polyisoprene
PRM	Perfume Raw Material
PtBA	Poly(t-butyl acrylate)
PVAc	Poly(vinyl acetate)
PVCL	Poly(vinyl caprolactam)
QCM-D	Quartz Crystal Microbalance with Dissipation Monitoring
SAM	Self-Assembled Monolayer
SAMCAPS	Self-Assembled MicroCAPSules
SAM-CH$_3$	Hydrophobic surface
SAM-COOH	Anionic surface
SAM-NH$_2$	Cationic surface
SAM-OH	Hydrophilic surface
SAXS	Small Angle X-Ray Scattering
SEM	Scanning Electron Microscopy
SFA	Surface Force Apparatus
SiO$_2$	Silicon Dioxide
SLP	Soluplus
SPM	Scanning Probe Microscopy
SPME	Solid Phase Microextraction
TGA	Thermogravimetric Analysis
UDV	Undecavertol
UV	Ultra-Violet spectrometry
UV/O$_3$	Ultra-Violet/Ozone
XPS	X-Ray Photo-Electron Spectroscopy
XRR	X-Ray Reflectivity

I. INTRODUCTION

This first Chapter gives an overview on the foundations of this project. The main factors that play a role in washing processes are first introduced. Then, a review on fragrance microencapsulation technologies is described, explaining the need for novel methods to be developed for their application in consumer products. The current methods to enhance the delivery of perfumes on target surfaces are summarized, followed by the methods applied to characterize the deposition of materials. Finally, the objectives of this project are defined.

I.1. Important factors in washing processes

As the SAMCAPS project aims at implementing a new encapsulation method in home- and beauty-care products, we have focused our attention on consumer goods that are used in cleaning processes such as laundry washing. This paragraph thus describes the main factors that play a role in such processes.

I.1.1. Surfaces

I.1.1.1. Fabrics in laundry

Textile fabrics used for garment production are materials presenting macro-, micro- and nanopores. They are obtained by interlacing yarns, which are composed of single or several strands of twisted fibers. The fabric properties thus depend on the type of fiber and construction. In modern fashion, cotton and polyester fabrics are by far the most commonly used materials.[1]

Cotton fibers

Cotton fibers being plant-derived, belong to the class of natural fibers along with animal fibers such as wool and silk. They are mainly composed of cellulose I, the most abundant organic polymer.[2] The d-

anhydroglucose ring units are linked together by β-1,4 glycosidic oxygen bonds (Figure I.1).[3]
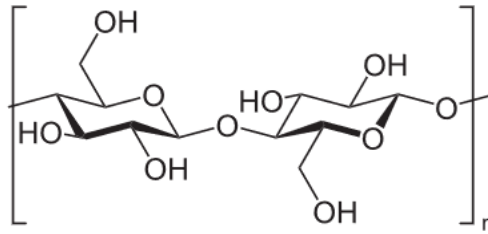

Figure I.1: Structure of cellulose.

Cotton fibers have a multilayered and fibrillar structure, consisting of a primary wall, a secondary wall and a lumen (Figure I.2). The outer surface layer has a great influence on the fiber properties, processing and use, which is why raw cotton fibers need to be chemically processed in order to remove the waxy cuticle and other non-cellulosic components. They have a flat, twisted, ribbon-like appearance with a rough surface. The quality of the fibers depends on various parameters, including their growth environment, which is why significant differences in fiber properties might be observed. The fiber dimensions vary between 12-22 μm diameter and 12-60 mm long.[4]
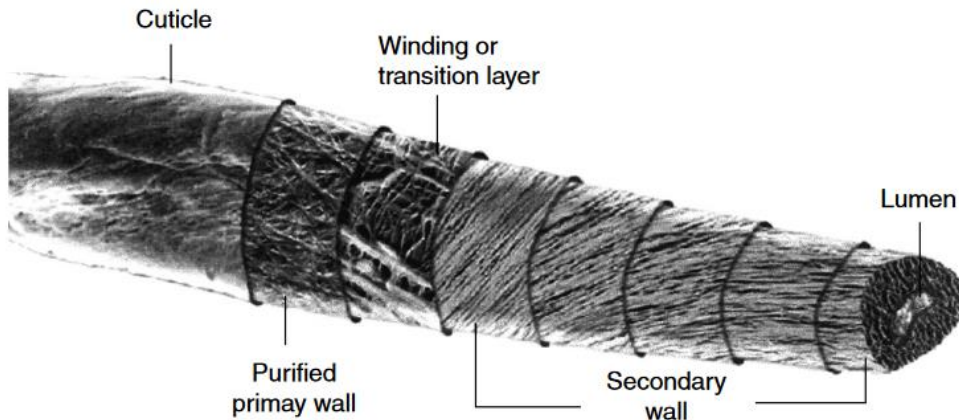

Figure I.2: Morphological model of cotton fiber.[4]

The abundant hydroxyl and hydroxymethyl groups, as well as the chain conformation of cotton fibers allow extensive inter- and intra-molecular hydrogen bonding. This results in highly hydrophilic and rigid fabrics.[2]

During the production of cotton fabrics, treatments such as bleaching or dyeing can be applied, which mainly consists in oxidation processes. Consequently, hydroxyl groups are transformed into carboxylic acid components, which confers a negative charge to cotton fabric surfaces.[2]

Polyester fibers

Polyesters are man-made polymers, one of the most synthesized in the world and are usually obtained by a polycondensation reaction. Polyester fibers are typically composed of polyethylene terephthalate (PET; Figure I.3), synthesized from terephthalic acid and ethylene glycol.[5]
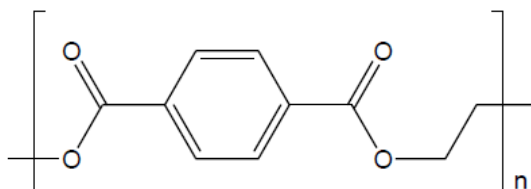

Figure I.3: Structure of polyethylene terephthalate.

The presence of ethylene and phenyl units in PET makes this polymer more hydrophobic than cellulose. However, PET exhibits slightly polar ester groups in the repeating unit and hydroxyl end groups, which allow the polymer to interact with polar molecules.
Similarly to cellulose, it has been reported that PET presents a negative surface charge, which was conferred to its high hydration capacity.[6]

I.1.1.2. Model surfaces

Topographical characteristics of textile fabrics depend on their construction parameters such as yarn fineness, yarn density and type of weave (i.e., woven, knitted or non-woven).[7] As a result, these characteristics have a strong impact on the wetting and adhesion properties and might in turn affect the targeted delivery of active compounds during the washing process. In fact, Kumar et al.[8] have demonstrated that the mechanism of deposition of cationic surfactants vesicles (typically contained in laundry softeners) is highly dependent on surface properties such as roughness. In this study, they investigated the

deposition of large and small vesicles on smooth and rough cellulose surfaces, namely viscose and cotton fibers, respectively. Using streaming potential measurements, they demonstrated that on viscose fibers, smaller vesicles predominantly adsorbed until the surface was covered, thus preventing the adsorption of larger vesicles. In contrast, the deposition of vesicles on cotton fibers was independent on vesicle size due to the increased roughness of the substrate. Similarly, Calvimontes et al.[7] demonstrated that the structure of polyester fabrics highly impacted their wettability behavior, where woven polyester fabrics presented a lower water penetration than their twilled equivalent.

These results stress the importance of the structure of textile fabrics in their adsorption capacity of perfume microcapsules during washing cycles. As the deposition mechanisms of the novel self-assembled microcapsules on various surfaces are yet to be understood, there is a need to merely investigate the influence of surface chemistry before considering other physical or mechanical properties such as geometry, roughness, yarn density, elasticity, etc. Consequently, in this Thesis, flat model surfaces were preferred for the preliminary investigation of particle-surface interactions. In the past decade, self-assembled monolayers (SAMs) have been used to study the adsorption of a wide range of materials including polymers,[9] surfactants,[10],[11] and lipids,[12] due to their simplicity and flexibility. These ultrathin membranes are commonly formed by spontaneous chemisorption of alkanethiols on gold (Au) substrates and produce stable and ordered surfaces, thanks to the strong gold-sulfur bond.[13,14] Functionalized alkanethiols with different chemistries are typically used to control surface properties at the nanoscale, in order to investigate the driving force for material adsorption at the solid/liquid interface.[15,16] In this Thesis, we studied the effect of wettability and surface charge on the targeted delivery of perfumes by creating hydrophobic, hydrophilic, cationic and anionic model surfaces.

I.1.2. Surfactant formulations

I.1.2.1. Cleaning formulations

Modern laundry detergents can contain twenty or more ingredients, depending on consumer needs such as white cleaning, color protection and so on. Nevertheless, the major ingredients remain similar and typical compositions of European products can be found in Table I.1.[17,18]
The main components in cleaning formulations such as liquid laundry detergents are surfactants, which combine hydrophilic and hydrophobic moieties within the same molecule. Their principal function is to reduce the interfacial tension between water and soil, in order to promote the removal of dirt from surfaces and its dispersion in water.
Anionic surfactants, which are the primary surfactants in terms of relative amount, comprise a negatively charged polar head group (typically a sulfate, sulfonate, or carboxylate) and a hydrophobic tail (typical alkyl chains between C10-C20).[17] Linear alkylbenzene sulphonate (LAS) is the most popular anionic surfactant for laundry detergents, while sodium lauryl sulfate (SLS) predominate in shampoo formulations.

Table I.1: Typical basic compositions of liquid laundry detergents.

Ingredients	Percentage in liquid laundry detergent (wt.%)
Primary (anionic) surfactants	15-35
Secondary (nonionic) surfactants	3-7
Builders	20-40
Perfumes	0-0.5
Secondary agents	0-12
Water	Balance

Secondary nonionic surfactants are mostly used to improve detergency and form mixed micelles with anionic surfactants. They are typically used in laundry detergents since they do not form complexes with calcium or magnesium ions present in water and soils, which makes them tolerant to water hardness.[18]

Builders refer to compounds that soften water by chemically binding to metal ions that cause water hardness, namely calcium and magnesium.[18]

Finally, other agents such as bleaching agents, optical brighteners, thickeners, dyes, preservatives, perfumes, etc. can be incorporated into fabric cleaning formulations to improve the quality of the products and match multiple consumer needs.

Laundry detergents are relatively concentrated formulations, which is why they need to be correctly dosed and diluted before use.

I.1.2.2. Softeners and conditioners formulations

Fabric softeners are used after the cleaning process to confer a soft texture to the washed fabrics. The process involves the adsorption of conditioning agents onto the surfaces, which affects properties such as surface potential, surface energy and friction. They leave a soft, antistatic, elastic texture to the fabrics. As cleaning products, their composition and main ingredients can vary between competitors and typical formulae of this kind of product on the European market can be found in Table I.2.[19,20]

Table I.2: Typical basic compositions of fabric softeners.

Ingredients	Percentage in fabric softener (wt.%)
Cationic surfactants	3-12
Perfumes	0-1
Secondary agents	0-5
Water	Balance

The principal conditioning agents used in laundry softeners are cationic surfactants as they have good affinity to most fibers.[21] The main present-day products contain esters of quaternary ammonium compounds, which exhibit good adsorption properties and are readily biodegradable.[19]

Other agents such as ironing aids, preservatives, dyes and dye fixatives, perfumes, etc. can also be added to fabric softener formulations to differentiate products from competitors.[1]

As cationic surfactants can interact with anionic surfactants present in cleaning products and produce neutral salts that have low water solubility, fabric softeners are only added in the last rinse of the washing cycle.

As seen in this section, laundry products contain many ingredients, mainly surfactant aqueous solutions, that could influence the stability of self-assembled capsules. Laundry detergents and softeners vary greatly in composition, but also in the deposition of perfumes on fabrics. In fact, with detergents, fragrances are applied at the beginning of the washing cycle. In this process, perfumes are deposited on the fabrics while dirt is removed from the same surfaces, and they should withstand several rinse steps before the end of the washing cycle. On the contrary with softeners, the perfumes are only deposited at the end of the washing process, during the last rinse step. This major difference in application complicates our investigation as the requirements for perfume deposition are not the same for both laundry products. Therefore, in this Thesis, we chose to focus on softener applications. To simplify the systems, model formulations were studied using either water or cationic surfactant solutions as media.

It is also evident that formulations such as detergents and softeners are diluted during use, which could result in the dissociation of the microcapsules. It is thus crucial to study the targeted delivery of fragrances in the case where microcapsules are destroyed before being adsorbed on the surfaces, which is why part of this work has been dedicated to the investigation of diluted systems.

I.1.3. Perfumes

The performance of laundry products is often associated to the odor of washed items. Perfumes are also used to mask unpleasant odors from the washing water and cleaning agents during the washing procedure. As a result, they confer a sense of freshness and cleanliness, which is why their delivery on target surfaces is so important. Fragrances used in consumer products are usually liquid, complex mixtures of many individual small molecules, which can be synthetic aroma compounds or natural essential oils.[1] Due to the high volatility and chemical instability of that class of compounds, they are often susceptible to premature evaporation and degradation caused by light, heat, pH or oxygen, which can alter their sensory perception.[22] As seen in the previous paragraph, home- and personal care products contain surfactants in high concentrations serving as oil removal materials, which can be an additional challenge for the stability of the fragrances and their deposition on the target surfaces during the use of the product. Therefore, perfumes are usually encapsulated in consumer products, which not only reduces losses during the manufacturing process and storage, but also provides a targeted delivery of the active ingredients and a sustained release for long-lasting effects.

I.2. Encapsulation of perfumes

The encapsulation of fragrances and aroma chemicals has been widely investigated as these additives are essential to provide olfactory and gustatory properties to consumer goods. Encapsulation technologies have been developed as a means to protect and stabilize active materials from the surrounding environment and/or control their delivery by entrapping them in another substance to form nano- or micro-scale cargoes. Generally, the structures of such systems can be divided into two broad categories: core-shell capsules and matrix systems. In the first class, the encapsulated active ingredient is referred to as the internal phase, core material or payload; it is surrounded by another material, referred to as the wall, shell or membrane. Wall materials typically include polymers (synthetic or natural), inorganic materials or polymer-

inorganic materials.[23] Variations of this type of capsules include multi-layer, multi-core or multinuclear capsules. In the second type of systems, the encapsulated material is dispersed in the carrier matrix, which typically consists of a polymer, thus forming microspheres. For the past twenty years, these systems have been employed to encapsulate a variety of active ingredients for applications in the pharmaceutical, food, textile, cosmetics, agriculture, and energy industries [24–29].

I.2.1. Microencapsulation methods

Active materials can be encapsulated in nano- or micro-sized objects, depending on the end application. In the case of perfumes, the formation of nanocapsules often involves high-energy processes and larger quantities of emulsifier compared to that of microcapsules, which is why the latter are favored for fragrance applications.[30] The currently available techniques to form microcapsules can be divided into three categories: chemical processes, physico-chemical processes and physico-mechanical processes. A list of the most important methods for the microencapsulation of flavors and fragrances is provided in Table I.3 with examples of typical capsule wall materials.

Table I.3: Common methods for the encapsulation of flavors and fragrances.

Type	Encapsulation method	Advantages	Limitations	Examples of encapsulating material
Chemical process	In situ polymerization [31,32]	Excellent thermal and mechanical properties High encapsulation efficiency Fast reaction times Low cost of raw materials Easy scaling up	Poor biocompatibility Limited biodegradability Difficult to control particle size dispersity Residual monomers Not thermally efficient	Melamine formaldehyde [33] Urea–formaldehyde [34]

Type	Encapsulation method	Advantages	Limitations	Examples of encapsulating material
Chemical process	Interfacial polymerization [23,31,32]	Excellent thermal and mechanical properties High encapsulation efficiency Fast reaction times Easy scaling up	Difficult to control the particle size dispersity Limited biocompatibility Poor biodegradability Residual monomers Production of high quantity residual solvents Not thermally efficient	Polyurea [35] Polyurethane [36]
Physico-chemical process	Simple or complex coacervation [31,32]	High encapsulation efficiency Efficient control of particle size Minimal or no heat during process	Expensive Possible aggregation of particles Hard scaling up Requires further processing to stabilize the shell (cross-linking)	Polyvinyl alcohol [37] Gelatin / Gum Arabic [38]
Physico-chemical process	Molecular inclusion [23,39]	Simple Economic Triggered release of active materials	Complexation efficiency varies greatly depending on guest molecule	β-Cyclodextrin [40]

Type	Encapsulation method	Advantages	Limitations	Examples of encapsulating material
Physico-mechanical process	Spray drying [23,31,41]	Simple Flexible Fast Economic Easily scalable	Increased particle size dispersity Low encapsulation efficiency Loss of low-boiling point compounds Not thermally efficient	Gum Arabic [42]
Physico-mechanical process	Electrospinning [39,43]	High encapsulation efficiency Simple Flexible Non thermal process	Low productivity Hard scaling up Removal of residual solvents	Polyvinyl alcohol [44]

The appropriate method of encapsulation should be selected considering the nature of the encapsulated materials, simplicity, reproducibility, scalability, and cost effectiveness of materials and process. On the other hand, the main physical and chemical properties of the resulting microcapsules such as compatibility with the core material, stability and release properties are determined by the carrier material. The methods described in Table I.3 produce microcapsules that present a solid wall material that acts as a physical barrier between the active material and the surrounding formulation. Even though the hardening of the capsule shell via chemical crosslinking offers many advantages in terms of capsule mechanical properties and active compound stabilization, it also presents some drawbacks. For instance, many of these processes involve high energy homogenization and/or elevated temperatures,[33–36] a release of the active ingredient limited to diffusion through the membrane pores and/or rupture of the capsule shell under mechanical force,[45] and the use of crosslinkers that can unfavorably affect the properties of active compounds and capsule biodegradability.[46] It is

clear that improvements can still be made in terms of biodegradability, process, release triggers and targeted delivery. It is thus worth looking into substitutes that are sustainable and can improve the environmental profile of microcapsule technologies, without compromising the performance of fragrance delivery sought in consumer products.

I.2.2. Self-assembled polymeric microcapsules

The microcapsules developed in the SAMCAPS project are formed spontaneously by phase separation of an amphiphilic polymer, via hydrophobic interactions and/or hydrogen bonds, to encapsulate guest molecules in aqueous media. Therefore, this method requires less time and energy to create microcapsules, making it a more sustainable approach for the encapsulation of fragrances. Additionally, the self-assembly process avoids the creation of covalent bonds. As a result, this type of microcapsules can easily disassemble under an external stimulus such as dilution, or other triggers depending on polymer functionalities. Indeed, research interests in the recent years turn toward stimuli-responsive materials that are able to control the release of fragrances using triggers such as pH, temperature, light, or hydrolysis.[47–51] Consequently, this technique shows advantages in terms of processability (e.g., easy preparation, scaling-up), sustainability and flexibility for the release of active materials.

I.2.2.1. Amphiphilic polymers

Similar to surfactants, amphiphilic polymers are macromolecules that simultaneously possess hydrophilic and hydrophobic moieties. Depending on the number of monomers and polymerization procedure, they can form alternating, random, graft, star or brush structures.[52] They have been widely used as nanocarriers for drug delivery applications as they allow for improved cellular internalization, circulation time in the bloodstream, and solubilization and prolonged release of poorly water soluble compounds.[53] The use of amphiphilic polymers to encapsulate hydrophobic molecules via self-assembly typically results in the formation of nanosized particles, such as micelles[53,54] or polymersomes.[55,56] However, the production of

microparticles from amphiphilic polymers is less trivial and often requires multi-step methods that include emulsification and cross-linking procedures.[57–59]

Recent examples show the development of microparticles based on poly(γ-glutamic acid)-dodecylamine[60] and poly(4-vinylpyridine)-b-poly{6-[4-(4-butyloxyphenylazo)phenoxy]hexyl methacrylate}[57,58] amphiphilic copolymers that do not make use of chemical crosslinkers for capsule preparation. In these studies, microparticles were produced in water via emulsion-solvent evaporation method and exhibited a narrow size distribution with diameters around 10 μm. Even though the resulting particles showed promising tunability of capsule morphology and functionality, this emulsion-solvent evaporation method is unfortunately not applicable for the encapsulation of volatile compounds such as perfumes.

Another example exploits the phase separation of an amphiphilic poly(ethylene glycol)-graft-poly(vinyl acetate) (PEG-g-PVAc) copolymer creating polymeric microdomains.[62] In this case, the formation of microparticles was induced by the dehydration of the hydrophilic PEG upon addition of a non-ionic surfactant and a salting-out agent, causing the depression of the copolymer's cloud point temperature which resulted in a liquid-liquid phase-separation. It was also shown that these microdomains were able to encapsulate both hydrophobic and hydrophilic materials, which release could be triggered by dilution of the capsule suspension. This study is of particular interest as these microstructures showed stability in the presence of anionic surfactants, which is an attractive parameter for the design of microcapsules in laundry products.

I.2.2.2. Soluplus®

Similar to PEG-g-PVAc, Soluplus® is an amphiphilic copolymer produced by BASF that is composed of a hydrophilic poly(ethylene glycol) (PEG) backbone randomly grafted with hydrophobic poly(vinyl acetate) (PVAc) and poly(vinyl caprolactam) (PVCL) moieties (13% PEG 6000/30% vinyl acetate/57% vinyl caprolactam; Figure I.4).

Due to its biocompatibility, it has been studied over the past decade for the formation of solid dispersions with active pharmaceutical ingredients to enhance their bioavailability, especially in hot melt extrusion processes.[63–65] Owing to its amphiphilic character, Soluplus® is able to self-assemble into micelles in water with a low critical micellar concentration (CMC = 7.6 mg/L at 23 °C)[66]. As a result, many authors have recently investigated its use to solubilize water insoluble drugs (among others: ipriflavone,[67] quercetin,[68] doxorubicin[69] and furosemide[70]). The presence of VCL monomers makes the grafted chains slightly more hydrophilic than that on the PEG-g-PVAc copolymer, which could broaden the range of solubilizing molecules to even hydrophilic ones. Consequently, Soluplus® poses as an excellent candidate for the formation of polymeric microcapsules with perfumes, which is why the work described in this Thesis has been conducted using this copolymer as encapsulating material.
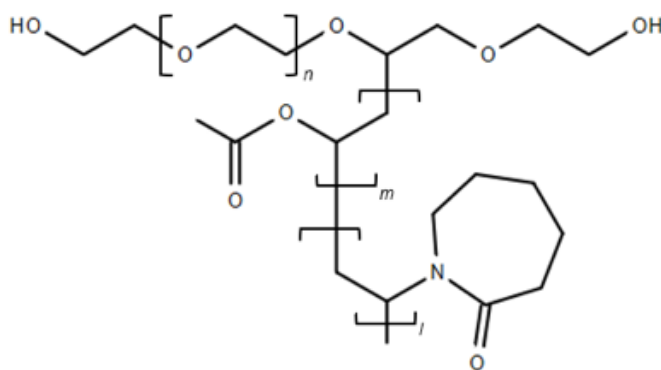

Figure I.4: Structure of the amphiphilic polymer Soluplus®.

I.3. Targeted delivery of particles

In cleaning processes, the deposition and retention of perfumes on target surfaces remains a challenge as the latter are subjected to multiple rinses during the washing cycle. Moreover, the surfactants present in the washing solutions aim at removing dirt from surfaces by entrapping the residues in micelles. Consequently, since perfumes are predominantly hydrophobic molecules, they are mostly located inside the micelles as well and rinsed off with water. Improving the targeted delivery of

fragrances during washing processes would thus decrease their consumption in consumer products, improving their industrial usage.

I.3.1. Current approaches to enhance the targeted delivery of perfumes

Different approaches have been used over the last few years to improve the targeted delivery of perfumes and their retention on surfaces and are described in the following categories.

Modification of the target surface

In the specific case of fabrics, microcapsules can be bound to the surface during the production of the textiles so that the benefit agent is able to withstand several laundry washing cycles. Such modifications can be performed by grafting the capsules to the surface after deposition using a cross-linker,[71] or by coating the substrates with the capsules during the finishing process of the textiles.[72] This is particularly relevant for smart textiles where the encapsulated active ingredient can provide benefits (e.g., thermoprotection, photochromism, insect repellent, etc.) in a sustained manner.[73] However, as the project is focusing on home care and beauty-care applications, modifying the target surfaces is not in the scope of our research and will not be exploited.

Modification of the perfume molecules

Perfume compounds can be polymerized or covalently bound to suitable substrates to form non-volatile and odorless precursors that are called profragrances. The release of these fragrant molecules is then controlled by cleavage of the covalent bond under certain environmental conditions (e.g., following a change of pH[74] or temperature,[75] exposure to light[51]). This method involves the modification of perfume molecules with specific chemical functionalities (alcohols, lactones, amines, etc.), which means that precursors usually release only one group of compounds. Forming profragrances is thus hardly applicable to consumer products that incorporate perfume mixtures with dozens of various molecules.

Modification of the bulk solution

Decreasing the solubility of the encapsulating polymer could improve its adhesion on substrates. In fact, by weakening the interactions between the solvent and the polymer, the latter should preferentially interact with the surface, hence increasing adsorption. Polymer solubility can be reduced by incorporation of additives such as electrolytes or alcohols in the solution.[76]

The addition of deposition aids in the formulation containing the microcapsules can also improve the adsorption of materials by increasing particle/surface interactions. The choice of the deposition aid depends on the nature of the capsule/active ingredient and more specifically which interactions they can have together. In general, positively charged polymers are used like polyacrylamides, polysaccharide derivatives or cationic polymers with quaternary ammonium centers.[77] Such polyelectrolytes can sometimes count on the presence of anionic surfactants in consumer products to form complexes that improve the targeted delivery of hydrophobic oils.[78,79] When dealing with charged particles, it is also important to consider and tune the ionic strength and pH of the solution to optimize the interactions.

Modification of the capsule properties

The size and flexibility of capsules can be adjusted to increase deposition. On fabrics, large and hard particles have shown an increased deposition on the external surface of the textile (filtering effect). On the other hand, softer particles with smaller sizes allowed for their permeation between the fibers, leading to a more homogeneous internal distribution.[80]

The improvement of microcapsule deposition on surfaces such as fabrics typically involves the functionalization of the capsule surface, usually with positively charged polyelectrolytes such as chitosan, polyvinyl formamide or polydopamine.[81] Capsules modified with peptide ligands[82] and protein-based coacervates[23,83] have also shown promising results for the deposition of volatile compounds on target surfaces. Yet, these methods can only be applied to microcapsules that present a solid shell material and are not suitable for the self-assembled

capsules studied in this project since the functionalization of the capsule surface would impact the stability of the capsule itself. Instead, modifying the encapsulating polymer could be a possible solution to this issue. For example, changing the molecular weight, composition or functional groups of the polymer could enhance its interactions with the target substrate. However, these modifications should be carefully designed as they could also affect perfume encapsulation.

Many reports can be found on the adsorption of amphiphilic block copolymers in the form of soft polymeric micelles on various surfaces.[84–88] Yet, these investigated systems do not contain any active ingredient in their core and similar studies on the delivery of molecules loaded in soft polymeric nano- or micro-carriers on solid surfaces are rather scarce.[89] Thus, one of the purposes of this project is to evaluate the potential for targeted deposition of perfumes from soft polymeric capsules and find possible improvements to this problem.

I.3.2. Current methods to characterize the deposition of materials

I.3.2.1. Targeted delivery of perfumes

To determine the amount of deposited ingredients on a substrate, two methods are generally used:[90]
- Indirect measurements, in which the ingredients are extracted from the surface before analysis;
- Direct measurements, where the presence of the compounds is directly analyzed on the treated surface.

Indirect measurements

These techniques require an extraction of the deposited active materials from the target surface using an organic solvent.[90] The extracts are then analyzed to determine the nature and concentration of the ingredients using systems such as headspace Gas Chromatography coupled with Mass Spectrometry (HS-GCMS), which is the main method in practice for the evaluation of complex fragrant mixtures.[91,92] In this

technique, the volatile compounds present in the headspace over the extract are first being separated in the gas chromatograph, then identified by the mass spectrometer. This powerful combination allows a quantitative analysis of the deposited materials. Other methods can involve different separation and identification techniques, such as High-Performance Liquid Chromatography (HPLC) combined with Ultra-Violet (UV) detection.[82,93]

Direct measurements

The involved techniques rely on the analysis of the target surface itself, which can allow visualization of the adsorbed ingredients as well as mapping of their distribution on the said surface. Depending on the nature and physico-chemical properties of the tracked compounds (polymer or perfume molecule), their targeted deliveries on fabrics or hair can be assessed by means of:

- Confocal Laser Scanning Microscopy, combined with fluorescence or Raman spectroscopy[94]
- Fourier transform infrared spectroscopy[95,96]
- Scanning electron microscopy[95]

By measuring the intensity of the response, some of these methods can even be used for quantitative characterization.

Other analytical methods use in situ conditions where the analysis takes place when the substrate is immersed in the solution containing the benefit agent. They provide valuable information that can help in the determination of the adsorption/desorption rate and process. Such techniques include:

- Ellipsometry[97]
- Quartz Crystal Microbalance with Dissipation[98]
- Surface zeta potential[99]

Finally, in the particular case of perfumes, human sensory panels can also be used to relatively quantify the targeted delivery of fragrance molecules.[23,100]

I.3.2.2. Adhesion of particles on surfaces

Investigating the adhesion of capsules on various substrates requires information about the physical and chemical properties of the surfaces of interest.

Techniques for the characterization of adhesion on surfaces

Methods that can be used to measure adhesive forces between particles and surfaces are described in Table I.4.

Table I.4: Characterization techniques for the measurement of adhesion on surfaces.

Characterization technique	Outcomes	Advantages	Limitations
Scanning Probe Microscopy (SPM)[101]	Measurement of intermolecular forces (between tip and sample) Measurement of surface forces and adhesion	Force sensitivity down to piconewtons X, y, z resolution down to the nanoscale No specific sample preparation needed Ambient operating conditions in air or liquid environments	Slow measurement speed
Surface Force Apparatus (SFA)[102]	Measurement of surface forces and adhesion	Force sensitivity down to nanonewtons Z resolution down to the angstrom-scale Ambient operating conditions in air or liquid environments	Base surface restricted to mica sheets (i.e., requirement to modify the mica surfaces by deposition of the tested material) Requires (semi)transparent samples with low surface roughness

Characterization technique	Outcomes	Advantages	Limitations
Quartz Crystal Microbalance with Dissipation monitoring (QCM-D)[103]	Information on binding and interactions between materials Adsorption kinetics Conformational changes Viscoelastic properties of the adsorbed layer	Mass detection sensitivity in the order of tens of nanograms Real-time measurements Reusable model sensor surfaces Operating in flowing or no-flowing conditions	Unable to distinguish the selective deposition of multiple component systems

Techniques for surface characterization

The techniques for surface characterization are described in Table I.5.

Table I.5: Surface characterization techniques.

Characterization technique	Outcomes	Advantages	Limitations
X-Ray Photo-Electron Spectroscopy (XPS)[104]	Elemental composition Chemical state Depth profiling	Chemical information from shifts in binding energy Quantitative elemental analysis of surfaces Chemical state analysis	Works in ultra-high vacuum (i.e., limited dry samples) Soft X-Ray irradiation
Confocal Raman Microscopy (CRM)[104]	Functional group identification Structural information	Depth profiles No sample preparation needed Non-destructive technique	Resolution (in x, y, z) limited to submicron scale (i.e., not suitable for the characterization of monolayers)

Characterization technique	Outcomes	Advantages	Limitations
Attenuated Total Reflection Fourier Transform InfraRed Spectroscopy (ATR-FTIR)[105,106]	Functional group identification Bonding properties Atomic and molecular structure, molecular interactions Imaging and mapping (when coupled with a microscope)	Suitable for soft and hard materials Identification of small concentrations of materials (0.1-1 mM) In-situ monitoring of adsorption processes at the solid/liquid interface	Possible spectral crowding and interferences with water Distinction between materials with the same functional groups can be challenging as frequency shifting due to a molecule's environment is minimal
Transmission Optical Microscopy	Imaging Morphology Topography	No sample preparation needed Enhancement of topographical features with phase contrast Non-destructive technique	Resolution limited to submicron scale No z information Not suitable for opaque samples
Scanning Electron Microscopy (SEM)	Topographical information (only in x, y) Chemical composition (when coupled to Energy Dispersive X-Ray Spectroscopy)	X, y resolution down to the nanoscale No need to pre-treat the surface (only with Field-Emission SEM)	Z information only qualitative Works in ultra-high vacuum (i.e., limited to dry samples) Radiation damage
Scanning Probe Microscopy (SPM)[107]	Microtopographic imaging Film thickness Profilometry Morphology Physical, chemical, mechanical, magnetic or electrical properties of the surface depending on the tip	Atomic resolution of flat surfaces in x, y, z No specific sample preparation needed Ambient operating conditions in air or liquid environments Suitable for very soft materials	Tip size can limit the measurement of narrow or deep indentations and steep slopes Slow measurement speed z direction range limited to 10 μm

Characterization technique	Outcomes	Advantages	Limitations
Grazing Incidence Small-Angle Scattering of X-Rays (GISAXS)[108,109]	Nanostructure analysis Shape, sizes, distribution of sizes and faceting of nanostructures Lateral dimensions and arrangements	Nanoscale structural method Non-destructive technique No specific sample preparation Fast measurements Possibility to perform in-situ experiments	Materials need a specific model to accurately describe the type of structure Measurement of the mean morphology of nanoparticle ensembles rather than individual morphological properties
Brunauer-Emmett-Teller (BET) analysis[110]	Surface area of a material Pore size distribution	Non-destructive technique Fast and easy measurements	Pre-treatment at elevated temperature in vacuum or flowing gas (i.e., limited to dry materials) Long degassing times
Contact Angle measurements	Surface wettability Surface free energy	Non-destructive technique Direct and easy measurements	Not suitable for materials that present roughness, chemical heterogeneity or porous nature
Streaming Potential measurements[99,111]	Surface charge of macroscopic solid surfaces	Suitable for the investigation of large planar solids as well as irregularly shaped samples, including fibers and fabrics Real time measurements allow for the investigation of adsorption processes of solutes on a surface	Measurements depend on the swelling and intrinsic conductance of the sample

Characterization technique	Outcomes	Advantages	Limitations
Electrophoretic Light Scattering (ELS)[112]	Surface charge of particles in suspension Dispersion stability	Non-destructive technique Compatible size range of particles between 5 nm - 100 µm (diameter)	Measurements depend on the particle size, polydispersity and optical properties of the sample (i.e., dilution of the sample might be needed)

In this project, understanding the adhesion mechanisms between capsules and substrates requires information on the surface properties of both entities. However, the techniques described in Table I.5 might not be suitable for all types of samples. Table I.6 below hence classifies the techniques that are recommended for the surface characterization of flat (model) substrates, fabrics and capsules.

Table I.6: Classification of techniques that are recommended for the surface characterization of flat (model) substrates, fabrics and capsules.

Techniques that are suitable for flat (model) surfaces	Techniques that are suitable for fabrics	Techniques that are suitable for capsules
XPS	XPS	Transmission Optical Microscopy
CRM	CRM	SPM
ATR-FTIR	Transmission Optical Microscopy	ELS
Transmission Optical Microscopy (if not opaque)	SEM	
SEM	BET analysis	
SPM	Streaming Potential measurements	
GISAXS		
Contact Angle measurements		
Streaming Potential measurements		

I.4. Objectives of this project

As seen from the literature review, there is a need to develop eco-friendly and cost-effective perfume encapsulation methods. By reducing the duration of the encapsulation process as well as the energy and raw materials inputs, self-assembled microcapsules present an improved sustainability profile. This Thesis thus describes the development of such microcapsules for the delivery of perfumes that are contained in consumer products, for home and beauty care applications. The SAMCAPS project has been established based on a previous research project from Bartolini et al.[62,113], in partnership with the Brussels Innovation Center (BIC) of P&G. As it targets end-use applications, business needs must be considered along with the fundamental understanding of this new technology. As a result, a number of factors need to be defined, including the choice of materials (ingredients involved in the encapsulation process and substrates), formulation parameters (surfactant solution, concentrations and process parameters), model systems, experimental conditions (deposition techniques and washing parameters), as well as characterization techniques.

Since soft microcapsules have previously been obtained with a PEG-g-PVAc copolymer in a prototype liquid detergent formulation, a PEG-PVAc-PVCL polymer called Soluplus® was investigated in this Thesis. The interactions between the amphiphilic polymer and three individual fragrant molecules were explored in binary systems of polymer and perfume, and their ability to form microcapsules and polymeric micelles was then assessed in water.

As this project focused on the targeted delivery of perfumes on various substrates, interactions between perfume carriers and surfaces were investigated. In this framework, the definition of perfume carriers includes both microcapsules and polymeric micelles. Indeed, it is expected that the soft microcapsules disassemble upon dilution and form micelles that entrap the hydrophobic perfumes. Keeping the business application in mind, it is thus as important to evaluate the fate of perfume ingredients following the capsule dissociation. Flat model surfaces were created for this study, to merely investigate physico-chemical

interactions between the particles and surfaces. Surface and perfume ingredients properties were explored in order to develop models for the deposition of capsules and micelles.

Finally, the technology was incorporated in a prototype softener formulation and used in small-scale washing tests to evaluate the applicability of the established models.

II. Investigation of Soluplus®-Perfume interactions

The numerous studies found in the literature for the solubilization of poorly water-soluble drugs using Soluplus® have shown that results highly depend on the nature of the loaded active material.[63,67,70,114] This type of study usually follows a top-down approach where the authors focus on the active molecules and screen for the best materials to solubilize them. As stated in the previous section, perfumes used in consumer products are composed of several dozens of fragrant molecules, which is why such a methodology might not be appropriate for our project as finding the right polymers to encapsulate each molecule would be highly ineffective. Instead, in this study we followed a bottom-up approach where the interactions between Soluplus® and three different fragrant molecules were investigated. As seen from the literature review, Soluplus® readily forms micelles with hydrophobic drugs, due to its amphiphilic character. The intention here is to extend its solubilization properties to perfume molecules, but also to investigate its potentiality for microcapsule formation. This study aims at observing potential correlations that could predict the capsule formation and in turn, their influence on perfume deposition on solid surfaces. In this Chapter, we chose to investigate the three molecules Eucalyptol (ECL), Citronellol (CTN) and Methyl nonyl acetaldehyde (MNA) and their physico-chemical properties can be found in Appendix II. We explored parameters such as hydrophobicity described as the water-octanol partition coefficient logP, water solubility, boiling point and Hansen Solubility Parameters. We first studied binary systems of polymer and perfume in solution as well as in thin polymeric films exposed to perfume vapors, and the results are explained in sections II.1.1 and II.1.2, respectively. Following this investigation, we incorporated the polymer-perfume systems in water and assessed their ability to form self-assembled microcapsules and perfume-loaded micelles, which is described in sections II.2.1 and II.2.2.

II.1. Soluplus®-perfume interactions in binary systems

Consumer products that are considered in this project are cleaning and softening formulations. When in use, products are applied on surfaces after dilution, rinsed off, and fabrics are then dried. Capsules and micelles will most likely collapse as the water evaporates, but the surfaces will still be left with polymer-perfume particles. If the interactions between the two components are strong enough, we could expect retention of the perfume on the surface and a sustained release. That is why understanding how the polymer and perfume interact together could bring light on the kind of molecules that will most likely be encapsulated in the amphiphilic polymer and slowly release after its delivery on the solid surfaces. In subsection II.1.1, we created concentrated polymer-perfume solutions to form gels as models for the microstructure of capsules. Interactions between the two materials were assessed via thermal analyses as well as X-ray scattering. In subsection II.1.2, we formed polymeric films of Soluplus® to absorb perfume and evaluate the changes in thickness and morphology of the films.

II.1.1. Interactions in solution
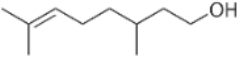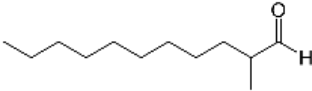
II.1.1.1. Sample preparation and characterization

The formation of Soluplus®-perfume solutions was conducted by mixing equal masses of the polymer and one of the investigated liquid fragrant molecules, namely ECL, CTN and MNA (

Table II.1). Samples were then tightly closed to prevent evaporation of the perfumes, mixed using a vortex mixer and finally stored at room temperature until homogeneous (about 15 days). The morphology of the samples was first assessed by optical microscopy, using bright-field illumination and polarized light. The samples were then characterized by Differential Scanning Calorimetry (DSC), Thermogravimetric Analysis (TGA) and Small-Angle X-ray Scattering (SAXS).

Table II.1: Structure of the studied perfume molecules.

Perfume name	Structure
Eucalyptol (ECL)	
Citronellol (CTN)	
Methyl nonyl acetaldehyde (MNA)	

II.1.1.2. Results

As seen on the optical micrographs (Figure II.1), neat Soluplus® exhibits non-spherical granules of about 340 µm in diameter[66] with micron-sized pores on its surface. When mixing the solid polymer to the perfume ECL, the liquid fragrance penetrated into the pores and flattened the granules surface to a certain extent, although the polymer was not able to dissolve in the perfume. Even several months after preparation, the sample still presented solid particles of polymer surrounded by the slightly more viscous liquid fragrance. On the other hand, the other two perfumes CTN and MNA formed colloidal gels when mixed with the polymer, with micron-sized aggregates present in a viscous fluid.

Under polarized light, all three samples containing perfumes exhibited birefringent structures, suggesting the orientation of polymer chains. In contrast, a Soluplus®-water sample was created in the same conditions and did not present any anisotropy (Figure II.1E), indicating that the orientation of the polymer chains observed in the other samples was caused by the presence of the perfumes.
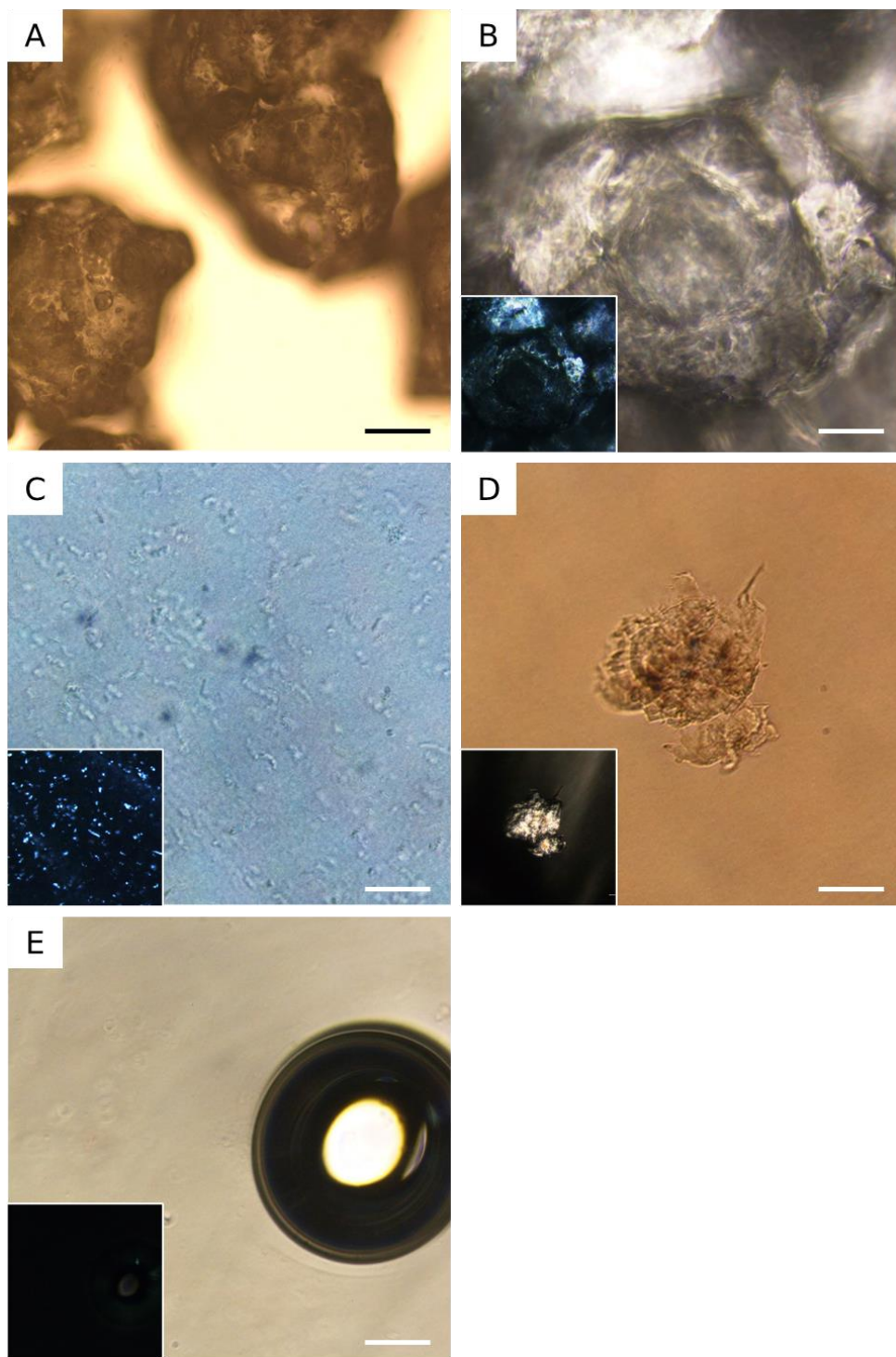
Figure II.1: Micrographs of A) Soluplus® particles and samples containing Soluplus® mixed with B) ECL; C) CTN; D) MNA; E) water under bright field illumination. The insets show the corresponding samples under polarized light. Scale bars are 50 µm.

When the samples were analyzed in DSC, the second heating cycle did not show any thermal event for any of the four tested samples (inset of Figure II.2), suggesting that the polymer did not have enough time after the cooling and isothermal steps to rearrange, which is why a third heating procedure was performed two weeks after the first analysis and the obtained curves are displayed on Figure II.3.
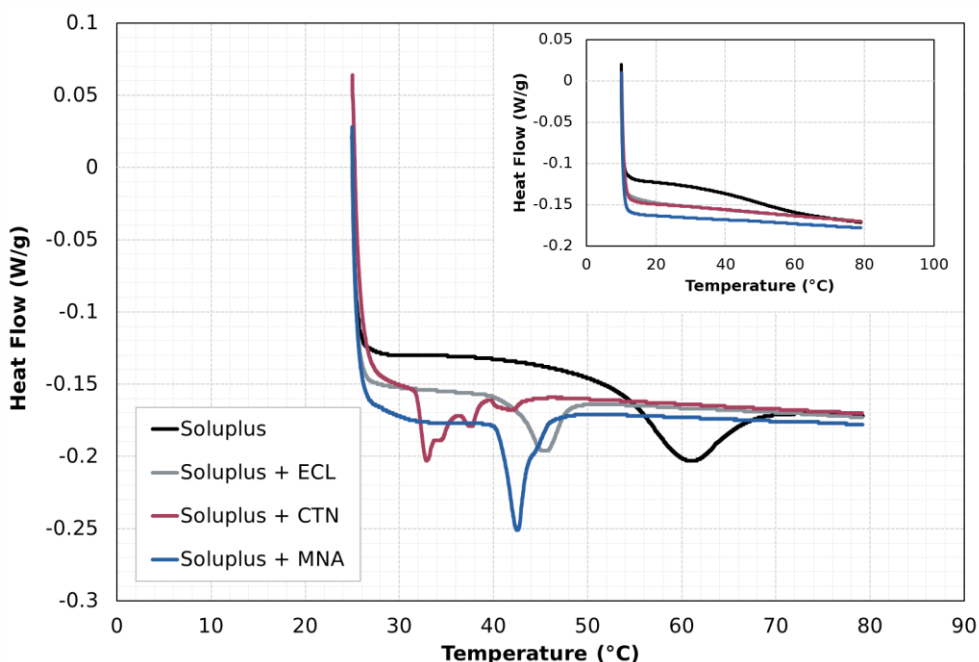
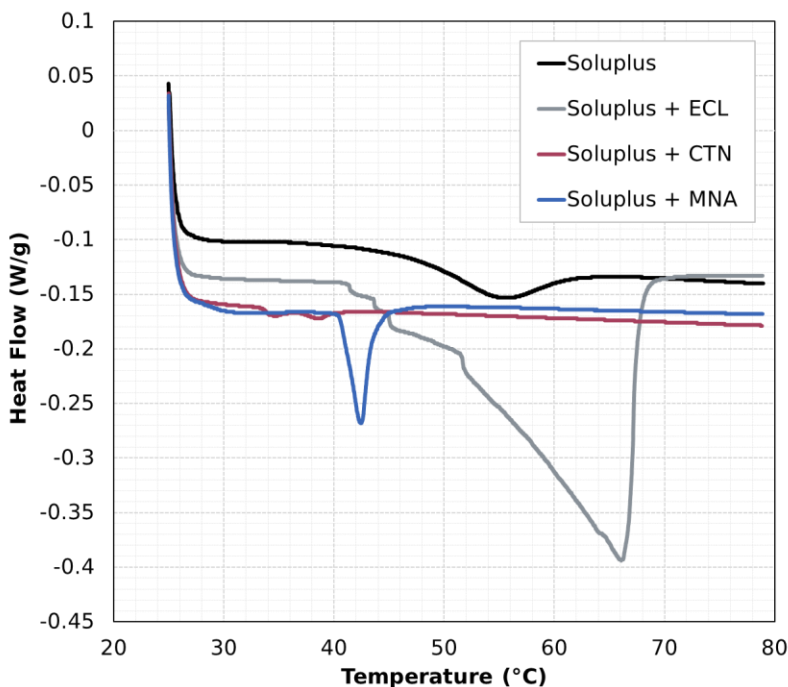**Figure II.2: DSC curves of first heating cycle of Soluplus® (black), Soluplus® + Eucalyptol sample (gray), Soluplus® + Citronellol gel (red) and Soluplus® + MNA gel (blue). Inset features the second heating cycle of the corresponding samples.**

The DSC curves of the pure perfumes did not present any thermal event in the 25-80 °C temperature range (data not shown), as the melting points of the three fragrances are located below 2°C. On the other hand, Soluplus® presented a glass transition temperature (T_g) coupled with a relaxation enthalpy contribution showing the thermal history of the sample.[115] The presence of this endothermic enthalpy relaxation peak made it difficult to precisely determine Soluplus®' T_g. However, the latter could still be approximated by drawing the tangents on the heat flow curve at temperatures below the glass transition and above the relaxation enthalpy contribution. The temperature at which the measured curve is equidistant between the two tangents was considered as the glass

transition temperature. The T_g of Soluplus® was thus measured at around 46 °C, much lower than values reported in the literature (about 70 °C [65,116]), which could be due to moisture present in the sample.[117,118]

After addition of the perfume molecules, none of the three samples showed a glass transition but melting peaks instead. The presence of ECL produced a very broad and asymmetric endothermic peak with shoulders, centered at around 66 °C, confirming that polymer-perfume interactions were present despite the persistency of polymer granules in the sample. In contrast, the Soluplus®-MNA gel presented a narrower melting peak with a minimum localized at around 43 °C, while the Soluplus®-CTN gel presented two melting peaks at around 34 °C (Tm_1) and 39 °C (Tm_2), indicating heterogeneity in the crystallites. The appearance of melting endotherms suggested the introduction of ordered structures in the samples, in accordance with the observation of birefringent areas observed under polarized light microscopy.

Figure II.3: DSC curves showing the third heating cycle of Soluplus® (black), Soluplus® + Eucalyptol sample (gray), Soluplus® + Citronellol gel (red) and Soluplus® + MNA gel (blue).

The TGA and DTG thermograms are reported on Figure II.4. Eucalyptol is the most volatile perfume and started evaporating at around 35 °C until 108 °C. When mixed with Soluplus®, one could observe several thermal events before the degradation of Soluplus® (not shown as the latter lies above 250 °C), first between 35-90 °C and then between 128-215 °C. The weight loss at lower temperatures corresponded to the evaporation of ECL surrounding the polymer granules, with a slight decrease in the evaporation rate (decrease in inflection peak) compared to that of the pure perfume. In contrast, the other weight losses at higher temperatures presented much lower evaporation rates and corresponded to perfume present in internal pores of Soluplus. Hence, it was evident that some interactions between the two materials were present even though this sample did not form a gel as with the other two fragrances.

The pure CTN and MNA presented very similar evaporation profiles having their TGA and DTG curves almost overlapping, with a slightly higher evaporation rate for the sample containing Citronellol. When combined with Soluplus®, the two gels showed only one weight loss which corresponded to the evaporation of both perfumes between 70-250 °C, with a lower evaporation rate compared to the pure ingredients. In the presence of Soluplus®, the evaporation rate of Citronellol was slightly lower than that of MNA, suggesting that this perfume could have stronger interactions with Soluplus® than MNA. However, the Soluplus®-CTN gel contained 47.4 % of polymer while the Soluplus®-MNA gel contained 40.7 % of polymer. Both gels were prepared in the same manner with a 1:1 polymer:perfume weight ratio and sampled from the top for the TGA analysis. Therefore, the difference in polymer content between the two gels reflected a slower diffusion of one material into the other in the case of the Soluplus®-MNA gel, thus suggesting stronger interactions in this system.
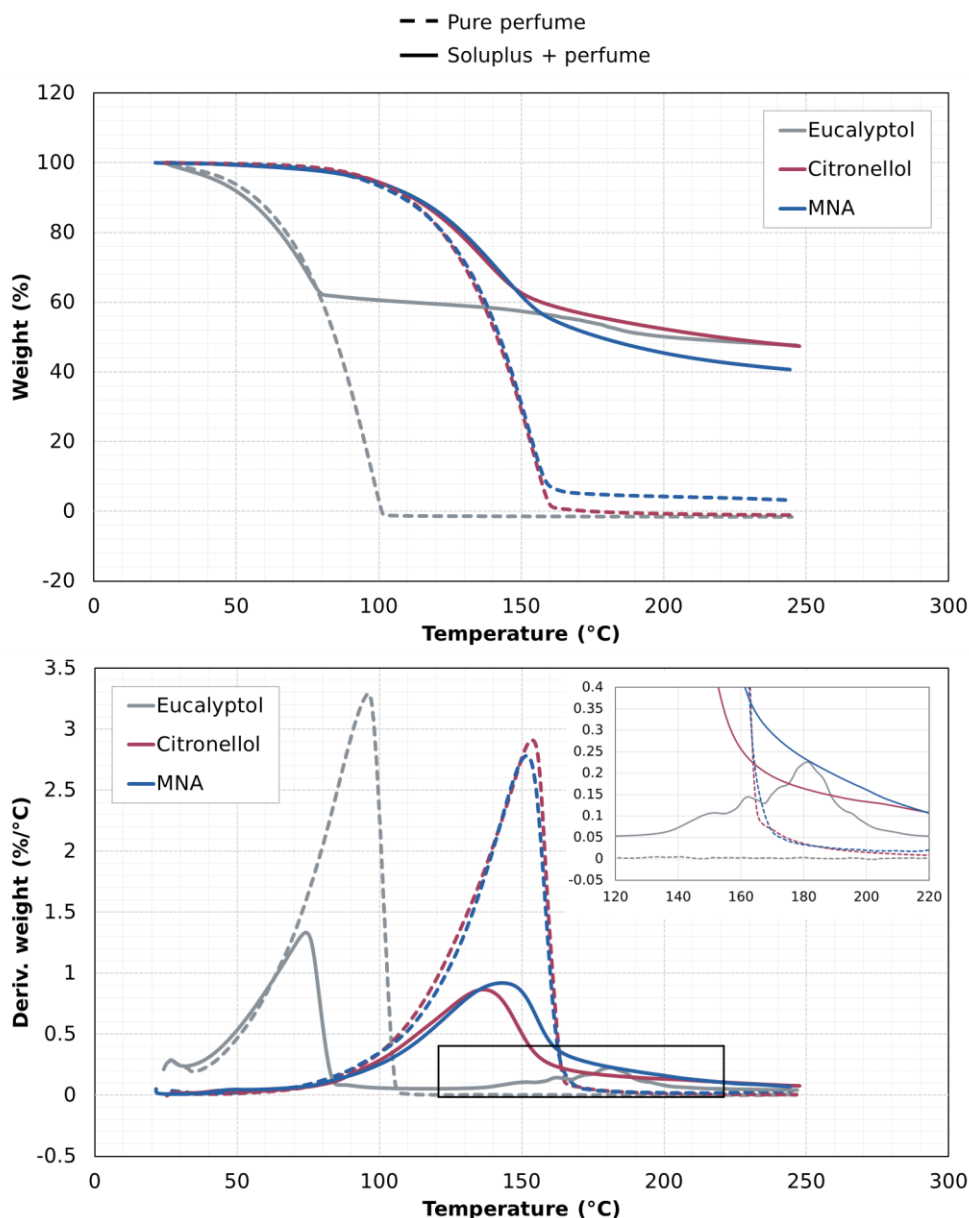
Figure II.4: TGA (top) and DTG (bottom) curves of the pure perfume molecules (dashed lines) including Eucalyptol (gray), Citronellol (red) and MNA (blue), vs. the Soluplus®-perfume samples (solid lines).

The SAXS profiles obtained for the Soluplus® + perfume samples are reported on Figure II.5 and highlighted once more the difference between Eucalyptol and the other fragrances. Small Angle Scattering of X-rays allows for the investigation of the structure of polymeric systems at the nanoscale. The gels of Soluplus® + CTN and Soluplus® + MNA both

showed a bump in the high Q region with a maximum intensity located at Q values of 0.29 Å^{-1} and 0.15 Å^{-1}, corresponding to characteristic distances of 2.1 nm and 4.2 nm, respectively.
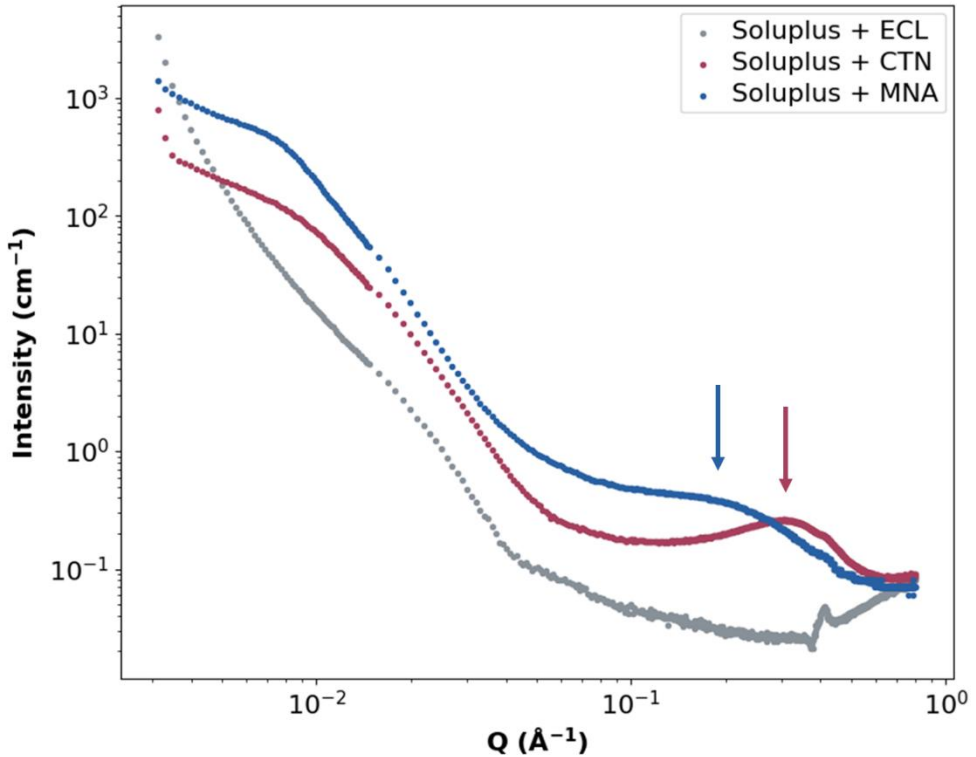
Figure II.5: Log-log representation of SAXS curves of the different samples containing Soluplus® mixed with Eucalyptol (gray), Citronellol (red) and Methyl Nonyl Acetaldehyde (blue). Arrows indicate the position of bumps in the high-Q region.

In contrast, the sample containing ECL only exhibited the beginning of a bump, and it is likely that its maximum intensity was located at larger Q values that cannot be obtained in the SAXS geometry. It is expected that this maximum peaked in the 0.9-3 Å^{-1} region, close to that of the pure Soluplus® around 1.4 Å^{-1}.[119] The position of this maximum in the high Q region corresponds to the molecular packing distances of the polymer chains: shifting the peak to lower Q values means that the packing of the polymer chains decreases, i.e., the polymer becomes more swollen. This showed that the polymer chains were only slightly swollen by the fragrance ECL, followed by CTN and finally MNA affecting them the most. The expansion of polymer chains in perfume took place in order to

maximize monomer-perfume interactions, which indicated that the perfume was a good solvent for the polymer. On the contrary, polymer chains adopted a globule configuration to maximize polymer-polymer self-interactions in the presence of a poor solvent. Thus, the strength of polymer-perfume interactions followed the order of MNA > CTN > ECL. Soluplus® + CTN and Soluplus® + MNA also showed strong scattering in the low Q region ($Q < 0.01$ Å^{-1}) while Soluplus® + ECL only showed a shoulder in the intermediate Q region ($0.01 < Q < 0.1$ Å^{-1}). This increased scattering intensity (for samples containing CTN and MNA) suggested the presence of aggregation.

II.1.1.3. Discussion

Among the three components of Soluplus® molecule, the homopolymer PEG is semicrystalline (T_g and T_m reported at around –55 °C[120] and 61 °C[121,122], respectively) whereas homopolymers PVAc and PVCL are amorphous (T_g reported at around 35 °C[123] and 145 °C[124,125], respectively). The branching of PEG with PVAc and PVCL moieties inhibits its crystallization by preventing the folding and alignment of the polymer backbone, thus making Soluplus® an amorphous polymer. However, the results presented here suggested that, at room temperature, the incorporation of the perfumes induced a crystalline state of the samples by driving the polymer chains to change their orientation and self-assemble into ordered structures. The self-assembly of Soluplus® in these binary solutions thus indicated that the fragrances did not have favorable interactions with all three of the PEG, PVAc and PVCL components, at least not at concentrations of 1:1 polymer:perfume. From the observation of the samples under polarized light (Figure II.1), it was evident that the crystalline structures were composed of the Soluplus® parts that seek to minimize their interactions with the fragrances. Since PVAc-co-PVCL side chains cannot crystallize, they were most likely the components that favorably interacted with ECL, CTN and MNA molecules, inducing the formation of PEG-rich aggregates. On the contrary, when water was mixed with the polymer, the PEG backbone interacted preferentially with this solvent rather than the PVAc-co-PVCL side chains and no crystalline state was observed. The dependence of the

orientation of polymer chains on solvent selectivity has already been reported for other three-components and multi-graft copolymers, where authors have investigated the micellization behavior of PI-g-Pluronics[126] and PGMA-g-(PCEMA-PtBA-MPEG)[127] in different organic solvents. They demonstrated that, in a selective solvent for both backbone and grafts, amphiphilic graft copolymers did not self-assemble and presented a stretched or swollen polymer coil configuration. In a solvent that was good for the backbone but not for the side chains, this type of polymers self-assembled into micelles with a "flower" type structure, having the side chains in the core. In contrast, when changing to a solvent that was nonselective for the main chain but selective for the grafts, the backbone collapsed and composed the micelle core, surrounded by the side chains. In addition, a recent study on the self-assembly properties of Soluplus® showed that this polymer formed micelles in water at a 50 wt% concentration, and the authors predicted that the latter were constituted of a PVAc-PVCL core surrounded by the PEG backbone.[128] Therefore, it is reasonable to assume that the three perfume molecules interacted preferentially with the PVAc-PVCL side chains rather than the PEG backbone.

The sample containing ECL perfume presented an increased melting point compared to the other two samples, which showed stronger polymer-polymer interactions and thus weaker polymer-perfume interactions. This was also corroborated by the increased packing of the polymer chains, as seen with the results from the SAXS measurements.
In the same manner, we concluded that Soluplus®-MNA interactions were greater than that between Soluplus®-CTN, seen as the melting point and swelling of polymer chains in the presence of MNA fragrance were greater than those comprising CTN molecule.

From these preliminary results, we could easily see that the amphiphilic polymer Soluplus® interacts differently with hydrophobic perfumes, due to the presence of three distinct components PEG, PVAc and PVCL. The random grafting and polydispersity of the polymer rendered the interpretation of results challenging, as it is likely that polymer-perfume

interactions cannot easily be explained through merely one of the perfume properties, but rather a combination thereof. So far, the defined interactions between polymer components PVAc and PVCL (i.e., the more hydrophobic parts of Soluplus®) and the studied fragrances seemed promising for the encapsulation of the latter in aqueous environment.

II.1.2. Interactions in thin films

In this study, we aimed at investigating the affinity of the different fragrances with the amphiphilic polymer by exposing thin Soluplus® films to perfume vapors. In fact, solvent affinity and solvent selectivity toward polymeric materials have been evaluated in the past through the study of swelling properties[129,130] and vapor sorption[131,132] in thin films. The thin polymeric films were first prepared by spin-coating as it is a fast and easy procedure yielding highly reproducible films.[133] The absorption of the perfume vapors was then studied through Quartz-Crystal Microbalance (QCM) and the resulting films were characterized using Atomic Force Microscopy (AFM) and X-Ray Reflectivity (XRR).

II.1.2.1. Experimental protocols

Preparation of Soluplus® films

Thin polymeric films were prepared by spin-coating Soluplus® solutions on glass substrates, using a spin-coater. In the first stage of this procedure, the coating solution is spread on top of the substrate with a pipette while the substrate is spinning at a rather low velocity. In the second stage, the substrate spins at a much higher rotation speed, allowing the excess solution to be propelled out of the substrate and the film to thin. In the final stage, the spinning velocity is increased even more in order for the solvent to evaporate out of the film. A scheme of the whole procedure can be found on Figure II.6. As a result, a dry film of polymer is obtained on top of the glass slide.
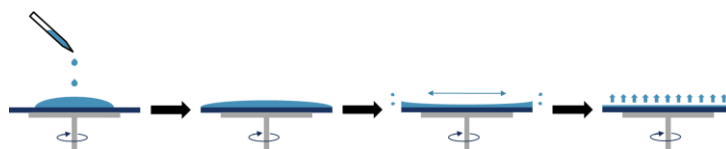
Figure II.6: Scheme of the spin-coating process.

The thickness of the resulting film is correlated to the angular velocity, the concentration of the polymer solution (and its viscosity) and the volatility of the solvent,[134–136] while polymer- and solvent-substrate interactions can affect the morphology and homogeneity of the film.[137] Thus, Soluplus® solutions of various concentrations and solvents, substrate hydrophobicities and spinning speeds were tested to obtain films of about 100 nm in thickness, and the experimental conditions are presented in Table II.2.

Table II.2: Tested parameters in the spin-coating process of Soluplus® solutions on glass substrates.

Soluplus® solutions		Substrate (glass slides)	Spin-coater rotation speed (RPM)
Solvents	Soluplus® concentration		
Ethanol Milli-Q Water	1 wt% 2 wt% 5 wt%	Hydrophilic Hydrophobic	1000 1500 1750 2000 2100 2500 2700

The optimization of the film formation procedure was conducted on glass substrates. To do so, glass microscope slides were cut to create substrates of about 1.5 x 1.0 cm^2. They were then cleaned thoroughly by immersion in a piranha solution (3:1 solution of H_2SO_4 : H_2O_2 30%) for 5 minutes, rinsed with Milli-Q water and dried with a flow of nitrogen (N_2) gas. Several pieces of glass were also hydrophobized after cleaning by exposing them to vapors of dodecyltriethoxysilane (DTES) by depositing a drop next to the substrates in a closed petri dish. They were stored as

such overnight to allow for the hydrophobization by chemical vapor deposition (i.e., reaction between ethoxysilanes and glass silanols).

Thickness measurement

Prior to determining the film thickness by AFM, it was necessary to scratch the surface of the film in order to remove the material from the glass substrate, and then create an image of the scratch. The scratches were produced via AFM using a silicon cantilever, by scanning a 0.75 x 1.00 μm^2 image at a 5 Hz frequency, first in contact mode (twice), then repeated in non-contact mode. Finally, the scratch was scanned over a 6 x 6 μm^2 area in non-contact mode. The difference in the z axis between the untouched film and the center of the scratch (i.e., the uncovered glass surface) was then defined as the polymeric film thickness, as can be seen from the line profile on Figure II.7. Three scratches per slide were performed in order to verify the homogeneity of the film thickness across the substrate, from the center of the film to the border.
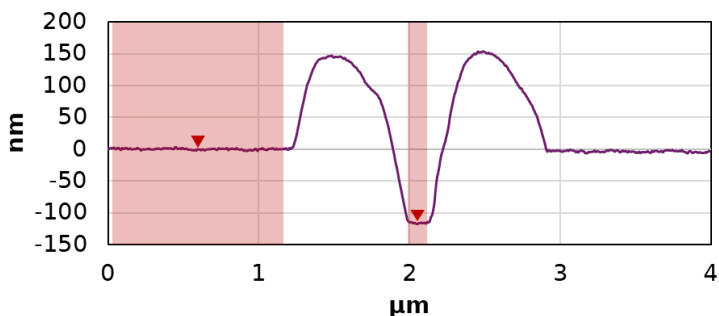
Figure II.7: Cross-sectional profile of a scratch created in a Soluplus® film, produced and characterized by AFM. Film thickness is determined from the difference between the averaged z height values in each red zone.

Sorption of perfume vapors on Soluplus® thin films

The affinity of perfumes with Soluplus® was evaluated by QCM through the sorption of vapors in thin polymeric films created on SiO_2 quartz sensor crystals. The experiments were performed following a protocol readapted from the literature,[138,139] which involved the transport of perfume vapors, using N_2 as a carrier gas, to a closed chamber containing the polymeric film, and a scheme of the system can be seen on Figure II.8.
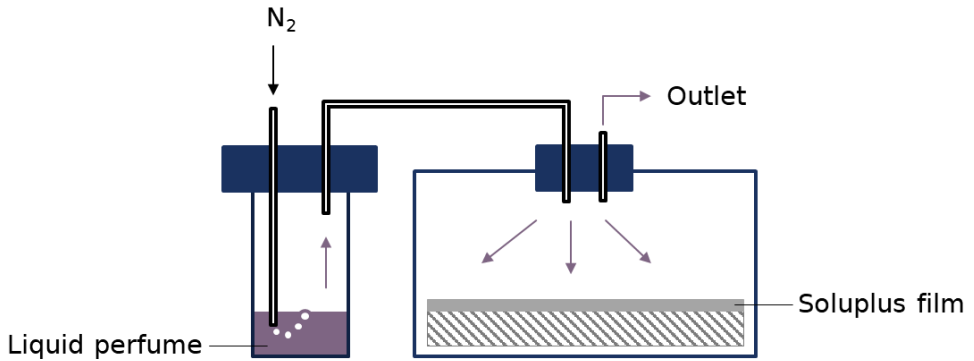
Figure II.8: Scheme of flow system used for the adsorption of perfume vapors on Soluplus® films.

First, a flow of dry N_2 gas was introduced into the chamber for at least 10 min to create a baseline of the frequency and dissipation shifts. The perfume vapors were passed through the QCM-D cell until a stable frequency signal was monitored for at least 5 min. Finally, nitrogen was flowed into the chamber again to obtain a desorption curve until a stable frequency signal was monitored for at least 5 min. The data was normalized by the vapor pressure of each perfume before quantification. All sorption experiments were then repeated in a flow cell of our own design on Soluplus® films created on gold-coated silicon wafers to evaluate their morphology by AFM and XRR, using the exact same protocol as with the QCM instrument.

II.1.2.2. Results

Preparation of Soluplus® films

The hydrophobization of the glass slides was confirmed by determining the wetting behavior of water using static contact angle measurements. Results showed that the treatment by DTES was effective to hydrophobize the glass surface as the water contact angle varied from 30 ± 6 ° to 90 ± 5 ° for the non-modified substrate and hydrophobized glass, respectively.[140]

The first step in the formation of Soluplus® thin films was to determine the solvent (water vs. ethanol) and surface properties (hydrophilic vs. hydrophobic) that would lead to the most homogeneous film. Figure II.9 presents the thicknesses of the created films, measured on three points across each slide.
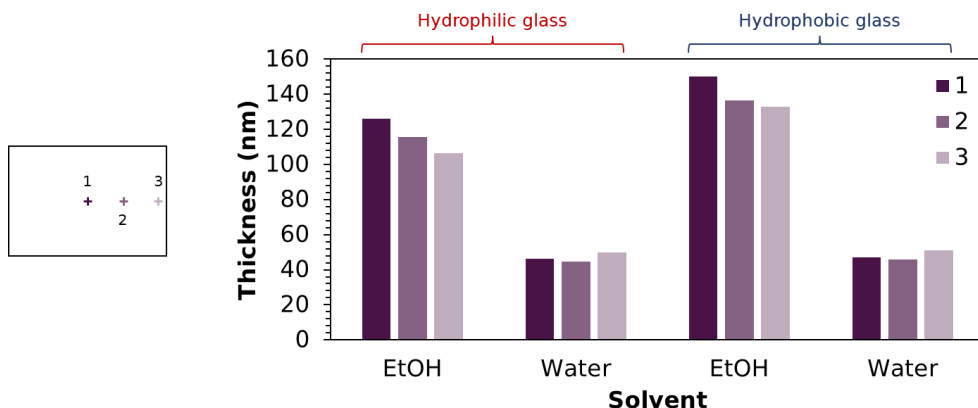
Figure II.9: Representation of a glass slide with location of the measured points. Thicknesses of Soluplus® films created from polymer solutions in ethanol or water on hydrophilic and hydrophobic glass slides, measured at different locations on the film.

The major difference in thickness between the films prepared from the aqueous or ethanolic solutions was mostly due to the polymer concentration (2 wt% Soluplus® in ethanol vs. 1 wt% Soluplus® in water). Additionally, it was observed that the ethanolic solution of Soluplus® produced films with a decreasing thickness from the center to the border of the substrate, while the aqueous solution resulted in more homogeneous films with a small border effect where the thickness was slightly increased. As this side of the substrate was not a relevant part in our study, this border effect was neglected, and water was chosen as the solvent for the polymer solution.

When considering the samples from the aqueous solution of Soluplus® on hydrophilic and hydrophobic glass slides, there was no significant difference in the film thickness and homogeneity between the two kinds of substrates. For practical reasons, the hydrophilic glass was chosen to continue with the next steps of the film optimization.

Increasing the polymer concentration in the coating solution while keeping the other process parameters intact increased the thickness of

the film as well (Figure II.10, left). Since the objective was to obtain a film about 100 nm thick, the 5 wt% Soluplus® aqueous solution was chosen to create the final films that would serve in the following experiments. Finally, increasing the angular velocity decreased the film thickness (Figure II.10, right) and the speed of 2700 rpm was selected for the following sorption studies, resulting in a film of 105 ± 2 nm thickness.
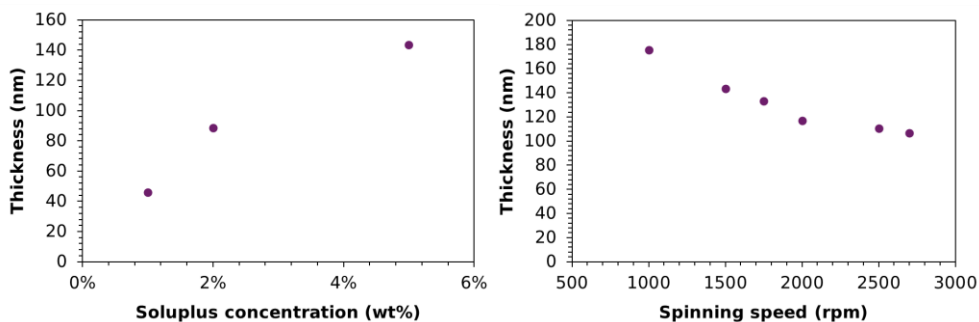

Figure II.10: Variation of film thickness as a function of polymer concentration (left) and spinning speed (right). Films were created from aqueous Soluplus® solutions on hydrophilic glass, using an angular velocity of 1000 rpm and a polymer concentration of 5 wt% to obtain the left and right graphs, respectively.

The procedure including all the chosen conditions (i.e., spin-coating of a 5 wt% aqueous solution of Soluplus® on a hydrophilic glass slide, using a 2700 rpm angular velocity) was finally repeated on SiO_2 QCM-D sensors and was used to study the perfume-Soluplus® interactions.

The morphology of the Soluplus® film was also characterized by AFM. As seen on Figure II.11, the film presented densely packed spherical objects with a diameter comprised between 50-100 nm, measured from the line profile on topographic images. These objects were identified as Soluplus® micelles, as their size aligned with that previously reported in the literature for Soluplus® micelles prepared in water.[67,70] Indeed, several authors reported on the transfer of polymer aggregates of various morphologies on surfaces by simply spin-coating a solution of these aggregates.[141–143]
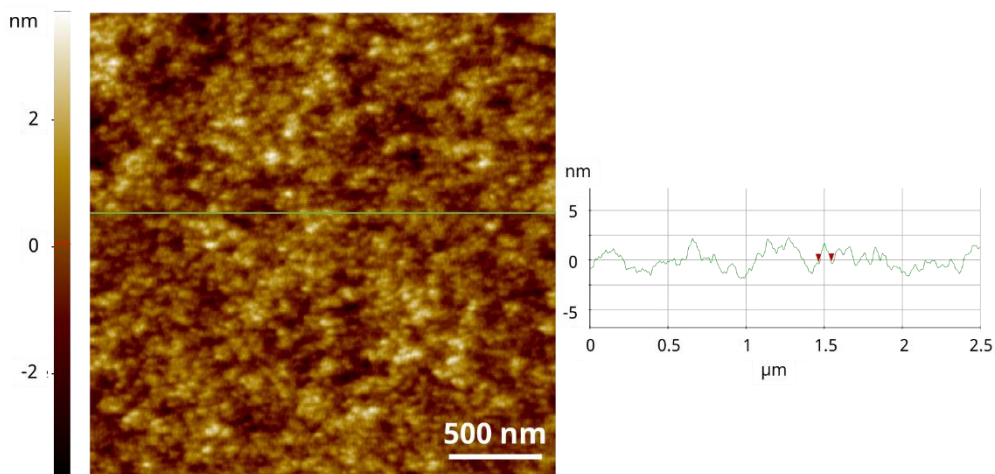
Figure II.11: AFM topographic image of a spin-coated Soluplus® film (left) and the cross-sectional profile corresponding to the green line (right).

Sorption of perfume molecules monitored by QCM-D

When a material is rigidly adsorbed and homogeneously distributed on the quartz crystal, assuming that the mass of the polymeric film is small compared to the mass of the sensor, the Sauerbrey relation[13] (equation II.1) can be used to calculate the absorbed amount of perfume vapors from the changes in resonance frequency:

II.1
$$\Delta m = -C \frac{\Delta f}{n}$$

where Δm is the areal mass of the adsorbed layer, C is a constant characteristic of the crystal, in our case 0.177 mg/m², Δf is the change in frequency and n is the overtone number. Here, the frequency shift is defined as $\Delta f = (f_0 - f)$, where f_0 corresponds to the fundamental resonance frequency of the sensor in solution prior to the start of the experiment, and f is the frequency at a given time during the experiment. The data from the 3rd overtone was normalized by the vapor pressure of the perfume molecules (Appendix II) and the Sauerbrey equation was applied to obtain the results plotted on Figure II.12.
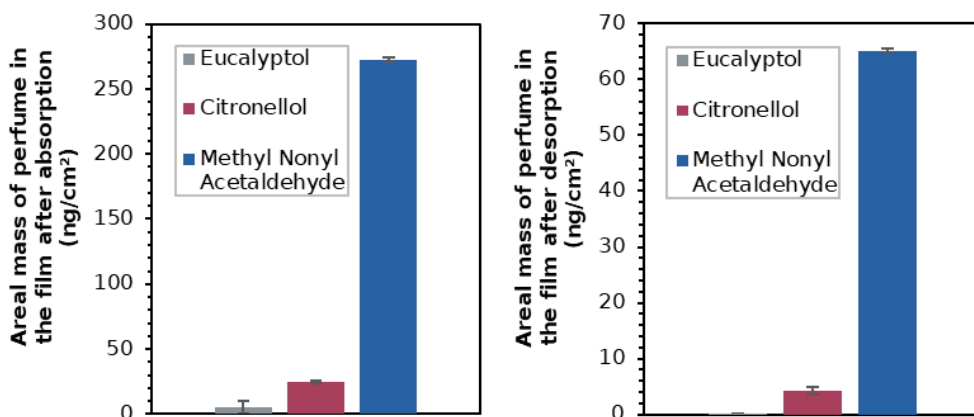
Figure II.12: Areal mass of perfumes in the Soluplus® films at the end of the absorption (left) and desorption (right) procedures.
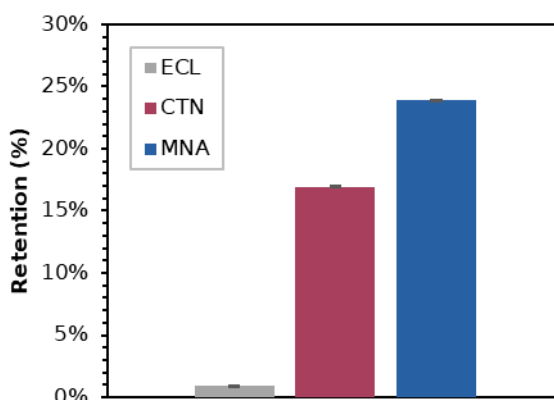

Figure II.13: Percentage of perfume retained in Soluplus® film after the desorption process.

It was evident that MNA had the greatest affinity with Soluplus® as this perfume showed the greatest absorbed mass in the polymeric film, as well as the greatest retention after desorption induced by the last flow of nitrogen gas in the chamber (Figure II.13).

The absorbed quantities and retained amounts of perfume in the polymeric film were plotted against the different physical-chemical parameters of the fragrances, including logP, vapor pressure, water solubility, Hansen Solubility Parameters (δ_D, δ_P, δ_H, HSP distance between perfumes and Soluplus® or its different components). Unfortunately, none of those properties seemed to be correlated to the affinity between the perfumes and Soluplus® (plots not shown), suggesting that several

parameters or less obvious ones should be considered to explain the polymer-perfume interactions.

Morphology of films

The polymeric films exhibited differences mainly in the micelle size after exposure to the various gas samples (Figure II.14). Indeed, while the roughness of the polymeric film did not significantly decrease, the diameter of the aggregates increased. More specifically, MNA raised the micelle size to 100-200 nm, ECL to 80-180 nm and CTN to 80-110 nm. However, these values were obtained by measuring the diameter of aggregates from the line profile of the AFM image, although using imaging particle analysis would certainly provide more accurate results.
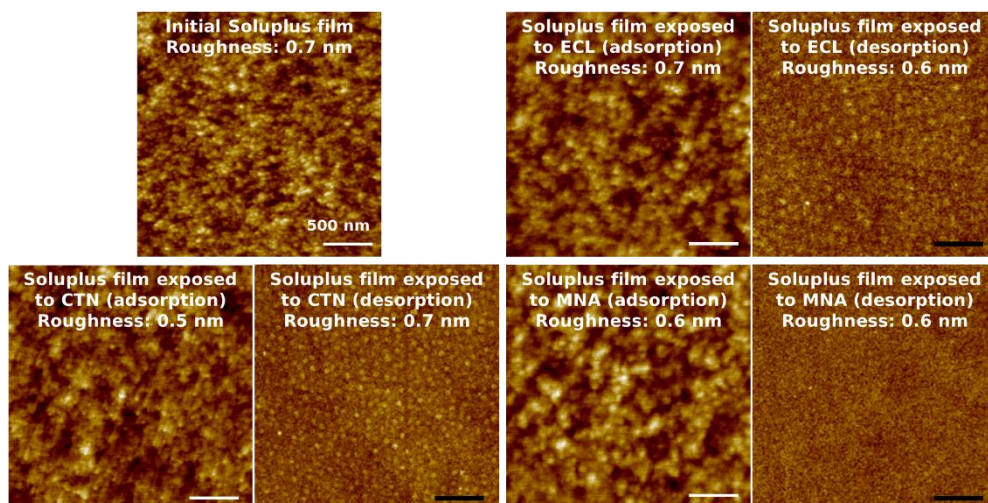
Figure II.14: AFM pictures of Soluplus® films exposed to the different perfumes. White and black scale bars are 500 nm and 10 µm, respectively.

It is worth mentioning that the film exposed to Citronellol was wet after the absorption experiment, which made it difficult to collect a proper image by AFM as the film was still diffusing during the analysis. Because of this phenomenon, the film had to be dried before the measurement by letting it rest in air to evaporate the perfume. It took more than 5 hours for the film to be dry enough for the analysis, which showed that when there is no flow of air passing above the surface to flush the perfumes, the desorption should be a slow process.

The polymeric film then showed greater differences in morphology after the desorption of Eucalyptol and Citronellol from the films (Figure II.14). It could be observed that the polymer rearranged into small "islands" for those two perfumes as the latter evaporated from their film, indicating a dewetting phenomenon. The sample that contained CTN exhibited aggregates of about 600-700 nm while ECL exhibited aggregates of about 700-1000 nm. On the contrary, the desorption of MNA from its polymeric film kept the morphology in a rather flat state, which supported the results from the QCM experiment where some MNA was still detected in the film after drying with nitrogen gas.
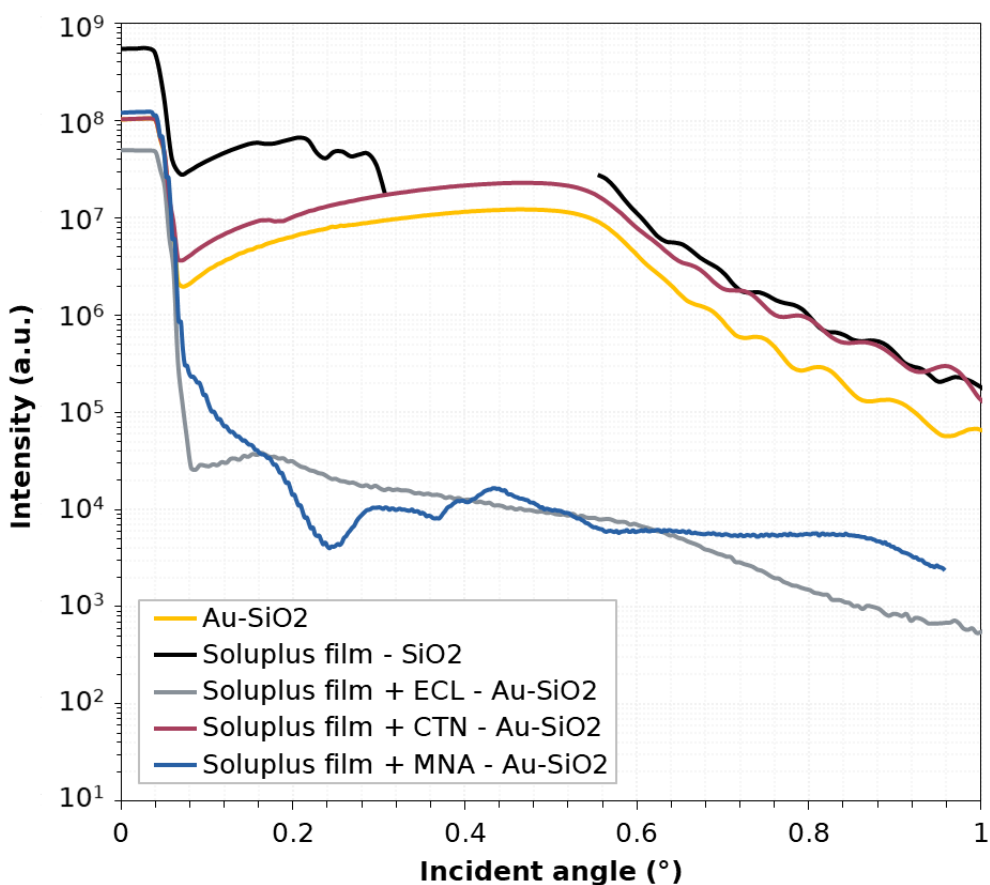
Figure II.15: XRR curves of Soluplus® films exposed to perfume vapors.

XRR is a technique that can be used to determine the thickness, density and structure of a relatively flat sample. Each layer of material can be distinguished by a set of bumps characterized by their periodicity, and a

decrease in the periodicity corresponds to an increase in layer thickness. A weak signal at around 0.15 ° (in incident angle) appeared only in curves of samples containing Soluplus® (black, gray, red and blue curves on Figure II.15), it was thus reasonable to assume that this bump was related to the thickness of the polymeric film.

The Soluplus® film that had been exposed to Citronellol vapors (red curve) showed a very similar curve to that of the references (Au/SiO$_2$ and Soluplus®/SiO$_2$), which indicated that the presence of perfume did not change the structure of the polymeric film, suggesting a low absorption of perfume. On the contrary, exposing the Soluplus® film to Eucalyptol or MNA caused the disappearance of the periodicity seen on the reference, which confirmed the presence of a different layer on top of the Au-SiO$_2$ wafer.

II.1.2.3. Discussion

The formation of a film by spin-coating makes use of the fast evaporation of the solvent of the spun solution, creating a dry film within a few seconds. Thanks to the rapidity of this process, polymer aggregates that are transferred to the substrate are thus "frozen" in the same state as they were in the initial solution. Hence, Soluplus® micelles composing the thin polymeric film should exhibit a structure with the hydrophobic PVAc-PVCL side chains in the micelle core and the PEG backbone on the outer part of the micelle, in order to protect the hydrophobic moieties from water that served as the solvent in the spun solution.[114] Moreover, the hydrophilicity of the glass substrate should also promote the preservation of the micelle structure as a hydrophilic PEG corona can favorably interact with the hydrophilic glass surface.

Eucalyptol and Citronellol substantially affected the morphology of the polymeric film but showed very little absorption and retention in the film, according to QCM results. When closely observing the topography of the various films after the desorption of perfumes (Figure II.16), one can notice the appearance of small and regular cavities in the films that were exposed to ECL and CTN, with a diameter of about 50 and 70 nm, respectively, whereas MNA did not present such elements. These features have already been reported in the past and have been attributed to the

opening of micelles when exposed to solvents that are selective for the micelle core.[144,145] In fact, the morphology of polymer micelles in solution is often controlled by the nature of the solvent(s) and its(their) selectivity toward the different polymer blocks. It has been shown that by exposing micelle films to solvents with a good selectivity for the micelle core, the polymer aggregates start to swell as the solvent diffuses through the film. Eventually, micelles rupture as the entanglement force of the corona chains cannot withstand this swelling any longer.[144]
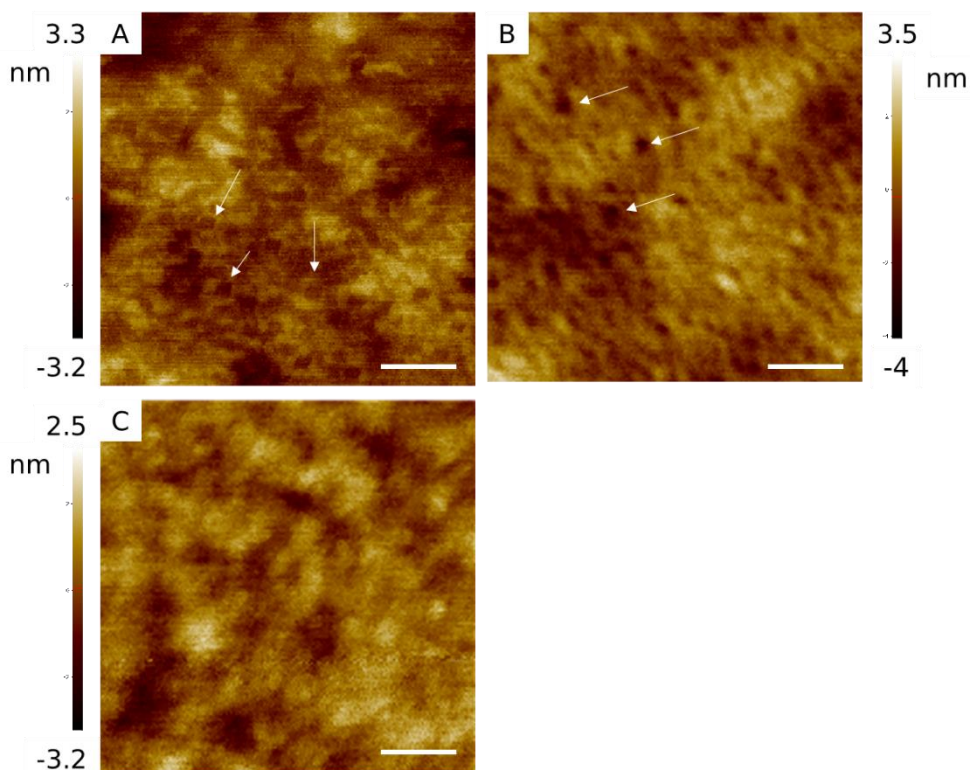
Figure II.16: AFM topographic images of Soluplus® films after exposure and desorption of perfume vapors, including A) ECL, B) CTN and C) MNA. White arrows point at examples of cavities formed in the film upon drying. Scale bars are 250 nm.

Since these openings were only visible in on the topographic images obtained after the desorption process, we could conclude that the rupture did not happen during the exposure to perfume vapors in our case, but at a later stage of the experiment while the film was being dried by the flow of N_2. As seen from the z-scale on Figure II.16, the depth and diameter of

the cavities seemed to be lower in the case of ECL, which suggested a lower swelling of the PVAc-PVCL core and thus a poorer affinity with this perfume compared to CTN. Additionally, the presence of larger aggregates in the micelle films after perfumes desorption (Figure II.14) suggested the rearrangement of the polymer chains as the fragrance vapors evaporated from the polymeric film.

The results reported in this section allowed us to evaluate the strength of interactions between perfume molecules and Soluplus®, following the order of MNA > CTN > ECL. This suggested that the hydrophobicity of the fragrant molecules plays a major role in the polymer-perfume interactions, though the extend of this correlation remains unclear as the obtained results were mainly qualitative and other parameters are certainly involved as well. Indeed, even though QCM experiments resulted in a quantitative analysis, the obtained findings led to the conclusion that Soluplus® micelles barely absorb ECL and CTN compared to MNA, which did not corroborate the swelling of Soluplus® micelles observed by AFM. Those discrepancies might come from the implementation of the QCM experiment itself, which would need to be revised and improved or replaced for better characterization. Nevertheless, we speculated that increased polymer-perfume interactions would serve in the formation of polymeric microcapsules and micelles. This could also be beneficial for the retention of fragrances after the deposition of capsules/micelles on surfaces, resulting in a slower perfume release.

II.2. Interactions in aqueous environment

In this project, we are exploring encapsulation systems that are to be contained in aqueous formulations. After investigating the polymer-perfume interactions in binary systems, it was then necessary to explore the ability of Soluplus® to encapsulate small molecules in aqueous environments. Therefore, in this section we are evaluating the encapsulation properties of Soluplus® in water with the same perfumes

previously investigated, in the form of microcapsules and polymeric micelles in subsections II.2.1 and II.2.2, respectively.

II.2.1. Formation of microcapsules

II.2.1.1. Experimental protocols

Formation of microcapsules

Capsules were created by incorporating the amphiphilic polymer Soluplus® in water with one of the three perfumes of interest, namely Eucalyptol, Citronellol and Methyl Nonyl Acetaldehyde, in a polymer:perfume 1:1 weight ratio. After incorporation of the three components (i.e., polymer, perfume and water) in a vial, samples were gently shaken for a few hours until no change was detectable. The obtained capsules were then characterized using optical microscopy and Raman Confocal Microscopy (CRM).

II.2.1.2. Results and discussion

The Raman maps (Figure II.17) were acquired in the liquid samples and showed moving capsules; it was thus challenging to obtain images displaying the inside and outside of capsules on the same map. Therefore, maps were also acquired outside of the capsules (data not shown) following the Raman signals of perfumes and Soluplus® (Figure II.19-21), showing the absence of the two components in these areas.
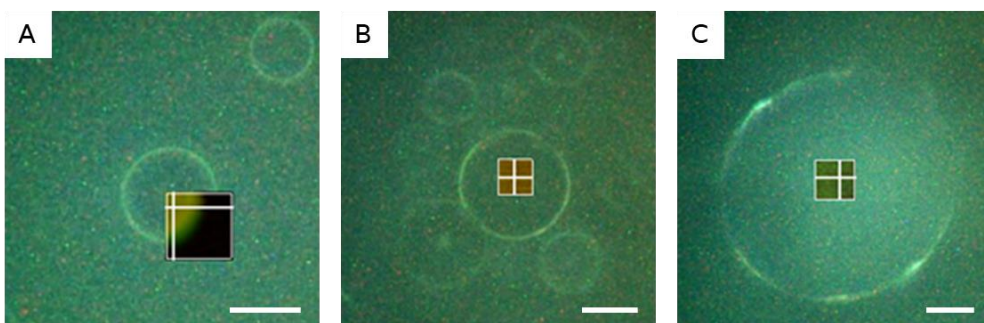
Figure II.17: Micrographs of Soluplus®-perfume microcapsules in water with 2D maps representing the location of the Raman signals corresponding to Soluplus® and the perfume A) Eucalyptol; B) Citronellol; C) MNA. Scale bars are 10 μm.
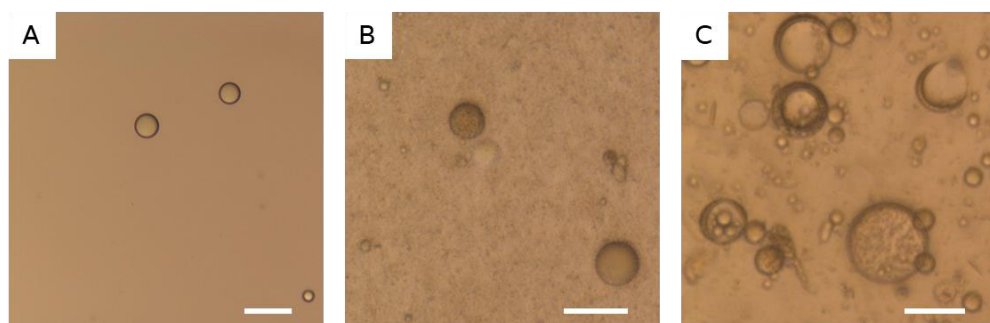
Figure II.18: Micrographs of microcapsules made of Soluplus® and the perfume A) Eucalyptol; B) Citronellol; C) MNA in water, in bright-field illumination. Scale bars are 50 μm.

When a simple aqueous Soluplus® solution was created (i.e., without perfume), the copolymer only formed polymeric micelles in water. On the contrary when a perfume was added to the mixture, Soluplus® was able to form spherical microcapsules of various dimensions and structures, depending on the encapsulated active molecule. The results confirmed the inclusion of perfume in the microcapsules of Soluplus®, with the colocalization of the Raman signals corresponding to the polymer and fragrances (Figure II.17).

As seen on the micrographs on Figure II.18, the ECL-capsules exhibited the smallest number density among the three samples, which was consistent with the poorer polymer-perfume interactions revealed in the first part of this Chapter. On the other hand, CTN-capsules possessed the highest number density with extremely small microcapsules, along with a few capsules having a diameter in the 40-50 μm range. Finally, MNA-capsules also exhibited great differences in capsule size and but also in internal structure, including core-shell, multi-core, matrix, as well as homogeneous capsules present in the same sample. However, the results obtained from the Raman mapping presented a homogeneous distribution of both polymer and perfume in the three tested samples. The observed difference between the results obtained with both techniques could come from the experimental conditions when producing the Raman 2D maps. In fact, each one of them was produced by acquiring signals every 0.5 μm in the x and y directions, eventually forming a grid of independent spectra. Consequently, the resolution of the

resulting bidimensional maps might not allow for the detection of small structural differences. Similarly, the resolution of the CRM was too poor to detect the presence of entrapped perfume in polymer in the form of micelles in the surrounding medium, although we suspected their presence alongside the microcapsules.

Since the procedure of capsule formation did not involve high-energy processes, the difference in capsule size and morphology between samples could only be attributed to differences in perfume properties (see Appendix II). This could for example be ascribed to perfume's hydrophobicity, perfume self-interactions and polymer interactions, etc.
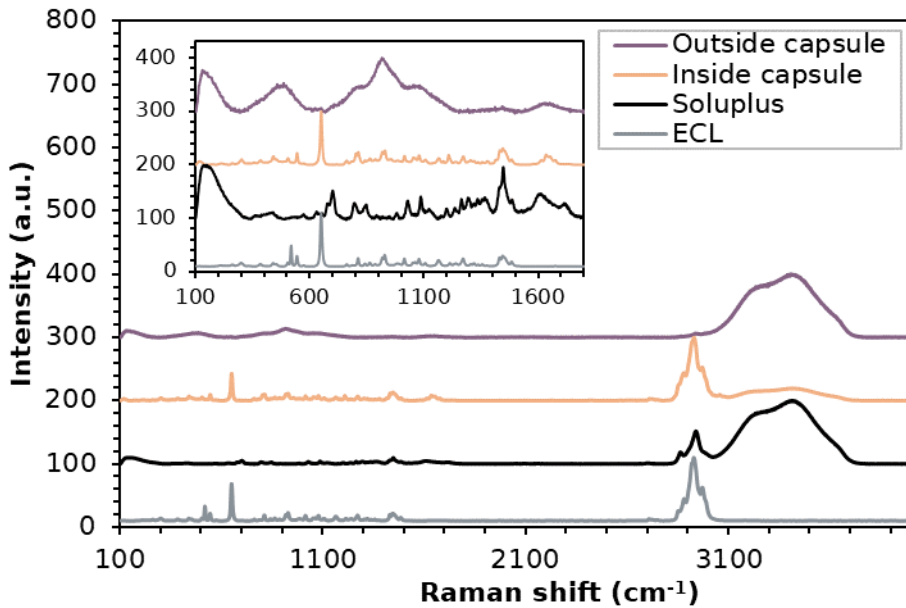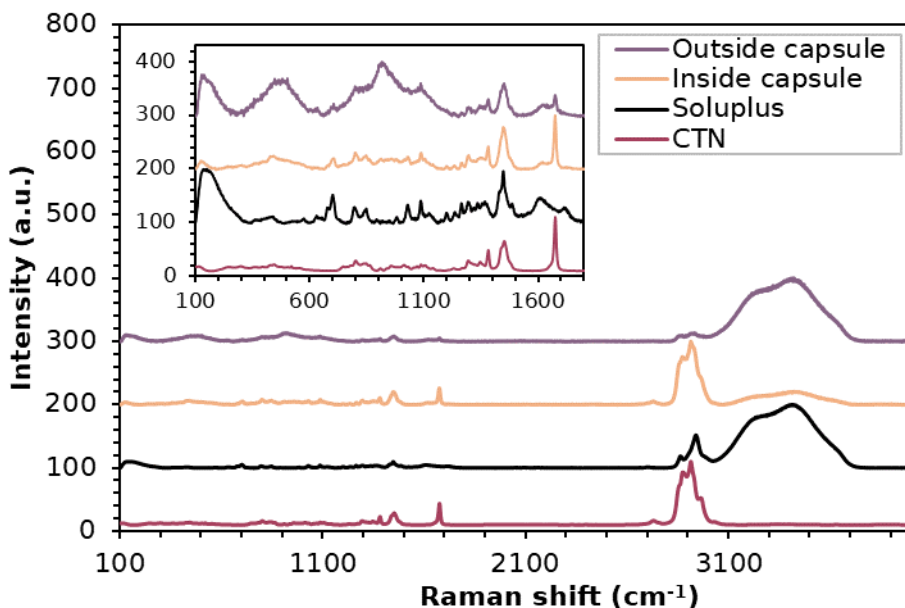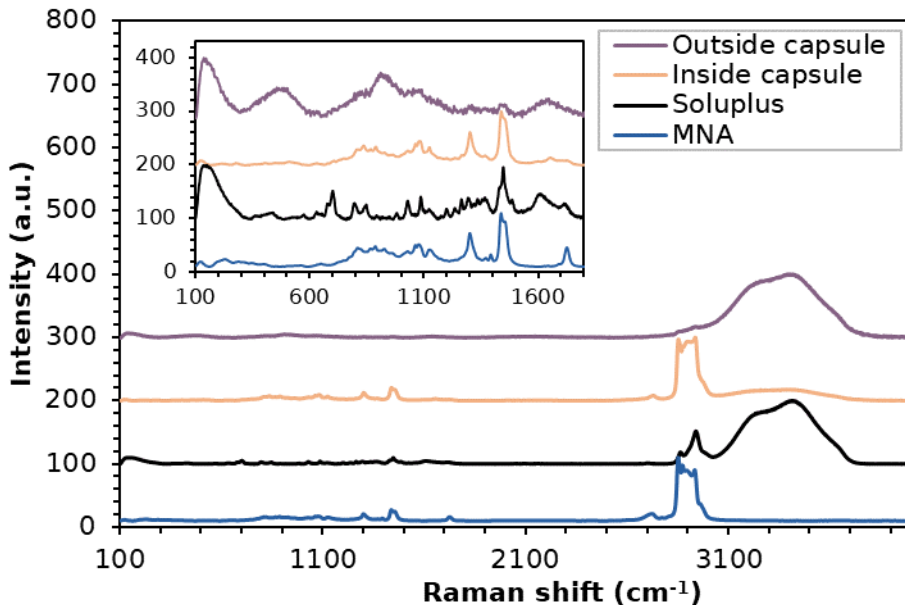

Figure II.19: Raman spectra characterizing Soluplus®-ECL capsule suspension, acquired on points located outside (purple) and inside (orange) of the microcapsules, and the corresponding Soluplus® (black) and Eucalyptol (gray) references. Inset shows a magnified view of the 100-1700 cm^{-1} range.

Figure II.20: Raman spectra characterizing Soluplus®-CTN capsule suspension, acquired on points located outside (purple) and inside (orange) of the microcapsules, and the corresponding Soluplus® (black) and Citronellol (red) references. Inset shows a magnified view of the 100-1700 cm^{-1} range.

Figure II.21: Raman spectra characterizing Soluplus®-MNA capsule suspension, acquired on points located outside (purple) and inside (orange) of the microcapsules, and the corresponding Soluplus® (black) and Methyl Nonyl Acetaldehyde (blue) references. Inset shows a magnified view of the 100-1700 cm^{-1} range.

As reported in this paragraph, the incorporation of the previously studied polymer-perfume systems in water produced a variety of spherical microcapsules, for which the properties cannot easily be predicted. As expected, the increased Soluplus®-MNA interactions observed in section II.1 induced the formation of big, numerous capsules, and the poor Soluplus®-ECL interactions resulted in the formation of few microcapsules in solution. Yet, the reason behind the different capsule structures and sizes appearing in the same sample remains unclear.

II.2.2. Formation of polymeric micelles

II.2.2.1. Experimental protocols

Formation of polymeric micelles

The same Soluplus®-perfume capsule suspensions were then diluted in water to a concentration of 25 mg/L Soluplus® to obtain polymeric micelles loaded with perfume.

Characterization of micellar solutions

The obtained solutions were characterized by Dynamic Light Scattering (DLS) to determine the particle size distribution. To evaluate the potential effect of viscosity on DLS results, density and kinematic viscosity of solutions were also estimated at 25 °C. The former was performed by measuring the mass of 1 mL of solution, while the latter was determined by recording the time to flow 50 mL of solution through a graduated burette. As the experiment was not performed using a standard gravimetric capillary, the flow time values could not be converted into kinematic viscosity values. However, since those two terms are proportional (kinematic viscosity = flow time x capillary constant), the flow time values could be used as measured to compare the solutions. Measurements are reported with a variation of ± 15 % to account for manipulation error.

Confirmation of perfume inclusion in micelles

Inclusion of ECL and CTN in the polymeric micelles had to be confirmed as these perfumes are water-soluble in the concentration range used in the following experiments, which was performed using a QCM-D instrument. To that end, SiO_2 sensors were first coated by a thin film of Soluplus® following the procedure described in section II.1.2.1. Once in the instrument, water was flowed over the sensor (0.1 mL/min) until the frequency and dissipation changes were stable ($\Delta f < 2$ Hz over 10 min). Then, a solution of Soluplus® micelles (25 mg/L) was introduced into the chamber (0.1 mL/min) in order to obtain a layer of micelles, again until the frequency and dissipation changes were stable (i.e., no more adsorption of polymer occurred). Finally, a solution of polymer + perfume (Eucalyptol or Citronellol) micelles was flowed over the sensor and the adsorption of materials was monitored over one hour, after which water was passed through the chamber for another hour to rinse the loosely bound materials.

II.2.2.2. Results and discussion
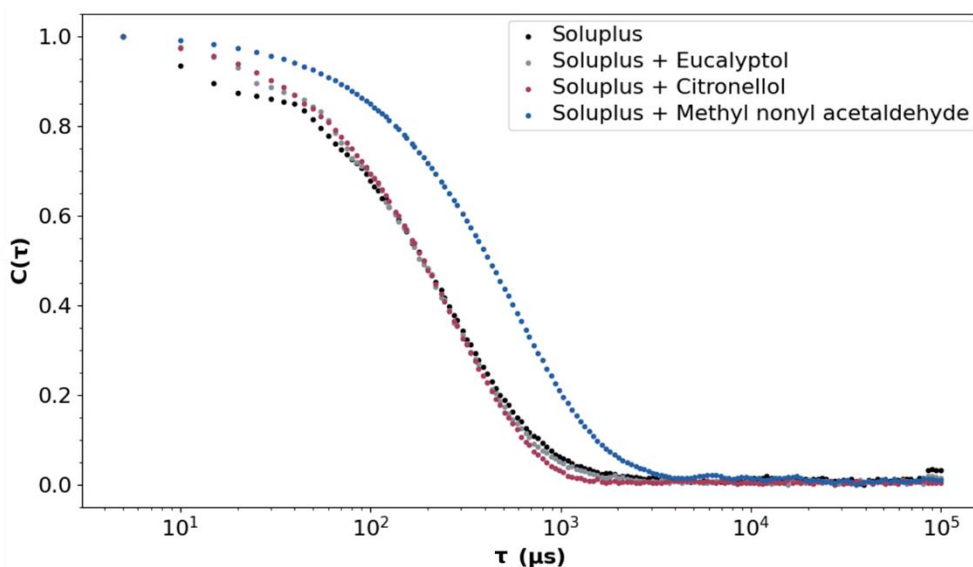
Characterization of polymeric micelles

Figure II.22: Intensity autocorrelation function of Soluplus® micelles containing perfume molecules.

When plotting the intensity correlation function of all samples, it can be noticed that only the solution containing MNA increased the size of the polymeric micelles (Figure II.22). This increase of the particle size induced by the inclusion of MNA perfume in the Soluplus® micelles corroborated the results obtained when investigating the absorption of MNA vapors in the Soluplus® micelle film. Indeed, this perfume being the most hydrophobic among the three studied analytes, it could easily be loaded in the polymeric micelles once the materials were placed in aqueous environment to decrease interactions between the hydrophobic molecule and water, hence increasing the size of Soluplus® micelles.

On the other hand, samples containing ECL and CTN showed little to no change in particle size for the polymeric micelles in the presence of the perfumes. However, the flow time of their respective solution was increased by a factor of 15-20 % (Table II.3), related to an increase in the viscosity.

Table II.3: Density and flow time of micellar solutions and calculated particle size and polydispersity of micelles.

Micelles	Density (g/L)	Time to flow 30 mL of solution (s)	Hydrodynamic diameter (nm)	Polydispersity index
Water	997	7.9 ± 1.2	-	-
Soluplus	995.5 ± 4.3	6.2 ± 0.9	86.7 ± 2.2	0.18 ± 0.01
Soluplus® + Eucalyptol	996.8 ± 4.3	7.1 ± 1.1	*79.9 ± 2.6	0.19 ± 0.03
Soluplus® + Citronellol	998.4 ± 8.4	7.3 ± 1.1	*84.0 ± 1.0	0.04 ± 0.02
Soluplus® + Methyl nonyl acetaldehyde	997.2 ± 0.3	6.3 ± 0.9	180.8 ± 1.8	0.11 ± 0.02

*Not corrected by the viscosity of the solution

The corrected micelle size was thus found to be around 70 nm in both samples, suggesting that Soluplus micelles collapsed in the presence of these perfumes. This raised the issue of whether these fragrances were entrapped in the polymer micelles when in aqueous environment, as

these perfumes are water-soluble at the experimental concentration and could simply be dissolved in the surrounding medium, as suggested by the change in viscosity.

Perfume inclusion in Soluplus® micelles

The adsorption of Soluplus® + perfume micelles onto the initial layer of Soluplus® micelles (Figure II.23) showed that the presence of Eucalyptol induced an increase in frequency shift corresponding to the desorption of materials, while the presence of Citronellol induced a decrease in frequency shift corresponding to the adsorption of materials.
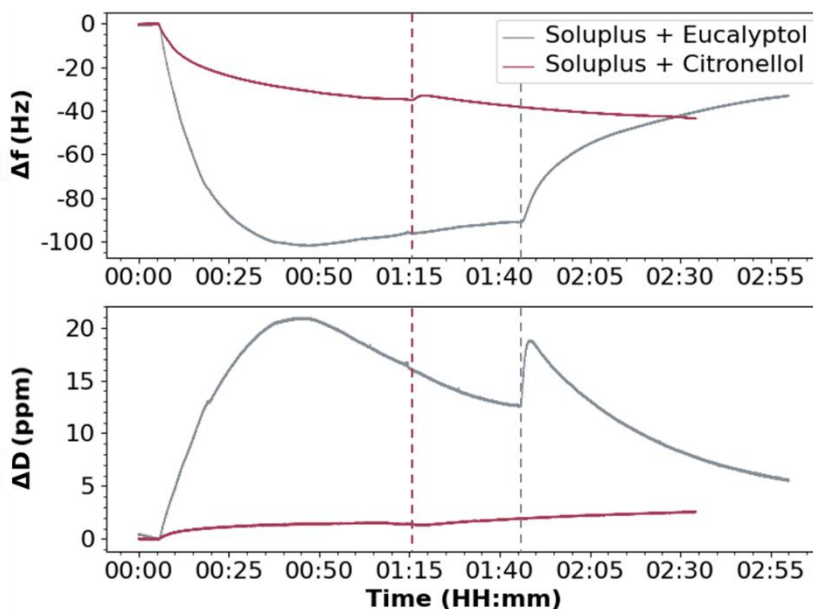
Figure II.23: Frequency (top) and dissipation (bottom) changes of the 3ʳᵈ overtone of Soluplus® + Eucalyptol (gray) and Soluplus® + Citronellol (red) micelles deposited on a layer of Soluplus® micelles. Dashed lines indicate the addition of the Soluplus® + perfume micelle solutions.

In the case of Eucalyptol, the observed result confirmed the interactions between the perfume and the polymer micelles, showing that some Soluplus® was removed from the sensor surface to solubilize Eucalyptol. At the same time, this indicated that Eucalyptol was not fully solubilized in the polymer micelles and was also present in the surrounding water. This desorption was first associated with a large increase in dissipation, suggesting that the polymer layer swelled in the presence of Soluplus® +

Eucalyptol micelles, followed by a decrease in dissipation as materials continued to desorb from the sensor. Here, the polymer-perfume interactions seemed to be stronger than the polymer-polymer interactions that kept Soluplus® on the surface. On the other hand, Soluplus® + Citronellol sample exhibited a decrease in frequency shift (i.e., adsorption) on the layer of micelles, which could either suggest that:

1) The interactions between this perfume and Soluplus® were unfavorable, hence the perfume was not contained in Soluplus® micelles, which induced further adsorption of neat Soluplus® micelles on the initial layer;

2) The perfume was in fact contained in the polymer micelles and the polymer-polymer interactions induced the adsorption of Soluplus® + Citronellol micelles on the polymer layer, resulting in the further decrease in frequency shift as more materials were added to the surface.

The first hypothesis, namely Citronellol was not included in the polymer micelles, should be associated with a first decrease in dissipation (before the increase due to the adsorption of materials). In fact, the presence of Citronellol in the aqueous environment should destabilize Soluplus® in this new solvent mixture and force it to recoil toward the sensor to minimize their interactions, resulting in a more rigid layer. Additionally, the plot of the dissipation vs. frequency changes (data not shown) indicated that during the flowing of the Soluplus® + Citronellol solution, the adsorption of materials was more viscoelastic than the adsorption of the pure Soluplus® micelles. This indicated that the adsorbed layer was more swollen or hydrated, discarding here again the first hypothesis.

This experiment hence confirmed the perfume inclusion in the polymeric micelles.

The results presented in this section showed that Soluplus® was in fact able to encapsulate the investigated perfumes of interest, in the form of microcapsules as well as polymeric micelles. We were able to confirm perfume inclusion for each system, which was a promising starting point for the encapsulation of small hydrophobic molecules in amphiphilic polymers such as Soluplus®. Similarly, the successful entrapment of

perfumes in this kind of materials opened up the possibility of using them as carriers for targeted delivery on surfaces. From these first results, we hypothesized that the deposition of perfumes on surfaces could be correlated to their ability to be encapsulated, hence expecting that MNA would adsorb the most on surfaces among the three perfumes.

This Chapter presented the preliminary study focused on polymer-perfume interactions for the encapsulation of hydrophobic molecules in aqueous formulations. It is clear that one needs to use a combination of several techniques in order to acquire a better understanding of these complex polymer-perfume interactions and there is still a need to develop protocols to reliably quantify them. Studying polymer-perfume interactions in binary systems allowed us to determine how the different polymer components are interacting with the various perfumes, which could be relevant in the following steps of the project such as perfume deposition or perfume release. The investigation of the absorption of perfume vapors in Soluplus® films also seemed to provide a good model for the screening of relevant perfumes and/or polymers to explore.

The created microcapsules presented great differences in their properties such as morphology, capsule size, etc. It is likely that the encapsulation of molecules is explained by a combination of several properties and the preliminary study pointed out the hydrophobicity of the fragrances as one of the major factors.

III. INVESTIGATION OF PARTICLE-SURFACE INTERACTIONS

The development of a new encapsulation technology for the delivery of perfumes on surfaces first requires the fundamental understanding of particle-surface interactions, as well as forces that play a role in the adhesion of materials on substrates. In this Chapter, we continued our study using the three perfume molecules that were investigated in the previous Chapter, namely Eucalyptol, Citronellol and Methyl Nonyl Acetaldehyde. The aim was to develop models for the deposition of hydrophobic molecules on surfaces, promoted by microcapsules and/or polymeric micelles. In this framework, we first prepared substrates to be used in each section of this Chapter, in order to use model surfaces with various properties, exploring surface hydrophobicity/hydrophilicity as well as surface charge, which is described in section III.1. We then studied capsule-surface interactions at the liquid/solid interface before investigating polymeric micelle-surface interactions, using Soluplus® as a perfume carrier, as reported in sections III.2 and III.3, respectively.

III.1. Preparation of model surfaces

In order to understand and describe the deposition mechanisms of capsules and micelles on surfaces, we created flat model surfaces to study the interactions between the different materials and get rid of the mechanical interactions that might occur with real substrates (e.g., filtration, adsorption on a porous surface). We chose to study model hydrophilic, hydrophobic, cationic and anionic surfaces.
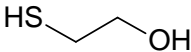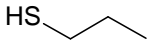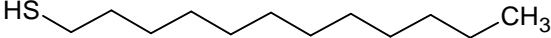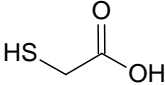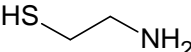
III.1.1. Experimental protocols

Model surfaces were created on gold (Au) substrates by chemisorption of thiols to create self-assembled monolayers (SAMs) with different functional end groups, following a protocol from literature.[146,147] Prior to the functionalization, gold substrates were cut in squares of about 1.5 x 1.5 cm². They were then placed in a hydrogen

peroxide:ethanol:acetone solution (1:1:1), cleaned using an ultrasonic bath for 30 min at 25°C, rinsed with Milli-Q water and dried with a N_2 stream.

Table III.1: Description of the created model substrates and the corresponding thiol used for the surface functionalization.

Model	Functional end group	Thiol
Hydrophilic	-OH	(2-mercaptoethanol)
Hydrophobic	-CH$_3$	(1-propanethiol) or (1-dodecanethiol)
Anionic	-COOH	(Thioglycolic acid; pKa$_{(COOH)}$ = 3.83[148])
Cationic	-NH$_2$	(Cysteamine; pKa$_{(NH_2)}$ = 10.75[149])

The functionalization of Au surfaces was performed using the thiols displayed in Table III.1. 5 mM ethanolic solutions of the different thiols were prepared and a gold substrate was placed in each solution. Hydrochloric acid and triethylamine were added to the ethanolic solutions containing thioglycolic acid and cysteamine, respectively, to adjust the pH to about 2 and 10, respectively.[16,146] All substrates were left to react with the thiols for at least 24 hours to allow for the monolayer to be formed. They were then rinsed thoroughly with ethanol (10-15 seconds), placed in an ultrasonic bath in ethanol for 5 minutes (twice), and rinsed with ethanol again (10-15 seconds) before being dried with
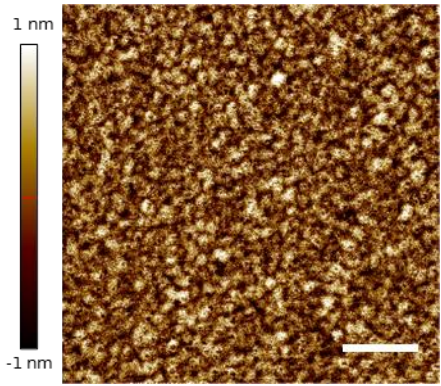
N_2. The substrates were stored in a closed petri dish until characterization by water contact angle and Atomic Force Microscopy.
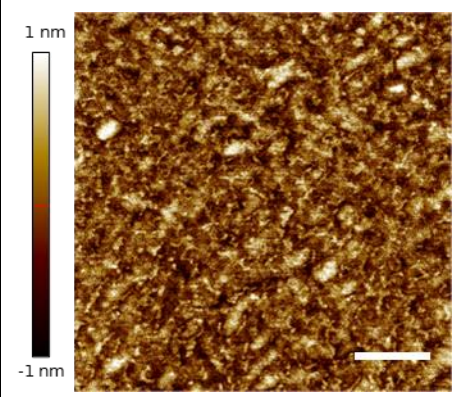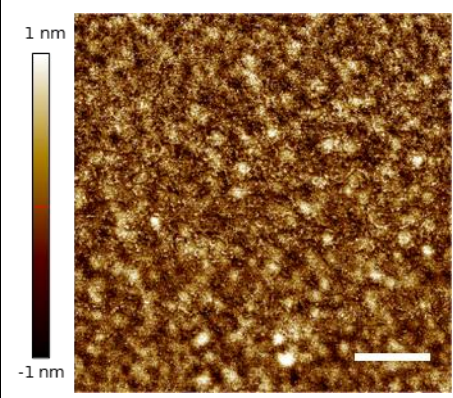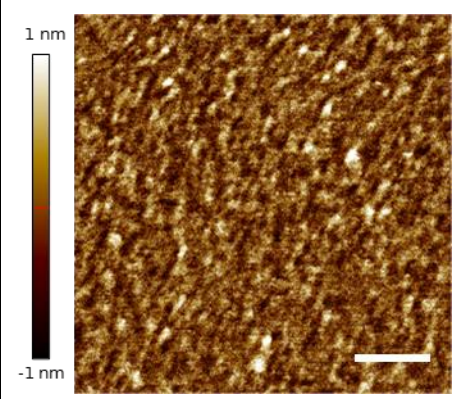
III.1.2. Results

Almost all substrates obtained contact angle measurements that were in accordance with the literature (see Table III.2),[9,15,150] which confirmed the correct formation of SAMs on Au surfaces.

The exception was made for the SAM-CH_3 prepared using 1-propanethiol (C_3), where the contact angle was found to be of 75.7 ± 3.9 ° instead of 100-110 °.[9,15] In fact, a surface is considered hydrophobic if its water contact angle is > 90 °,[140] which was not the case for our model hydrophobic surface. As the obtained value was close to that of bare gold, it is likely that the 1-propanethiol did not bind successfully to the surface. Another attempt at creating a hydrophobic surface was performed using this time a thiol with a longer alkyl chain, namely dodecanethiol (C_{12}). The resulting contact angle was 92.1 ± 0.5 °, which fulfilled the hydrophobic criteria.
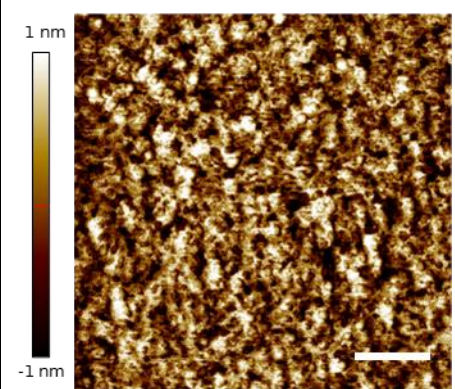
Table III.2: AFM topographic images, average roughness and contact angle measurements of the gold substrate and the created model surfaces. Scale bars are 500 nm.

Surface	Aspect	Roughness	Contact angle
Bare gold		0.4 nm	71.3 ± 3.6 °
Model hydrophobic (propanethiol) (SAM-CH_3/C_3)	Not analyzed	Not measured	75.7 ± 3.9 °

Surface	Aspect	Roughness	Contact angle
Model hydrophobic (dodecanethiol) (SAM-CH$_3$/C$_{12}$)		0.4 nm	92.1 ± 0.5 °
Model hydrophilic (SAM-OH)		0.4 nm	51.0 ± 4.7 °
Model anionic (SAM-COOH)		0.4 nm	57.6 ± 2.0 °

Surface	Aspect	Roughness	Contact angle
Model cationic (SAM-NH$_2$)		0.5 nm	49.8 ± 5.7 °

According to the pKa values of thioglycolic acid and cysteamine (Table III.1), the formed SAM-COOH and SAM-NH$_2$ presented a negative and a positive charge at neutral pH conditions, respectively.[15,151–153] As seen from the obtained results, we successfully created the four model surfaces that could be used to study the particle-surface interactions. This protocol was thus repeated on other gold wafers, as well as QCM-D gold sensors.

III.2. Capsule-surface interactions

In this section, we chose to study the interactions between the soft microcapsules and two model substrates, namely hydrophobic and hydrophilic surfaces. Using the created SAMs, we investigated the adhesion of microcapsules on the two surfaces by Confocal Raman Microscopy to visually determine the quantity of materials deposited on the substrates, and the results are reported in subsection III.2.1.

Critical factors to consider when studying the adhesion between capsules and surface are the surface properties of the systems of interest, such as surface energy, roughness, surface morphology, etc. However, the soft matter capsules created in this project are not surrounded by any solid shell as in the typical hard matter, polymeric microcapsules. This means that the properties of the bulk and the surface of the capsules can be the same, which suggests that the microcapsules might be elastic,

viscoelastic, or even viscous liquids depending on the composition and polymer properties. Thus, they could easily be subjected to deformations when in contact with another capsule or a surface, which can in turn impact their deposition. That is why in subsection III.2.2, we used Atomic Force Microscopy to determine the cohesive forces in the soft microcapsules, in order to understand how to tune their adhesion on surfaces.

III.2.1. Deposition of microcapsules

III.2.1.1. Experimental protocols

The deposition of microcapsules containing the three perfume molecules was investigated on model hydrophobic and hydrophilic surfaces, as created from the protocol described in section III.1. In these experiments, the two flat substrates were exposed to a flow of capsule suspension, using a flow cell of our creation (Figure III.1).
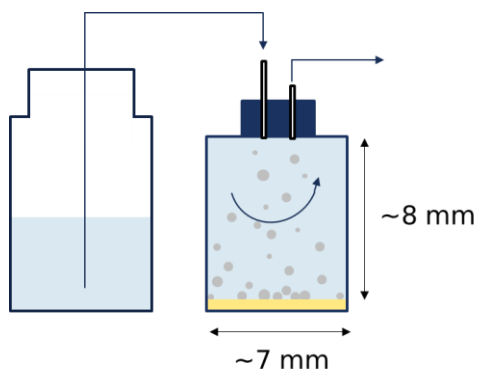

~8 mm

~7 mm

Figure III.1: Scheme of the flow system used for the adsorption of soft perfume microcapsules on model substrates.

Water was first passed in the flow chamber containing one of the studied model substrates (i.e., hydrophobic and hydrophilic or SAM-CH$_3$ and SAM-OH, respectively) for 20 min using a peristaltic pump at a 0.5 mL/min flow rate, to immerse the surface in the medium. The capsule suspensions were then flowed in the cell for an hour at a 100 µL/min flow rate to adsorb the capsules on the solid surface, and then removed from the system. The surfaces were kept in the flow cell under a thin layer of

solution, to prevent capsules from drying. The surfaces were thus characterized in liquid, using Confocal Raman Microscopy.

III.2.1.2. Results and discussion

Because of the density of the perfumes, it was first observed that no adsorption on either surface occurred during the experiment as the microcapsules creamed at the top of the solution, thus not approaching the surface. However, forcing the capsule to come into contact with the surfaces by placing the latter at the top of the solution (i.e., turning the flow cell upside down) led to the adsorption of materials. This indicated that these soft microcapsules need to come in close contact with the surface to be adsorbed, optimally at the air/water interface.

Once the experiments were repeated in the new configuration, we were able to detect materials on the analyzed surfaces. It is worth mentioning that the analysis of the surfaces was not performed with the substrate upside-down, hence the detected materials on the surface did not cream back up and were effectively adsorbed.
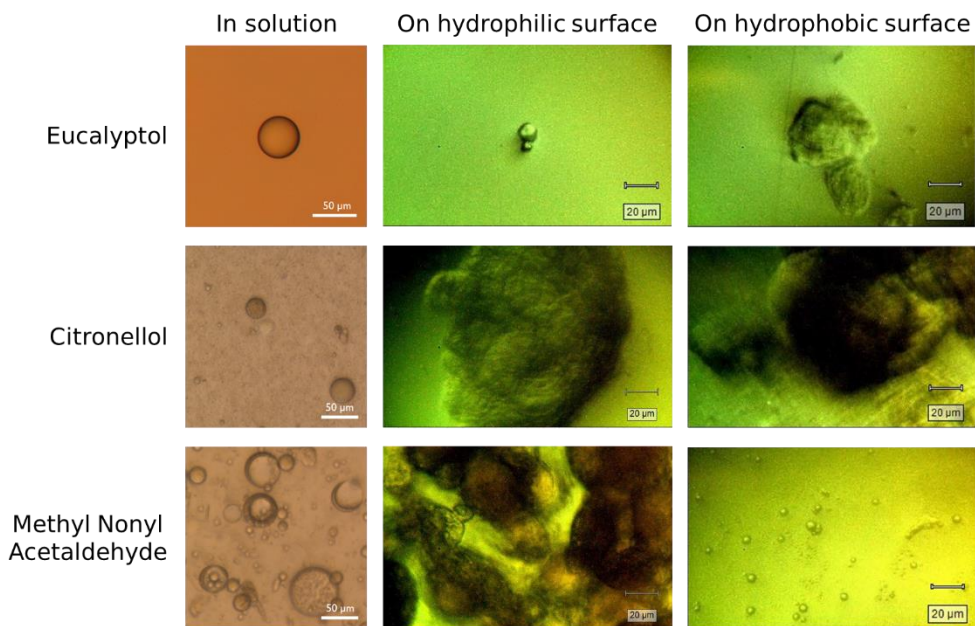

Figure III.2: Morphology of microcapsules of the copolymer Soluplus® containing the perfume molecules Eucalyptol (top row), Citronellol (middle row) and Methyl nonyl acetaldehyde (bottom row). Light microscopy images of capsules in solution (left) and CRM images of capsules adsorbed on the model hydrophilic (middle) and hydrophobic (right) surfaces.

As seen on Figure III.2, the microcapsules presented extremely different morphologies, depending on perfume and/or surface properties. More specifically, we observed that all three types of capsules changed their structure upon adsorption on the substrates, but only CTN-capsules exhibited the same morphology on both surfaces (which was also different from that in solution). ECL exhibited smaller and less capsules on the hydrophilic surface, while MNA showed the opposite.

As ECL did not form many microcapsules with Soluplus® in solution, we were not expecting much adsorption either and the visual examination of the surfaces in the microscope confirmed the poor presence of microcapsules. However, this characterization method could not detect perfume that might have been deposited on the surface through polymeric micelles of Soluplus®, because of the spatial resolution of the microscope but also that of the Raman spectrometer, which was not sensitive enough for the experimental concentration range of these materials.

On the other hand, CTN-capsules adsorbed on the substrates were found to be much bigger than in solution. They exhibited a non-spherical shape with a rough surface that suggested the aggregation of particles. Since capsules were not observed over the whole surface, it could be assumed that for both hydrophilic and hydrophobic surfaces, the particle-particle interactions were stronger than particle-surface interactions, as capsules preferred aggregating to each other rather than spread over the surface. However, this aggregation phenomenon did not take place in the bulk solution, indicating that the introduction of the surface in the system changed the stability of the CTN-capsules.

Finally, in the case of MNA-capsules, the hydrophilic surface was covered with big, aggregated capsules whereas the hydrophobic surface only exhibited small, spherical capsules. This difference in size could be explained by the surface energy of the substrates and their interactions with the sample. In fact, the adsorption of large microcapsules indicated favorable particle-surface interactions, allowing for a large contact area between the two systems. This implied that the surface of the capsules would be highly hydrophilic, likely with PEG chains facing the outside of the particles. This would also explain the low adsorption on the

hydrophobic substrate, as the interaction with the particle's surface would be unfavorable.

It was clear that the adsorption of MNA-capsules increased with the surface energy of the substrate, however the conclusions for the other two samples remained uncertain as only a few particles were observed on the surface and might not be representative of the whole sample. Since these experiments included only three different perfume molecules, it was difficult to draw any further conclusions on the capsule-surface interactions and the possible adsorption mechanisms. Moreover, the characterization methods available for these experiments did not allow for a quantitative determination of the adsorbed materials, which is why a proper model for the deposition of microcapsules on the different surfaces could not be established. However, it was concluded that good encapsulation properties might facilitate the deposition of capsules on surfaces as more microcapsules were available to interact with surfaces.

III.2.2. Adhesive force measurements

When studying adsorption, one would typically measure the adhesion properties between capsule and surface.[81,154] However, this type of experiment requires the isolation and immobilization of a single capsule on a surface, which was not obtainable with our studied systems. Instead, we attempted to determine the cohesive energy of the different capsules, hypothesizing that their mechanical properties could impact their deposition on surfaces.

III.2.2.1. Experimental protocols

Soluplus® soft microcapsules containing either ECL, CTN or MNA were first deposited on surfaces by dipping glass slides directly in the capsule solutions. The substrates were left to dry in air for about one hour before the measurements. As stated in section II.2.1, Soluplus® did not form microcapsules on its own without perfume, which is why Soluplus® microcapsules could not be measured as a control case.

A topographic image of the sample was first obtained by AFM, then force-distance curves of the dry capsules were acquired in spectroscopy mode. To do so, the deflection of the cantilever was monitored as the latter was

approaching the sample surface or retracting using a piezoelectric actuator in z-direction. The measured deflection was in turn translated as a force exerted on the cantilever, following Hooke's law:[155]

III.1 $$F = -k\delta_c$$

where F is the applied force, k is the spring constant of the cantilever (in our case 42 N/m), and δ_c is the deflection. The absence of deflection corresponds to a flat cantilever when it is not subjected to any attractive nor repulsive force. When the cantilever bends away from the sample, the deflection is positive, and the exerted force is repulsive. On the contrary, when the cantilever bends towards the sample, the deflection is negative, and the exerted force is attractive.

Along with the deflection of the cantilever, the piezo displacement (i.e., the distance between the sample surface and the resting position of the cantilever) was also acquired. The tip-sample distance D was then calculated as follows:

III.2 $$D = Z - \delta_c$$

where Z is the displacement of the piezoelectric scanner. Before the measurement, the cantilever is approached to the sample surface and the position is arbitrarily set as the Z = 0 position. The piezo is raised to a minimum position; the data acquisition starts as the cantilever is lowered to the maximum position (approach) and then stops once the cantilever is raised to the minimum position again (end of retraction).

III.2.2.1. Results and discussion

Typical force-distance curves can be seen on Figure III.3A, and the adhesion energy is determined as the area between the retraction curve and the baseline. In our case, this adhesive energy truly corresponded to the cohesion energy in the polymer-perfume capsule. Indeed, to acquire the topographic image of the sample surface, the sharp tip was set to scan a 100 x 100 μm^2 area of the dry capsule, eventually amassing material along the way, which resulted in a tip covered with the analyzed sample. Therefore, when force-distance curves were produced afterwards, the evaluation of the adhesive energy between the sample and the sample-

covered tip resulted in the measurement of the cohesive energy in the sample. Values of the obtained adhesive/cohesive energy of different zones in the sample can be found in Table III.3, along with the topographic images of the samples' surface.
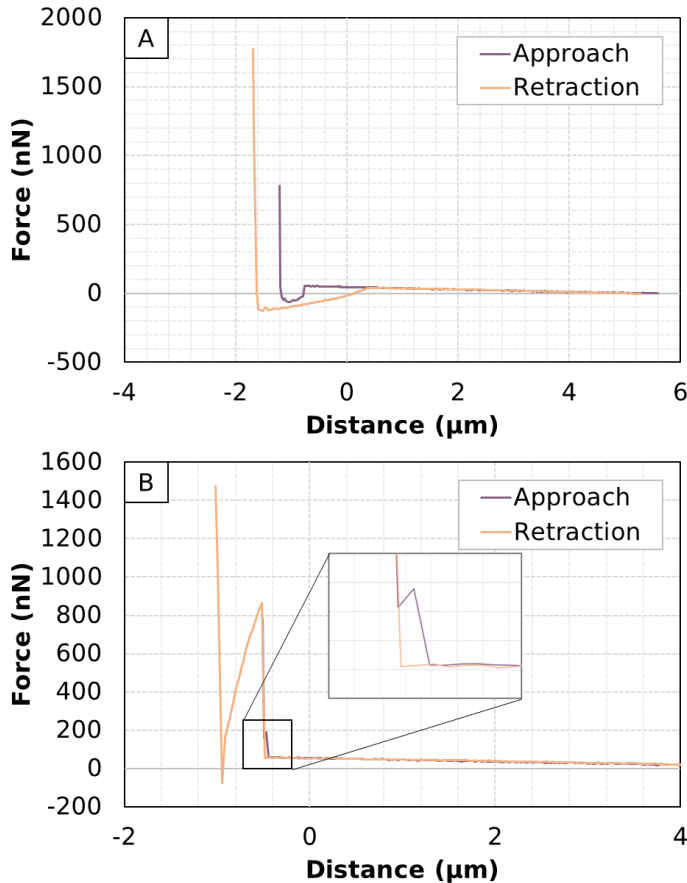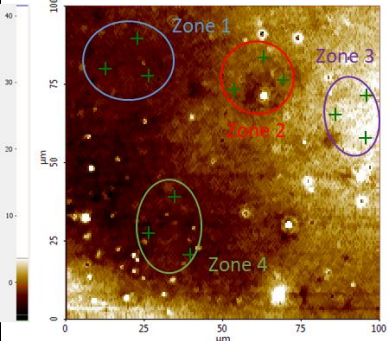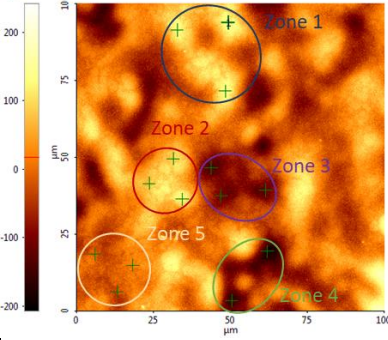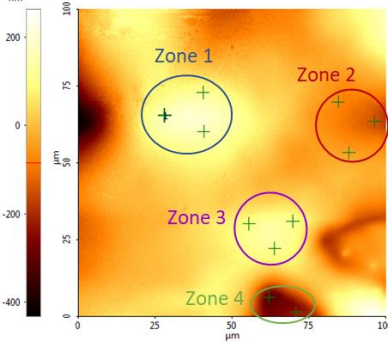

Figure III.3: Examples of force-distance curves obtained on samples containing A) Soluplus® + MNA dry capsules and B) Soluplus® + CTN or ECL dry capsules. Curves display the force exerted on the cantilever as the tip is approaching the surface (purple) and retracting from the surface (orange).

Table III.3: Morphology of dry capsules containing ECL, CTN or MNA and the corresponding rupture force, layer thickness and adhesive energy measured from the force-distance curves obtained in the featured zones.

Perfume	Surface topography	Zone	Measured value	
ECL			Rupture force (nN)	Thickness (nm)
		1	206.7 ± 12.4	24.0 ± 0.2
		2	206.5 ± 10.5	23.4 ± 0.2
		3	182.8 ± 11.0	23.9 ± 0.1
		4	198.2 ± 11.9	23.8 ± 0.3
CTN			Rupture force (nN)	Thickness (nm)
		1	201.4 ± 20.0	24.0 ± 0.6
		2	209.5 ± 23.0	23.7 ± 0.9
		3	183.0 ± 26.0	23.1 ± 0.04
		4	224.7 ± 24.7	22.6 ± 0.9
		5	178.9 ± 19.7	22.0 ± 0.9
MNA			Adhesive energy (J)	
		1	3.07E-13 ± 1.1E-14	
		2	2.03E-13 ± 1.2E-14	
		3	2.23E-13 ± 1.2E-14	
		4	4.16E-14 ± 1.0E-14	

In air, when the cantilever approaches the sample, the tip would normally be pulled down to the sample surface due to Van der Waals and capillary attractive forces, before being subjected to repulsive contact forces as the distance between the cantilever and the sample decreases further (Figure III.3A). When the piezo then retracts from the sample, the force exerted on the cantilever would decrease as the latter recovers its resting position and would then become negative due to adhesion keeping the tip in contact with the sample as the piezo continues to go up. Eventually, when the attractive forces can no longer overcome the spring constant of the cantilever, the tip would break free from the sample and the cantilever would find its flat position back.[155,156]

In contrast to MNA-capsules, samples containing ECL and CTN perfumes presented unusual force-distance curves where no adhesion energy could be measured, and an example of their obtained profiles can be found on Figure III.3B. The approach curve exhibited repulsive forces induced by the contact between the tip and the sample, followed by a quick decrease in the measured force, corresponding to a breakthrough in the sample surface, before the tip encountered a stiffer surface underneath. Similarly, when the tip retracted from the sample, the force decreased to 0 nN before increasing and exhibiting repulsive forces as the piezo continued to go up. At a certain point, the tip suddenly recovered its resting position (i.e., flat cantilever). This phenomenon has been observed for lipid bilayers,[156,157] where the tip first comes into contact with the bilayer before compressing and breaking through it as the cantilever further approaches the sample. Then, as the tip retracts from the sample, the bilayer reforms and pushes the tip out of the sample, thus only exhibiting repulsive forces in the force-distance curve.

We then measured the thickness of this surface layer and the force needed to break through it (see Table III.3), and we observed very reproducible and homogeneous values across the different zones, for both ECL and CTN-containing samples. More specifically, after one hour of drying, the force required to break through the layer was for both types of capsules about 200 nN, with a thickness of 25 nm. As the capsule films dried (and the perfumes evaporated) overnight, the thickness of the layer

increased to about 65 nm, while the force required to break through the film decreased to about 120 nN (Figure III.4).
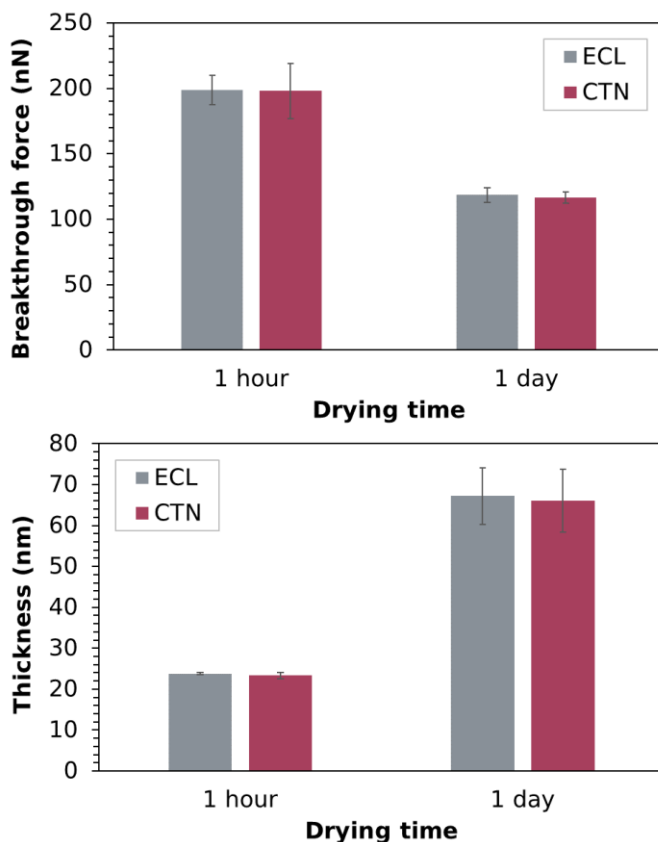

Figure III.4: Graphs presenting properties measured on the sample surface of the dry caspules containing ECL (gray) and CTN (red) perfumes after 1 hour and 1 day of drying: force required to break through the layers (top) and thickness (bottom) of the latter.

These results suggested the rearrangement of the layer as the perfumes evaporated, which was supported by the observations made in section II.1.2, where the evaporation of ECL and CTN perfumes from the Soluplus® thin film induced the rearrangement of the polymer chains with the appearance of the small "islands" (Figure II.16). Additionally, the decrease in the breakthrough force after desorption of the perfumes indicated a looser packing of the polymer chains in the layer, which was also supported by results from section II.1.1 in which we observed that the presence of perfumes induced the ordering and crystallization of the polymer chains (Figure II.3). It was thus assumed that when perfumes

evaporated, Soluplus® chains lost their packed order and returned to a glassy state. Therefore, it seemed like the drying process induced the formation of an elastic polymer layer at the top of the samples surface, with a swelling of the polymer upon further evaporation as it tried to maintain its interactions with the perfumes, thus "following" them upwards.

This phenomenon was not observed for the sample containing MNA as no breakthrough took place during the obtention of the force-distance curves, even after a day of drying. However, according to the results from Chapter II showing the increased polymer-MNA interactions and the lower vapor pressure of this molecule (see Appendix II), we could assume that the content of MNA in the capsules was still high enough after a day to prevent the sample surface from breaking.

The results presented in this section showed that the prediction of capsules interactions with surfaces is rather challenging, as the introduction of a new component in the capsule system changes the initial equilibrium between polymer, perfume and water. We then attempted to measure the cohesive energy of the different capsules by AFM. Unfortunately, we were unable to determine those values for two of the three tested samples, which was ascribed to the formation of an elastic polymer layer upon perfume evaporation, and this prevented us from finding a possible correlation between capsule mechanical properties and adsorption on a surface. It would thus be interesting to develop a method to perform the same measurements in water, which would allow one to follow the evolution of the capsule properties when interacting with different surfaces. However, the experiments in water would require the modification of the support to promote capsules' adhesion and the capsules would probably be too soft to allow for an accurate measurement.

III.3. Micelle-surface interactions

We showed in Chapter II that the soft microcapsules developed in this project can be destabilized by water dilution and produce polymeric

micelles of Soluplus® that entrap the fragrant molecules. That is why it was necessary to understand the capacity of this type of perfume carrier to deliver its payload to the target substrates. Therefore, we investigated the interactions between the polymeric micelles containing the fragrant compounds and the four model surfaces developed in section III.1, namely the hydrophilic, hydrophobic, cationic and anionic surfaces.

We used Quartz Crystal Microbalance with Dissipation monitoring to follow the adsorption and desorption of materials on surfaces. However, this method is not selective, and it is not possible to determine which material is interacting with the sensor surface in multiple components systems. As seen in section II.2.2, Eucalyptol and Citronellol are water-soluble at the experimental concentration, but both were contained in the polymeric micelles even though we did not observe any increase in particle size between the neat Soluplus® micelles and that in presence of these molecules. Nevertheless, it could be assumed that they were only partially incorporated in the nanocarriers, which is why it was first necessary to assess the possible adsorption of these perfumes in water on the model substrates to make sure that they did not present any initial interactions with the surfaces, before investigating the interactions between micelles and surfaces.

We also complemented these results with topographic images of the surfaces after adsorption, using Atomic Force Microscopy. This allowed us to visualize the morphology of the adsorbed particles in order to understand the deposition mechanisms.

III.3.1. Experimental protocols

Interactions between perfumes and surfaces

Aqueous solutions of ECL and CTN were first prepared at a 100 mg/L concentration and were then diluted to obtain a 25 mg/L concentration for both perfumes. The interactions between the different perfumes and surfaces were then studied using the QCM-D chamber by first flowing Milli-Q water as a baseline. Then, the aqueous perfume solution (containing either ECL or CTN) was passed over the functionalized sensor for an hour. Finally, the sensor was rinsed with Milli-Q water for the same

duration. Flow rates were kept constant at 50 µL/min and the temperature in the chamber was regulated to 25 °C.

Adsorption on model surfaces promoted by polymeric micelles

Soluplus® micelles containing ECL, CTN or MNA were prepared following the protocol described in section II.2.2. The micelle solutions were then passed in the QCM-D cell to investigate their interactions with all model surfaces (i.e., SAM-CH$_3$, SAM-OH, SAM-NH$_2$ and SAM-COOH). To do so, milli-Q water was first passed through the chamber for at least 20 min using a flow rate of 0.5 mL/min, to immerse the surfaces in the medium and get a baseline for the frequency and dissipation values. The sample solution (namely, Soluplus® or Soluplus® + perfume solution in water) was then flowed in the cell for an hour with a flow rate of 50 µL/min to adsorb the micelles on the sensor surface. Finally, milli-Q water was flowed again in the chamber to simulate a rinse and remove the non-adsorbed materials for one hour at a 100 µL/min flow rate.

The frequency and dissipation changes were monitored throughout the whole experiment at different overtone harmonics (from 3rd to 13th).

The deposition experiments were then repeated in our home-built flow cell (Figure III.1) to characterize the deposited micelles by AFM. After the adsorption of particles, the substrates were retrieved from the cell and placed in the oven for at least 15 min at 70 °C to dry the sample. It has been reported that the morphology of the deposited micelles would not change in the drying process,[158] which is why AFM images were obtained in air.

III.3.2. Results and discussion

In QCM-D, we are monitoring in real time the changes in resonance frequency of the quartz crystal sensor (Δf), which are related to variations in thickness or mass of the crystal, i.e., adsorption and desorption events taking place at the sensor surface. Changes in energy dissipation of the crystal (ΔD) are also recorded and characterize the viscoelasticity of the adsorbed layer. Similarly to Δf (see equation II.1), the dissipation shift is defined as ΔD = D – D$_0$, where D$_0$ corresponds to the energy dissipation of

the crystal sensor in solution prior to the start of the experiment, and D is the dissipation at a given time during the experiment, expressed as:

III.3
$$D = \frac{E_{dis}}{2\pi E_{st}}$$

where E_{dis} and E_{st} describe the energy dissipated per oscillation and the total energy stored in the system, respectively.

Typical QCM-D curves obtained from the adsorption/desorption of micelles on a sensor surface can be seen on Figure III.5, presenting the frequency and dissipation shifts measured at different overtone harmonics.
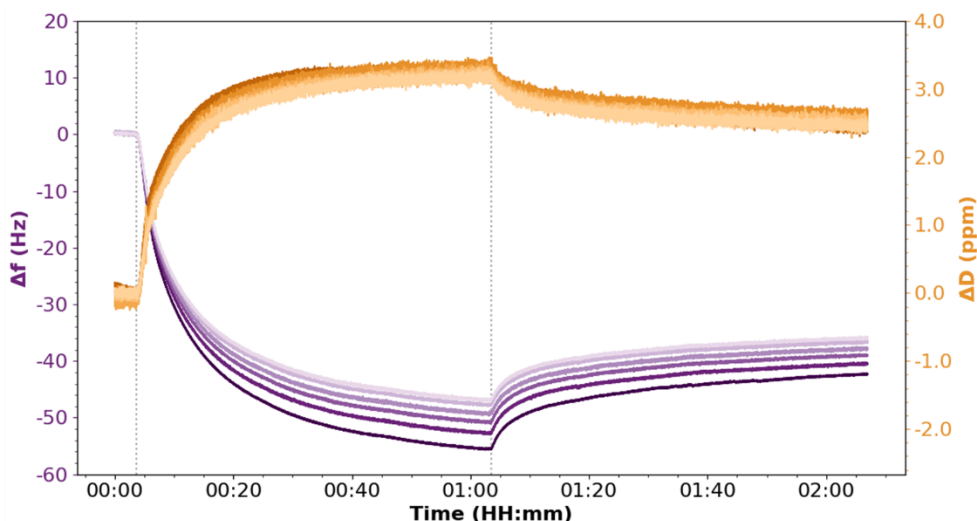

Figure III.5: Frequency (purple) and dissipation (orange) shifts induced by the adsorption/desorption of Soluplus® micelles containing Citronellol on the model cationic surface. Overtone harmonics from 3rd (darker shade) to 13th (lighter shade) are depicted. Vertical dotted lines represent the changes of solution passed through the chamber: the first line (at 5 min) marks the beginning of the adsorption; the second line (at 1h05) marks the beginning of the desorption.

For a thin, rigid and homogeneous adlayer, the resonance frequency shifts are proportional to the areal mass of the adsorbed layer Δm, following the Sauerbrey equation (II.1). In this case, the changes in dissipation are negligible and the changes in resonance frequency are independent of the overtone number n. The thickness h_{eff} can then be determined using the following equation:

III.4
$$h_{eff} = -\frac{\Delta m}{\rho_{eff}}$$

where ρ_{eff} is the effective density of the adsorbed layer.

However, when the dissipation is important and the frequency shifts are overtone dependent, the QCM-D response is often translated into viscoelastic properties of the adsorbed layer, through the model developed by Voinova et al.[159] that is based on the Voigt viscoelastic elements, where a spring (elastic response) is connected in parallel with a dashpot (viscous response).
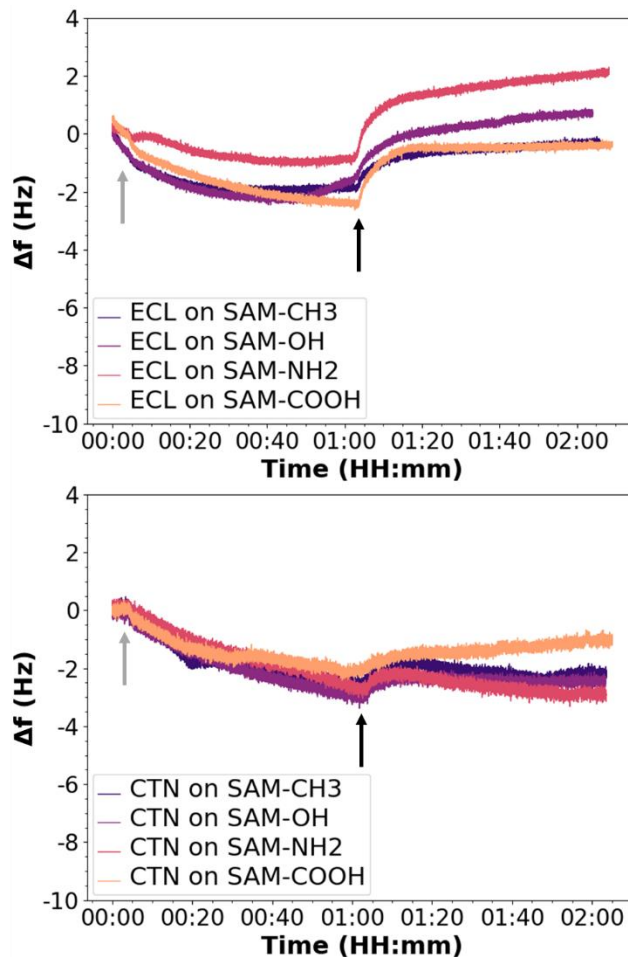
Perfume-surface interactions

Figure III.6: Frequency changes (3rd overtone) induced by the adsorption and desorption of Eucalyptol (top) and Citronellol (bottom) on the different surfaces. Arrows indicate the different steps of the experiments: introduction of the tested perfume solution following the water baseline (gray), then beginning of water rinse (black).

As seen from the small frequency shifts (Figure III.6), the Eucalyptol and Citronellol have little interactions with the four surfaces. The dissipation shifts of all samples was negligible (<1 ppm, data not shown) and the formed layers were thus considered rigid. The mass and thickness of the adsorbed layer were calculated using the Sauerbrey equation (II.1). The obtained layer thickness lied below 0.5 nm in all samples, confirming that the interactions were minimal between the perfumes dissolved in water and the different surfaces.

Adsorption of micelles monitored by QCM-D
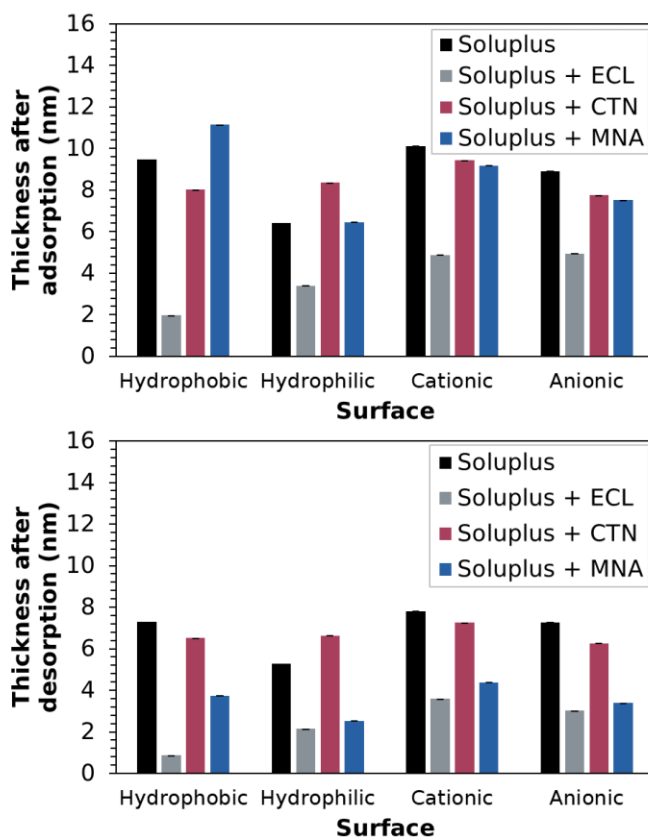
Figure III.7: Layer thickness calculated suing the Sauerbrey equation, obtained after the adsorption (top) and desorption (bottom) of neat Soluplus® micelles (black) and micelles containing the perfumes Eucalyptol (gray), Citronellol (red) or MNA (blue) on the different model hydrophobic, hydrophilic, cationic and anionic surfaces.

Reviakine et al.[160] suggested that the Sauerbrey equation can be used when $|\Delta D_n/(\Delta f_n/n)| \ll 4 \times 10^{-7}$ Hz^{-1}, which was the case for our results.

We thus applied equations (II.1) and (III.4) to determine the thickness of the adlayers after adsorption and desorption of materials. The results were grouped by surfaces and showed a correlation between thickness of the adsorbed layer (i.e., quantity of adsorbed materials) and surface properties (Figure III.7). We observed that the systems containing fragrances behaved differently on the model hydrophobic surface compared to the hydrophilic surfaces (SAM-OH, SAM-NH$_2$ and SAM-COOH). We could thus consider that the adsorption of materials was governed by the hydrophobicity / hydrophilicity of the surface.
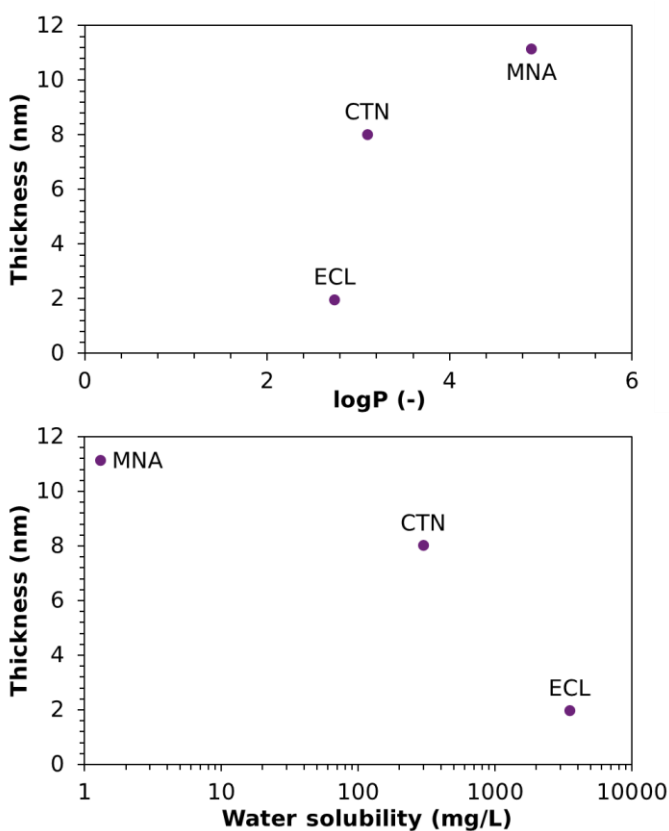
Figure III.8: Thickness of the layer deposited on the quartz crystal caused by the adsorption of polymeric micelles containing fragrances on the model hydrophobic surface, plotted against the logP (top) and water solubility (bottom) of the studied perfumes.

More specifically, on the hydrophobic surface, the deposition of polymeric micelles containing the fragrant molecules increased with the hydrophobicity of the perfume molecule, suggesting that the adsorption was governed by hydrophobic interactions between the surface and the

polymer-perfume systems. In fact, this correlation was confirmed when plotting the thickness of the adsorbed layer against the water solubility and logP of the perfumes (Figure III.8).

On the other hand, the adsorption of polymeric micelles on the three hydrophilic surfaces followed a different trend. Micelles containing ECL presented the lowest adsorption on surfaces, while micelles containing CTN presented the highest adsorption, which could be explained by none of the perfume properties that were investigated. This suggested that several properties should be considered at the same time to explain the differences in deposition between the perfumes, including functional groups or structure of the perfumes. For instance, the increased deposition of micelles containing Citronellol could be justified by the presence of a hydroxyl group on this molecule, which could form hydrogen bonds with the hydrophilic surface as well as ion-dipole interactions with the cationic and anionic surfaces. On the other hand, Eucalyptol, being the least hydrophobic perfume, is likely more stable in the aqueous solution, which decreased its adsorption on surfaces.

When considering the adsorption of neat Soluplus® micelles, we generally observed a higher deposition than that in presence of perfumes although more materials were present in the system. This showed that this amphiphilic polymer maintained its solubilizing role rather than exclusively delivering materials to target surfaces.

We also noticed that the adsorption of the four kinds of micelles was increased on the cationic surface, suggesting that polymer-substrate interactions are dominant in this case. In fact, it has been reported that Soluplus® micelles present a slight negative charge with a zeta potential value of -0.58 ± 0.53 mV (12 wt% Soluplus® solution at pH~6.8).[161] It was thus understandable that these polymeric micelles would present an increased interaction with the positively charged surface due to electrostatic interactions.

Sensors were also rinsed with water for an hour, during which frequency shifts increased as materials desorbed from the surfaces. We observed that none of the studied system reached the baseline of 0 Hz by the end of the experiment, indicating that materials were irreversibly adsorbed

on the surfaces. The thickness of the resulting adlayer can be found on Figure III.7. These results allowed for the calculation of the retention capacity (RC), defined as:

III.5 $\qquad \% \text{ RC } = \frac{Thickness\ after\ desorption}{Thickness\ after\ adsorption} \times 100$

The retention of micelles on surfaces loaded with fragrances followed the order of CTN > ECL > MNA (Figure III.9), regardless of the surface properties. Soluplus® and Soluplus®-CTN micelles had similar retention capacities which were relatively important and constant across all surfaces (around 80%). This indicated that the desorption of these micelles did not depend on surface-micelles interactions, but rather on micelle-micelle interactions, which were strong enough to keep the materials on the different sensors. These strong particle-particle interactions were also observed in section III.2.1 with the aggregation of microcapsules containing CTN upon adsorption on surfaces (Figure III.2). On the contrary, the retention of micelles loaded with ECL or MNA showed differences between the various surfaces, highlighting the influence of micelle-surface interactions in the retention of materials. The most hydrophobic perfume, namely MNA, was retained the least (RC < 50 %) on all surfaces as the amphiphilic polymer resolubilized it into the aqueous environment. This showed that the technology would not present the same efficiency for every perfume on the target substrates when used in rinse-off products such as detergents.
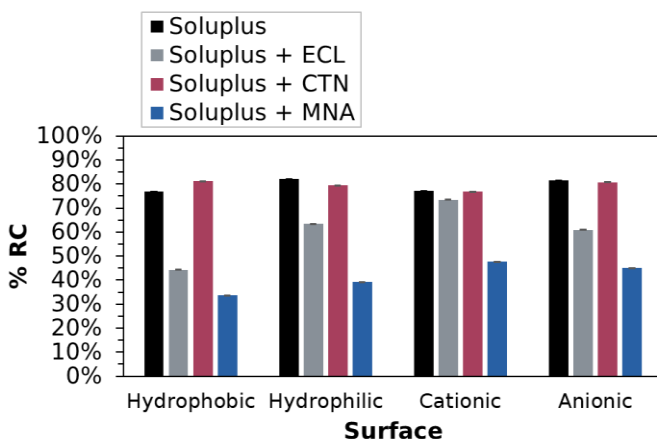

Figure III.9: Retention capacity of Soluplus® micelles.

Deposition mechanisms

The AFM images of micelles adsorbed on surfaces gave complementary information on their deposition mechanisms (Figure III.10). Small spherical objects were observed on the three hydrophilic substrates after the adsorption of the polymeric micelles containing all three perfume molecules, suggesting that the micelles had deposited as discrete particles. This result was easily explained by the arrangement of the amphiphilic polymer in the micelles: in order to diminish the unfavorable interactions between water and the hydrophobic moieties, the polymeric chains directed their PVAc-PVCL parts inward while the PEG backbone could interact with water and stay on the surface of the micelle. The interactions between PEG and the hydrophilic surfaces were thus favorable, which is why micelles were not disrupted as they adsorbed on these substrates.
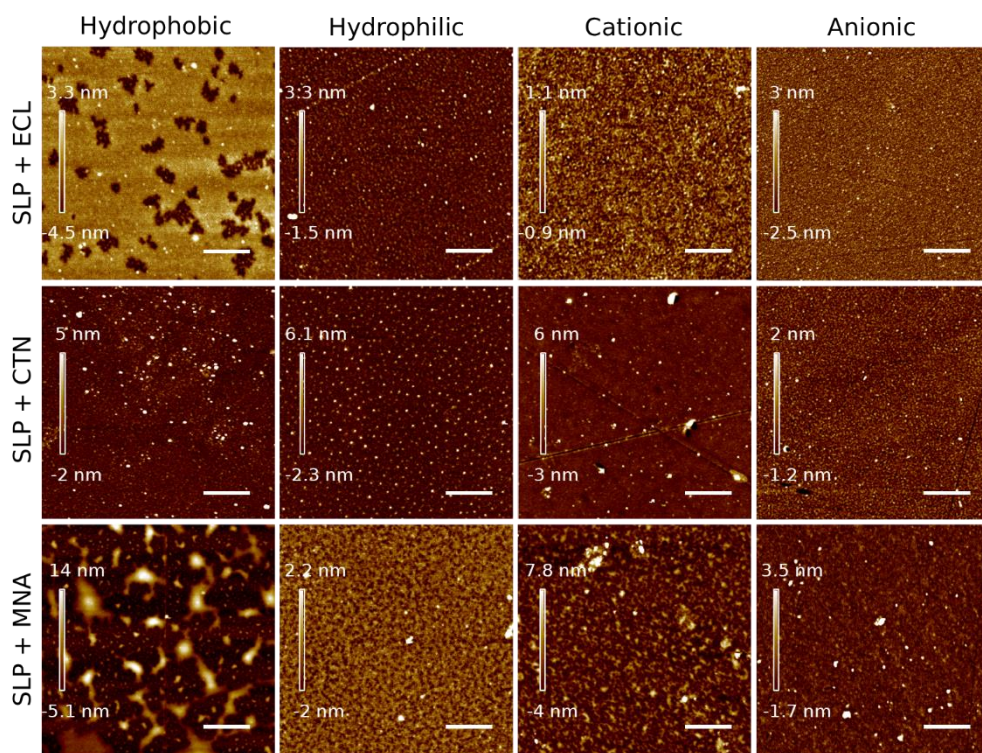

Figure III.10: AFM topographic images of model hydrophobic (left column), hydrophilic (middle-left column), cationic (middle-right column) and anionic (right column) surfaces after adsorption of Soluplus® micelles containing Eucalyptol (1st row), Citronellol (2nd row) or MNA (3rd row). Scale bars are 2 µm.

On the other hand, the hydrophobic surface showed different structures depending on the perfume molecule. The substrates that had been exposed to micelles containing ECL and MNA presented morphologies corresponding to homogeneous films, while the substrate that had been exposed to Soluplus®-CTN micelles presented small particles instead. The former observation could be explained by the fact that a hydrophobic surface would tend to minimize its interactions with the aqueous environment, hence spreading the adsorbed materials over the surface and disrupting the micelles in order to enhance the interactions between the SAM-CH$_3$ and the hydrophobic polymer moieties. In the case of ECL, the AFM image of the adsorbed layer presented microdomains seen as cavities, most likely corresponding to the location of perfume that evaporated during the drying procedure. On the other hand, the sample containing MNA featured a dewetting pattern, suggesting that micelles deposited homogeneously (i.e., without segregation) because of the strong polymer-perfume interactions and a good affinity between the micelle core (containing perfume and hydrophobic parts of Soluplus®) and surface.

In contrast, the polymeric micelles loaded with Citronellol kept their spherical structures upon adsorption, indicating stronger polymer-perfume interactions or weaker perfume-surface interactions.

In conclusion, the results obtained from this study allowed us to develop a model for the deposition of perfumes through polymeric micelles on a hydrophobic surface, in which the adsorption of materials is driven by hydrophobic interactions. However, the deposition of perfumes on hydrophilic surfaces is a complex mix between surface-polymer-perfume-water interactions and a more complicated model still needs to be developed, considering several parameters at the same time. By coupling the QCM-D experiments with AFM analysis, we were able to visualize the adsorbed particles and understand the different deposition mechanisms. Depending on the nature of fragrances and surfaces, micelles adsorb either as discrete, spherical particles or homogeneous, flat films.

In this Chapter, we studied the interactions between flat model surfaces and particles such as capsules and micelles loaded with fragrant molecules. It was clear that the introduction of a new component (i.e., a surface) into the system disrupted the initial polymer-perfume-water equilibrium. Developing models for the delivery of perfumes promoted by polymeric capsules or micelles thus requires a systematic understanding of the interactions between each component of the system, as well as their effect on the other interactions. As a result, only one model could emerge from this study, showing a correlation between the adsorption of perfumes in polymeric micelles and the hydrophobicity of the investigated fragrances and surfaces.

IV. Evaluation of the efficiency in small-scale washing tests

In this Chapter, the efficiency of the technology was assessed in a real-life application at Procter & Gamble. The microcapsules and micelles solutions were used in small-scale washing tests to deliver perfumes on fabrics. Using Gas Chromatography coupled with Mass Spectrometry (GCMS), we were able to quantitatively determine the amount of fragrance deposited on the surfaces.

Section IV.1 first describes practical aspects regarding the GCMS instrument and methods that needed to be set up at Procter & Gamble for the assessment of the deposition efficiency of perfumes on fabrics. We then investigated the deposition of perfumes assisted by Soluplus® microcapsules in water. We were thus able to test the hypothesis formulated in Chapter II, that the deposition of perfumes would increase with the encapsulation of perfumes and the results are reported in section IV.2. Finally in section IV.3, we evaluated the deposition of perfumes promoted by polymeric micelles in a prototype softener formulation and tested the models developed in the previous chapter.

IV.1. Development of protocols to evaluate the deposition of perfumes

Typically, the performance of perfume technologies is evaluated in washing tests where fabrics are washed with the prototype laundry product that contains the tested microcapsules.[162,163] These procedures include the dilution of the formulation, the cleaning of the fabrics with the washing solution and the rinse in clear water. The fabrics are then sampled and directly analyzed via Headspace Gas Chromatography coupled with Mass Spectrometry (HS-GCMS). In this technique, the volatile compounds in the headspace of the vial (i.e., above the fabric), in equilibrium with the sample, are captured by a Solid Phase Microextraction (SPME) fiber and injected into the instrument for quantitative analysis.

Due to the dilution of the microcapsule formulation and the rinse of the fabrics at the end of the washing procedure, the concentration of the perfume blend adsorbed on the substrates is usually quite low. Additionally, since perfume mixtures are composed of several dozens of fragrant ingredients that are present in various amounts, the concentration of each individual molecule detected by the GCMS is eventually measured in micrograms of perfume per gram of fabric. In the experiments presented in section IV.2, the dilution and rinse steps were omitted to prevent capsule destabilization, which resulted in a considerably higher concentration of perfumes on fabrics compared to that from standard washing tests. This could cause the broadening and overlapping of peaks in the obtained chromatograph from the GCMS analysis, leading to inaccurate results as well as the overloading of detectors that could damage the instrument. That is why the samples had to be diluted before the analysis and the appropriate concentration range of detection was thus defined for the tested perfumes, using calibration curves.

The typical protocol to assess the performance of microcapsules described above measures the concentration of perfumes in the headspace of the sample vial, which is influenced by both the deposition of perfumes on fabrics during the washing cycle and their release from the microcapsules during the analysis. As we focused on the delivery of active compounds on surfaces, it was thus necessary to develop a method that would solely assess the adsorption of perfumes in order to evaluate the deposition efficiency of the polymeric soft microcapsules or micelles. To do so, an extraction step was added after the cleaning process to remove the fragrances from the fabrics, and the extract was analyzed in GCMS instead of the substrates.

IV.1.1. Experimental protocols

Determination of the concentration range of individual perfumes

Five perfume molecules were analyzed, including Methyl Anthranilate (MA), Eucalyptol, Delta-Damascone (DD), Undecavertol (UDV) and Methyl Nonyl Acetaldehyde (Appendix II). They were mixed all together

in equal parts (in weight) to form a perfume blend, then the latter was diluted in ethanol to create four solutions of 25, 50, 100 and 500 ppm of blend concentration. Two replicates per concentration were produced and analyzed via headspace-GCMS. At the end of the analysis, the chromatogram of each solution concentration was observed to detect a possible overload of the instrument in the peaks.

Calibration curves

To account for the selectivity and sensitivity of the HS-GCMS, each fragrance was calibrated individually to ensure accuracy and repeatability of the results. To do so, ethanolic solutions of 1000 ppm of fragrance were created and evenly transferred to pieces of cotton fabrics with a pipette. The sprayed amounts of perfume solutions were calculated so that the final GCMS sample vials contained between 0.5 and 50 ppm of perfume. 5 g of ethanol were then added to extract the perfume from the substrate, and the extracts were analyzed by GCMS. Finally, the calibration curves were traced plotting the measured area under the peak as a function of the known deposited perfume concentration.

Extraction of perfumes

The perfumes were extracted from the substrates to assess the efficiency of deposition. To that end, we modified an extraction method that had been developed for other types of microcapsules.[164] In the initial protocol, the washed substrate sample was incorporated in a vial with 12 mL of ethanol. The vial was gently shaken in the oven at 60°C for 1 h, and then placed in an ultrasonic bath for 15 min. This method was modified to be applied to soft microcapsules to improve extraction times and obtain a more efficient procedure. For this purpose, microcapsules were created in water using Soluplus® and the perfume Delta-Damascone. The solution was then used to wash small pieces of polyester fabrics (4 x 4 cm²) in a closed container for 20 min, using a magnetic stirrer to gently mix the solution. Fabrics were then retrieved from the pots, squeezed gently to remove the excess of solution and placed separately in vials for extraction. Table IV.1 describes the different extraction procedures that were compared.

Table IV.1: Tested extraction procedures.

	A	B	C	D (initial extraction method)
Extraction procedure	EtOH + gentle shaking (30 min)	EtOH + ultrasonic bath (15 min)	EtOH + oven (1h, 60°C)	EtOH + gentle shaking in oven (1h, 60°C) + ultrasonic bath (15 min)

Following the extraction, ethanol was used to dilute the extracts in order to avoid saturation of the GC detector.

To ensure repeatability of the results, each procedure was applied to three different pieces of fabric, and the experiment was performed twice.

IV.1.2. Results

Determination of the concentration range of individual perfumes
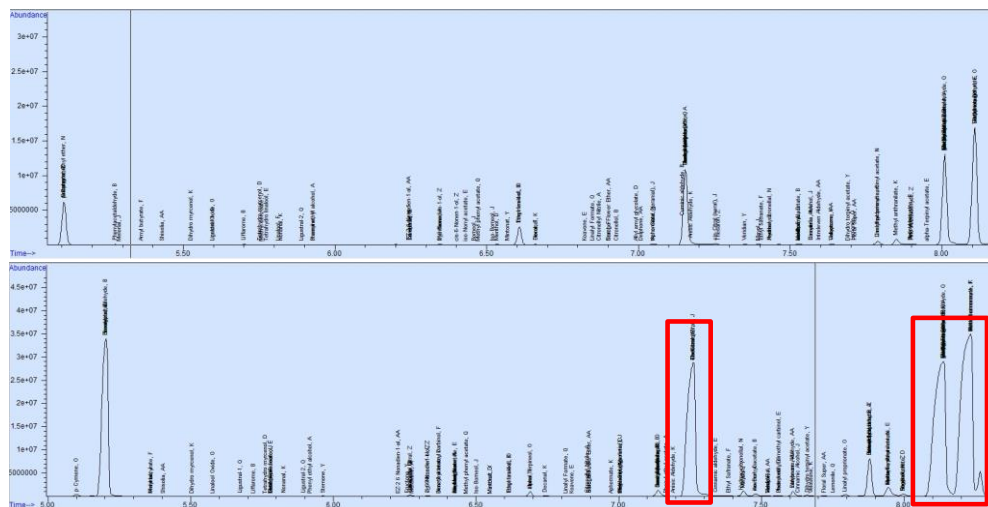

Figure IV.1: Chromatograms of the solutions containing 50 ppm (top) and 500 ppm (bottom) of the created perfume blend. Red rectangles highlight overloaded substances, exhibiting fronting peaks.

The chromatograms reported on Figure IV.1 showed that at 500 ppm of perfumes blend, peaks of Delta-Damascone, MNA and Undecavertol were showing an overloaded peak (fronting of the peak), meaning that the area under the curve used for the determination of the perfume blend concentration could not be trusted. These results showed that samples

needed to be diluted to contain a maximum of 100 ppm of individual perfume.

Calibration curves

The area under the peak corresponding to each fragrance was obtained from the chromatograms and plotted against perfume concentration to obtain calibration curves. The sensitivity and selectivity of the HS-GCMS analysis can be seen on Figure IV.2, where the response of the GC detector was considerably lower in the case of MA compared to DD for the same perfume concentration (the other studied fragrances were not plotted for clarity purposes). Among the five tested perfumes, MA was the only one showing a linear curve up to the highest concentration of 100 ppm.
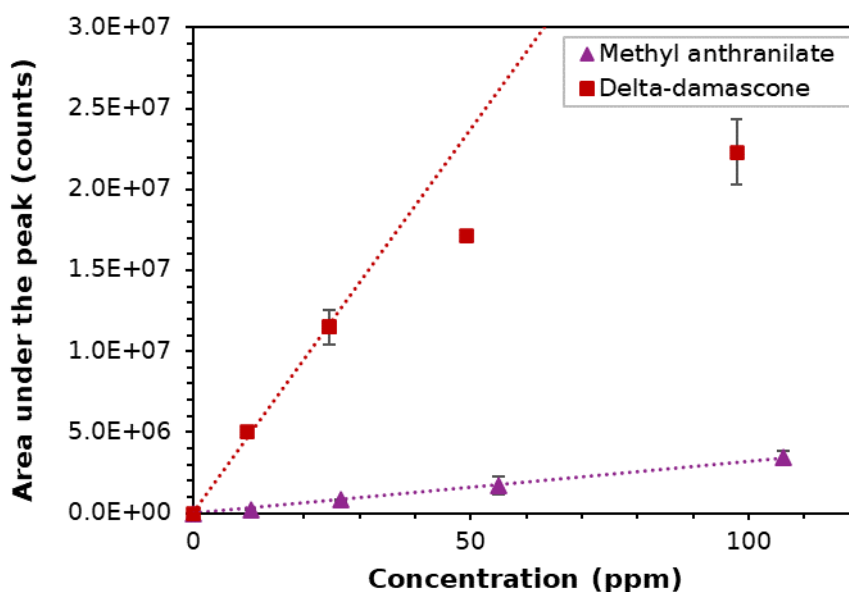

Figure IV.2: Calibration curves of Delta-Damascone (squares) and Methyl Anthranilate (triangles). Straight lines were added to point the loss of linearity of the calibration curve in the case of Delta-Damascone. Non-visible error bars are within markers.

In order to work with the same concentration and dilution factor for all perfume molecules, the maximum perfume concentration to be analyzed was set to 25 ppm and the linearity of all calibration curves in that concentration range is depicted on Figure IV.3.
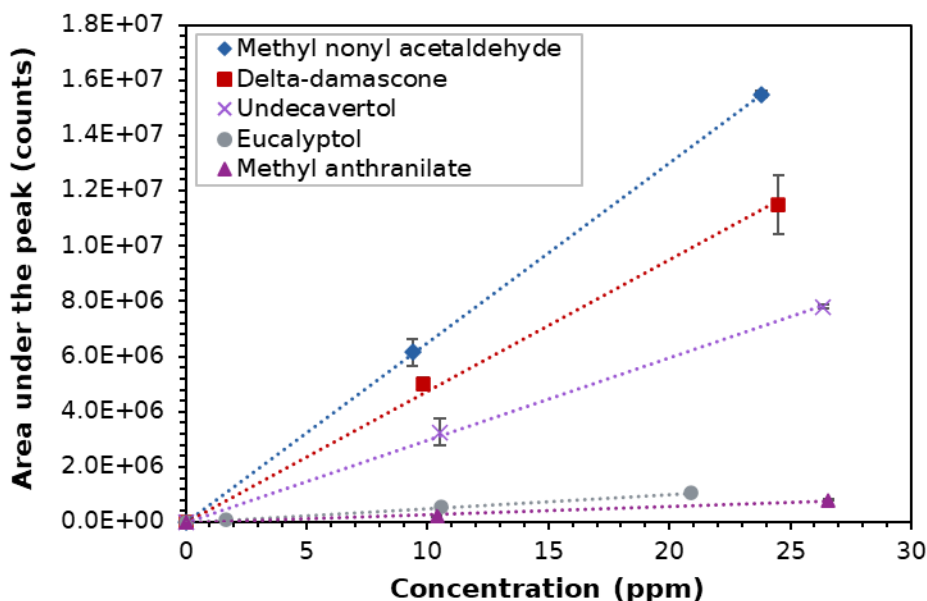
Figure IV.3: Calibration curves of MNA (diamonds), DD (squares), UDV (crosses), ECL (circles) and MA (triangles) for perfume concentrations up to 25 ppm. Non-visible error bars are within markers.

Extraction of perfumes
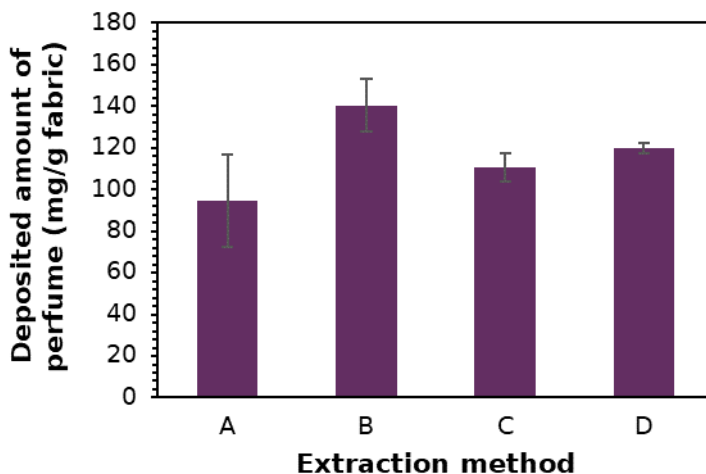
Figure IV.4: Average deposited amount of Delta-Damascone on polyester vs. extraction method.

The calibration curve of Delta-Damascone was first traced using standard solutions, which allowed for the determination of the perfume concentration in the GCMS sample vials. The latter was then multiplied by the dilution coefficient to obtain the amount of perfume deposited on each piece of fabric, and finally normalized by the weight of the fabric

piece to obtain the amount of deposited perfume per g of fabric. Figure IV.4 presents the results comparing the different extraction procedures and shows that protocol B, namely extraction in EtOH with 15 min in an ultrasonic bath, gave the highest amount of perfume detected in the GCMS. This method was hence kept for the deposition experiments.

In this section, we developed protocols for the evaluation of the deposition efficiency of perfume carriers using the HS-GCMS technique. We first determined the maximum perfume concentration that can be contained in the GCMS sample vials and detected without saturating the instrument. We then observed the differences in selectivity and sensitivity of the method towards various perfumes, which highlighted the need to use a calibration curve for each tested molecule and adjust the perfume concentration in the analyzed sample depending on the limit of linearity of the calibration curve. Finally, we optimized an extraction method to ensure the correct determination of the deposition efficiency of perfumes. All of these results will be used in the next sections to evaluate the efficiency of soft microcapsules and polymeric micelles to deliver fragrances on fabrics in washing tests.

IV.2. Deposition of perfume using microcapsules

In this section, we evaluated the targeted delivery of perfumes on fabrics, assisted by soft microcapsules of Soluplus®. The aim of this study was to determine the influence of encapsulation on the deposition efficiency of perfumes on real substrates such as fabrics. Herein, we investigated two types of fabrics, namely hydrophilic cotton and hydrophobic polyester.
As mentioned in the previous section IV.1, wash tests would normally include the dilution of the laundry product (namely detergent or softener) before being exposed to the fabrics, and the latter would be rinsed following the use of a detergent. In this study, it was necessary to maintain the presence of microcapsules in solution, which is why a standard wash test could not be performed due to the destabilization of the soft microcapsules by water dilution. Therefore, fabrics were simply

"washed" directly in the tested capsule suspensions in small, closed containers and not rinsed at the end of the experiment.

We used the same five perfume ingredients as in the previous paragraph, namely Methyl Anthranilate, Eucalyptol, Delta-Damascone, Undecavertol and Methyl Nonyl Acetaldehyde.

IV.2.1. Experimental protocols

Preparation of microcapsules

Soft microcapsules were prepared by mixing the amphiphilic copolymer Soluplus® with one of the five perfumes of interest in water. Incorporating a small amount of polymer that had been labeled with Rhodamine B enabled the characterization of the capsules using Confocal Laser Scanning Microscopy (CLSM).

Deposition tests

The solutions containing microcapsules were first sampled to accurately determine the initial perfume concentration by GCMS. Three pieces of cotton and polyester fabrics were then cut in small squares of 4 x 4 cm² and placed in different jars containing one of the Soluplus®-perfume capsule solutions, which was gently mixed for about 20 min using a magnetic stirrer. The fabrics were retrieved from the pots, gently squeezed to remove the excess of water and two pieces were individually placed in vials. Perfumes were extracted from the fabric and liquid (containing the initial capsule solution) samples using ethanol with a 15 min ultrasonic bath treatment. Each extract was then diluted further in EtOH, and the dilution coefficient was calculated to obtain a maximum perfume concentration of 25 ppm in the analyzed solution for a deposition efficiency (DE) of 100 %, defined as:

$$IV.1 \quad DE = \frac{\text{Concentration of deposited perfume on fabrics}}{\text{Initial concentration of perfume in capsule suspension}}$$

Each extract was analyzed three times by GCMS, and all experiments were performed twice (external replicates). We prepared three standard solutions for each perfume in ethanol with concentrations ranging from

5 ppm to 25 ppm to build a calibration curve. By plotting the integrated area under the peak obtained from the GCMS data as a function of the perfume concentration, the slope of the linear calibration curve was used to determine the concentration of perfume in the samples. The latter was then normalized by the mass of fabric to account for the differences in fabric grammage between cotton (287 ± 6 g/m^2) and polyester (120 ± 20 g/m^2).

IV.2.2. Results and discussion

Preparation of microcapsules

The morphology of the different microcapsules observed in CLSM can be found in Table IV.2, with the red color corresponding to the location of the polymer. As seen in Chapter II, Soluplus® only formed very few capsules with the fragrance Eucalyptol, which was once again observed using the labeled polymer. Capsules were moving too fast in the CLSM to take a proper picture and only red dots are featured here, corresponding to capsules with a diameter below 3 µm. On the other hand, the sample containing MNA showed numerous, bigger capsules (diameter > 10 µm) which was also consistent with the observations made in the previous chapters. Between the other three perfumes, Methyl Anthranilate and Undecavertol presented solid particles of various shapes and dimensions. The sample containing MA showed many spherical particles seen as microcapsules with a diameter of about 2 µm or less, as well as a few bigger aggregates of about 10 µm. Even though the CLSM was only able to track Soluplus®, it was believed that the perfume was contained in these aggregates. In fact, the latter sedimented whereas all of the other samples presented some creaming. This was due to MA having a greater density than water (see Appendix II), thus bringing the particles at the bottom of the vial. On the contrary, Undecavertol had the opposite effect, and large aggregates (visible to the naked eye) were found at the top of the solution. The observed objects contained spherical shapes surrounded by the red polymer in the corresponding micrographs, marking the location of polymer-free areas. These black spheres should thus represent perfume droplets dispersed in a polymer-rich matrix.

Table IV.2: CLSM micrographs of soft microcapsules created using Soluplus® and perfumes in water, including Methyl Anthranilate, Eucalyptol, Undecavertol, Delta-Damascone and Methyl Nonyl Acetaldehyde. The red signal corresponds to the location of the polymer, labeled with Rhodamine B. Scale bars are 50 μm.

Methyl anthranilate	Eucalyptol
Undecavertol	Delta-Damascone
Methyl Nonyl Acetaldehyde	
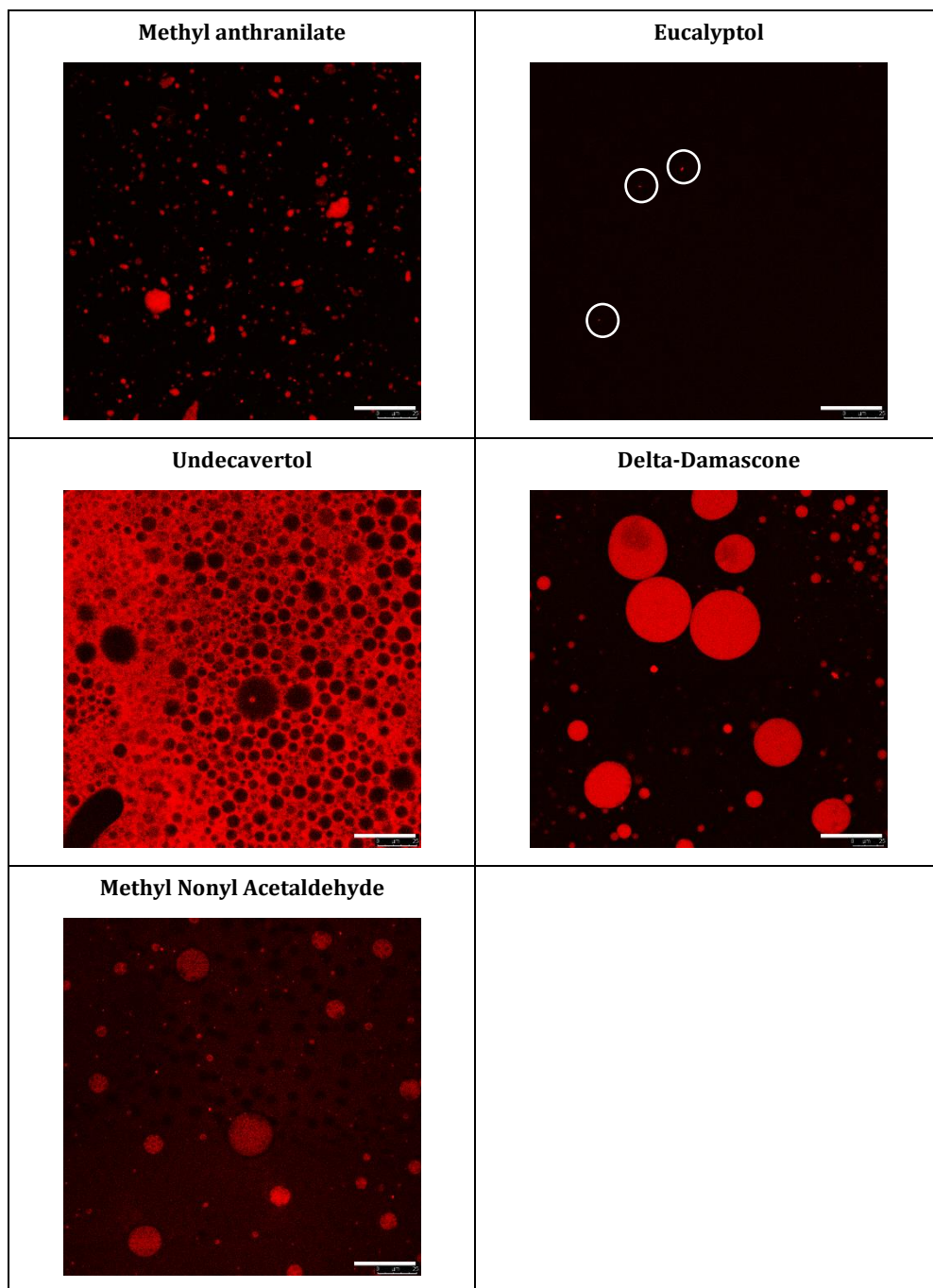
Finally, the last sample with the perfume Delta-Damascone presented highly polydisperse microcapsules, with a diameter varying from 5 to 60 μm (measured from CLSM micrographs).
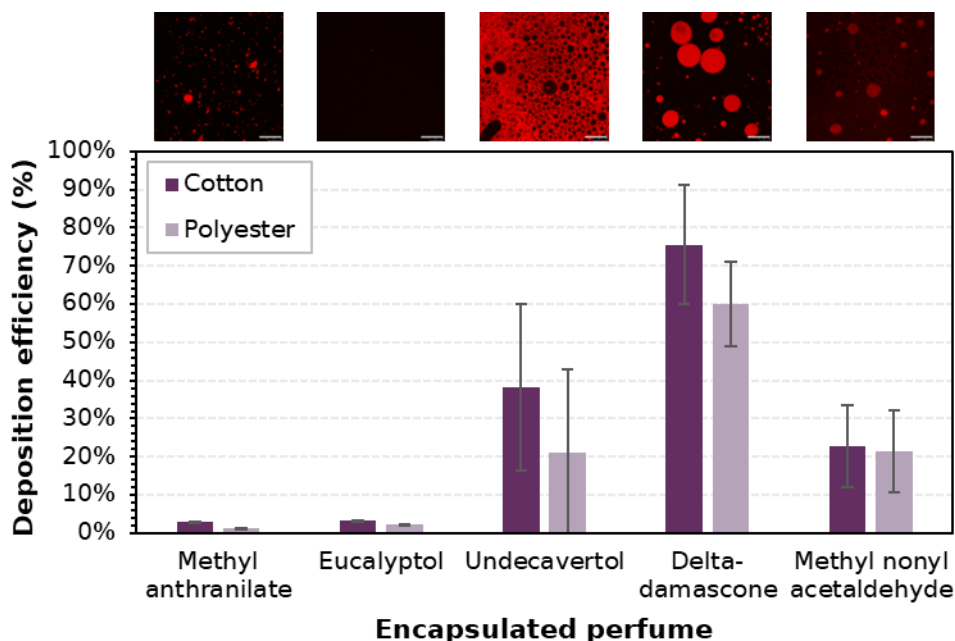
Deposition tests

Figure IV.5: Deposition efficiency of fragrant molecules promoted by the polymeric capsules of Soluplus® on cotton (dark purple) and polyester (light purple) fabrics and fluorescence-CLSM micrographs of the corresponding capsules in solution. The red signal marks the location of the polymer thanks to the Rhodamine B label.

The deposition efficiency of the perfume molecules of interest assisted by microparticles of Soluplus® was evaluated on cotton and polyester fabrics. The results depicted on Figure IV.5 showed a similar trend between cotton and polyester, namely an increased deposition efficiency for samples containing a higher number of capsules with a larger size (diameter > 10 μm). In fact, samples with ECL and MA with few/small microcapsules showed a poor adsorption on the surfaces whereas DD and MNA showed an increased deposition associated with big and numerous microcapsules. On the contrary, UDV did not present microcapsules but rather large aggregates, with a perfume adsorption comparable to that of MNA and a great variability in the measured results, which was a direct consequence of the presence of chunks in solution. Indeed, at the end of

the deposition experiment, aggregates present at the air/water interface stuck to the fabrics as the latter were pulled out of the solution, leading to a very inhomogeneous deposition.

It is also worth noting that the deposition efficiency was slightly increased on cotton than polyester, which could be attributed to the differences in roughness and/or yarn density of the fabrics which are more important for cotton.

The results thus indicated that the adsorption of materials was due to the entrapment of microcapsules between the yarns rather than adsorption, confirming that capsules need to get in close contact with the fabrics to adsorb.

The results described here confirmed that the encapsulation of new perfume molecules is difficult to predict. However, we were able to verify that a better encapsulation leads to an increased deposition of fragrances on real substrates, for both types of surfaces. In this study, the difference in perfume adsorption between cotton and polyester was associated to differences in the physical properties of the fabrics, such as roughness, fiber size, weight, etc. This suggested that perfumes were mainly delivered to fabrics by physical interactions between the microparticles and the substrates.

IV.3. Deposition of micelles

In this last section, we assessed the delivery of perfumes assisted by polymeric micelles on fabrics. The goal was to test the model developed in the previous Chapter on a real-life application. To do so, we created the microcapsules in a prototype laundry softener containing a cationic surfactant and used this formulation on fabrics in a small-scale washing machine. In total, ten fragrant ingredients were tested, and cotton and polyester fabrics were mixed in the same load to evaluate the partitioning between the two types of fabrics.

IV.3.1. Experimental protocols

Preparation of microcapsules in the prototype softener formulation

In this study, the tested fragrances included the five molecules used in the previous section (namely MA, ECL, UDV, DD and MNA), as well as Citronellol (CTN), Limonene (LMN), Alpha-Pinene (APN), Habanolide (HBN) and Iso-E Super (IES), and their physical chemical properties can be found in Appendix II. Soluplus® was first incorporated in a vial with one of the tested perfumes. The softener formulation (already containing the cationic surfactant) was then added to the vial and each solution was shaken for a few hours until homogeneous.

Calibration of the GCMS

Each capsule solution was diluted in water to obtain 3 different standard solutions, containing about 4, 20 and 70 ppm of perfume, respectively. The three calibration solutions were then spread on 4 x 4 cm² pieces of cotton fabrics and ethanol was added to extract the perfume molecules from the substrates with an ultrasonic bath treatment for 15 min. The spread amounts of standard solutions were calculated to reach 0.5, 4 and 10 ppm of perfume in the different GCMS vials.

Wash tests

Soluplus®-perfume microcapsules were deposited on cotton and polyester fabrics using a small-scale washing machine called a launderometer (Figure IV.6) to mimic washing conditions. In this procedure, the capsule solutions were first diluted in water to obtain 200 mL of solution in a container from the launderometer. This diluted solution was sampled and analyzed by HS-GCMS to determine the initial amount of perfume in solution before deposition. 25 g of cotton and 25 g of polyester (in square swatches of 20 x 20 cm²) were introduced in the same washing pot, soaking in the diluted washing solution. The container was then placed in the launderometer and rotated for 20 min at room temperature.

2 samples of fabric were cut into 4 x 4 cm² pieces in 2 different swatches for both cotton and polyester (i.e., 4 samples per type of fabric). The perfumes were extracted from the fabrics with the extraction procedure developed in section IV.1 (i.e., extraction in EtOH with 15 min in an ultrasonic bath) and quantified by HS-GCMS. No further dilution of the extract was necessary this time because of the dilution step incorporated in the wash test; the final concentration of perfumes in the GCMS vial could not exceed the chosen limit of 25 ppm. Each wash test was performed twice.

Figure IV.6: Launderometer containing eight slots for individual washing pots with a capacity of 500 mL. Once placed in the instrument, the washing containers revolve around a horizontal axis.

The deposition efficiency of each perfume molecule was then calculated using equation (IV.1). The partitioning between cotton and polyester was also calculated as the percentage of total amount of deposited perfume that was adsorbed on each type of fabric.

IV.3.2. Results and discussion

The deposition efficiency of perfumes was plotted against their physical chemical parameters for both cotton and polyester, and the results featuring the perfumes' logP and water solubility can be seen in Table IV.3. Due to technical issues with the GCMS, the fragrance Methyl

anthranilate was not detected correctly and gave unexploitable results, which is why this molecule does not appear in the graphs.

Table IV.3: Deposition efficiency of perfumes on cotton and polyester vs. their different physical chemical properties.
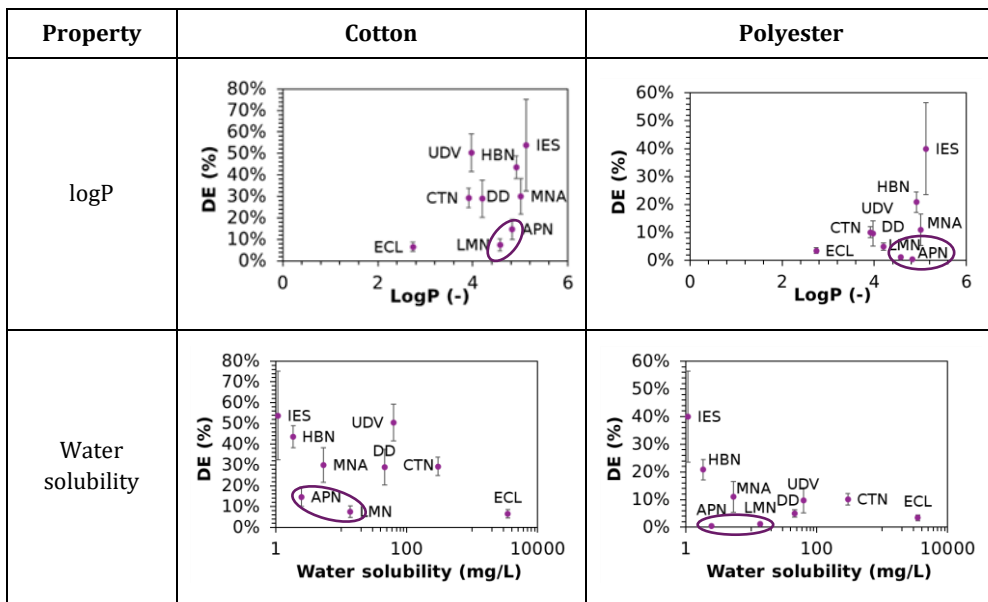
Interestingly, perfumes preferentially deposited on the hydrophilic cotton than on the hydrophobic polyester, although the results obtained on the flat model substrates did not predict such a trend. This was ascribed to the presence of cationic surfactant in the prototype softener formulation. As seen from the results in section III.3.2, the polymeric micelles of Soluplus® interact preferentially on the cationic surface, which was attributed to the slight negative charge present on the polymeric micelles (Figure III.7). Therefore, it was reasonable to assume that cationic surfactant could also interact with the Soluplus® micelles, thus forming polymer-surfactant complexes that entrap the hydrophobic perfume. Additionally, it has been reported that cationic surfactants adsorb twice as much on natural fibers such as cotton than on synthetic fibers such as polyester, due to the lower specific amount of charge on the latter.[1,6] These observations suggested that the polymer-surfactant complexes might have been positively charged and long-range electrostatic forces played an important role in the delivery of perfumes on surfaces, attracting the particles close to the substrates. Future studies

should evaluate the zeta potential of polymeric micelles (with and without perfume) and assess variations in presence of cationic surfactant.

Even though the model from the previous chapter was developed without cationic surfactant, the results obtained on polyester fabrics were in accordance with that of the model hydrophobic surface, with an increased deposition as water solubility decreases or logP increases (Figure III.8). On the other hand, we also observed the same trend on cotton, even though the latter is considered as a hydrophilic surface. It is also worth noting that the two perfumes Alpha-pinene and Limonene did not follow the trend and their deposition efficiency was very low, which was surprising considering the nature of these two molecules. Indeed, being the only two hydrocarbons among all the investigated active ingredients, it was expected that their increased hydrophobicity would benefit their deposition on fabrics. This differing result thus highlighted the limitations of the model and suggested that nonpolar molecules might follow a different deposition mechanism, which stressed once again the importance of the perfume's functionality on its targeted delivery.

The results presented in this section showed that fragrances can efficiently be deposited on substrates such as fabrics in a small-scale washing machine, using polymeric micelles as perfume carriers. The cationic surfactant present in the prototype softener formulation most likely formed a polymer-surfactant complex with Soluplus®, providing a positive charge to the perfume carrier. This induced the preferential adsorption of fragrances on natural fibers rather than on synthetic ones. It was observed that the perfumes' deposition efficiencies on cotton and polyester fabrics both followed the model developed in Chapter III on the flat hydrophobic surface, indicating that the latter could be used to predict the deposition of new fragrances. However, some limitations arose when investigating hydrocarbons, suggesting the need to develop a new model for nonpolar molecules.

In this last Chapter, the performance of the technology was investigated on real substrates such as fabrics, using HS-GCMS as the main

characterization technique. We first developed methods to evaluate the deposition of single molecules by including an extraction protocol and evaluating the appropriate working concentration for each molecule. Various perfume ingredients were then deposited on cotton and polyester fabrics using the soft microcapsules or polymeric micelles in small-scale washing tests. It was seen that the targeted delivery greatly depended on the fragrance's nature, just as encapsulation. When investigating microcapsules, perfumes were adsorbed on the substrates by physical interactions between the perfume carriers and fibers, confirming that improving encapsulation also improves deposition. On the other hand, the delivery of fragrances through polymeric micelles was correlated to their water solubility and logP, showing that the active material's hydrophobicity played a major role in its deposition. Yet, the influence of other parameters such as polarity, functionality, etc. need to be investigated further as the developed model presented some limitations.

V. CONCLUSIONS AND PERSPECTIVES

This Thesis focused on the development of a new encapsulation process that relies on the self-assembly of amphiphilic polymers to deliver fragrances on various surfaces, for home care and beauty care applications. Even though the encapsulation of perfumes has been developed for the past few decades, there is still a need for novel processes that present improved biodegradability, sustainability and chemical use, all the while maintaining the performance sought in consumer goods. As the SAMCAPS project aims at creating a new technology, there was a need to define and obtain the systems of interest. Soft microcapsules had previously been obtained with a PEG-g-PVAc copolymer in a prototype liquid detergent formulation, which is why Soluplus®, a PEG-g-(PVAc-co-PVCL) polymer, showed potential for microcapsules formation as well. Its biocompatibility, amphiphilic nature and its already well-known ability to solubilize hydrophobic drugs in aqueous media strengthened our choice for this material. Prior to forming perfume carriers, I focused my attention on the understanding of interactions between this polymer and three different perfume molecules, namely Eucalyptol (ECL), Citronellol (CTN) and Methyl Nonyl Acetaldehyde (MNA).

The primary objective was to develop methods and models to study these interactions, with the ultimate goal of relating the physical-chemical properties of fragrances with their ability to form microcapsules with Soluplus®. We started by investigating polymer-perfume (1:1) binary systems in solution and thin films in order to assess how the different perfumes affect the polymer properties. Combining thermal analyses, X-ray scattering, acoustic sensing and microscopy techniques, we learned that the studied perfumes interact preferentially with the hydrophobic parts of Soluplus®, namely PVAc and PVCL, driving the polymer to self-assemble. Stronger polymer-perfume interactions were observed with the most hydrophobic perfume MNA which predicted good encapsulation properties in aqueous environment, though it is likely that polymer-

perfume interactions cannot easily be explained through merely one of the perfume properties. Following this investigation, we incorporated these polymer-perfume systems in water and studied the formation of microcapsules and micelles. We were able to confirm that all three perfumes formed microcapsules with Soluplus® due to their favored interactions with the hydrophobic moieties of the polymer, producing a variety of spherical capsules of various sizes and structures. Interestingly, the strength of polymer-perfume interactions observed in the preliminary study was correlated to the encapsulation properties of Soluplus®, with weak interactions leading to the formation of few, small capsules and vice versa. The dilution of these microcapsule suspensions then resulted in the creation of polymeric micelles, where the most hydrophobic molecule with strong polymer-perfume interactions (i.e., MNA) once again showed effective entrapment in the polymer aggregates, and we used Quartz-Crystal Microbalance with Dissipation monitoring (QCM-D) to confirm the inclusion of the other fragrances. These findings unlocked the possibility of using Soluplus® as perfume carrier for targeted delivery on surfaces, and we hypothesized that the deposition of perfumes on surfaces could be correlated to their ability to be encapsulated.

As a next step, we used the perfume carriers obtained from the previous study to assess their adsorption on surfaces, examining the effect of surface chemistry and perfume properties. More specifically, self-assembled monolayers (SAMs) with alkyl, hydroxyl, carboxyl and amino terminal groups were created as model substrates to explore the effect of wettability and surface charge on the adsorption of particles containing the three perfumes of interest. The adsorption of microcapsules on hydrophobic and hydrophilic surfaces was observed using confocal microscopy imaging technique and the inspection of the substrates revealed that predicting capsules interactions with surfaces is a rather challenging task. Indeed, the introduction of a new component (i.e., a surface) in the capsule system changed the initial structure of the microcapsules, thus exposing the delicate balance between polymer, perfume and water to form such perfume carriers. Yet, even though the

results obtained in this study did not allow us to establish deposition models for microcapsules on surfaces, we still observed that good encapsulation properties facilitate the deposition of capsules on surfaces as more microcapsules are available to interact with surfaces. Using Atomic Force Microscopy (AFM), we attempted to determine the cohesive energy of capsules. Unfortunately, we were unable to systematically estimate this property, which prevented us from connecting mechanical properties of microcapsules with their adhesion on surfaces. Nevertheless, this experiment could serve in release studies of perfume from microcapsules, as we observed that properties of the capsule surface layer changed upon perfume desorption.

To ensure that perfumes could be delivered to surfaces even after the destabilization of microcapsules in real applications, we also studied the adsorption of perfume-loaded micelles on the four model surfaces. By coupling QCM-D experiments with AFM analysis, we were able to visualize the adsorbed particles and understand the different deposition mechanisms. Depending on the nature of fragrances and surfaces, micelles adsorb either as discrete, spherical particles or homogeneous, flat films, which could prove to be an important factor in the retention of perfumes on surfaces following cleaning processes. A model for the deposition of perfumes on a hydrophobic surface was developed, in which the adsorption of materials is driven by hydrophobic interactions. On hydrophilic surfaces, it was shown that perfume chemistry as well as surface charge play critical roles in the adsorption of micelles. As seen from our results, electrostatic interactions could significantly impact the adsorption of fragrant active, which is why it is fundamental that the charge of microcapsules and micelles, as well as the model surfaces are characterized in further studies by measuring their (surface) zeta potential.

As half of this PhD took place at the Brussels Innovation Center of Procter & Gamble, we were able to apply the technology on real-life applications. We thus developed protocols to evaluate the efficiency of soft microcapsules and polymeric micelles to deliver fragrances on

fabrics, and we employed Gas Chromatography coupled with Mass Spectroscopy (GCMS) analyses to quantify the deposition of perfumes. In the first part of the investigation, five different perfumes were encapsulated in water and the microcapsule suspensions were used to wash cotton and polyester fabrics. Our findings confirmed that an increased encapsulation results in an improved deposition of perfume, particularly because microcapsules deposited through physical entrapment between the yarns. This shed light on the capsule properties to tune so as to improve the deposition of fragrances on fabrics, such as capsule size, elasticity, compressibility, etc. The second part of the study dealt with the targeted delivery of perfume-loaded polymeric micelles. The latter were incorporated into a prototype laundry softener and the formulations were once again applied to wash cotton and polyester fabrics in a small-scale washing machine. Testing ten different fragrances, it was shown that the perfumes' deposition efficiencies followed the model developed for the adsorption of perfumes on the flat hydrophobic model surface, namely adsorption increases with the hydrophobicity of the loaded perfume. However, the influence of other perfume properties such as polarity, functionality, etc. need to be investigated further as the developed model presented some limitations. Interestingly, the model was followed on both types of fabrics even though cotton is considered a hydrophilic surface, which indicated that the flat hydrophobic surface could be further used as model surface for these fabrics in future work. However, it would also be interesting to create model surfaces that have closer chemistries to cotton and polyester fabrics, for instance by forming spin-coated thin films from cotton and polyester solutions.[165,166]

In the framework of consumer products, the encapsulated perfumes that need to be delivered on surfaces are composed of dozens of fragrant molecules. It would thus be interesting to address the encapsulation and delivery of perfume blends and determine the potential synergistic or competitive effects between fragrances so as to enhance the encapsulation and deposition of fragrances that poorly perform in these matters. Similarly, this technology is destined to be used in high surfactant environments, which can drastically shift the delicate

equilibrium between polymer-perfume-water and result in the destruction of microcapsules or the creation of novel self-assemblies. The addition of new components requires a comprehensive study of their effect on the initial system, which is why it would be crucial to develop fast and easy procedures to study those interactions. For instance, one could study the effect of surfactants on capsules and micelles by investigating their interactions with SAMs terminated with long-chain anionic and/or cationic surfactants as new model surfaces.

As perfumes are added to home care and beauty care products to give a pleasant scent after washing processes, it would also be essential to investigate the release properties of the perfume carriers after their deposition, in order to determine the applicability of self-assembled microcapsules as novel perfume delivery systems in the field of consumer goods.

To conclude, the results presented in this Thesis participates in the expansion of the knowledge on the use of amphiphilic polymers for the targeted delivery of hydrophobic active compounds such as perfumes. As this project is still in its preliminary stage, many questions remain to fully understand all the facets of self-assembled microcapsules and further studies would unlock their full potential.

ACKNOWLEDGEMENTS

REFERENCES

[1]   E. Smulders, W. Rähse, W. Von Rybinski, J. Steber, E. Sung, F. Wiebel, in: E. Smulders, W. Rähse, W. Von Rybinski, J. Steber, E. Sung, F. Wiebel (Eds.), Laundry Detergents, Wiley-VCH Verlag GmbH & Co. KGaA, Weinheim, FRG, 2002, pp. 98–120.

[2]   Y.-L. Hsieh, in: Cotton: Science and Technology, Woodhead Publishing, 2006, pp. 3–34.

[3]   M.P. Ansell, L.Y. Mwaikambo, in: Handbook of Textile Fibre Structure, Woodhead Publishing, 2009, pp. 62–94.

[4]   L. Segal, P.J. Wakelyn, in: Handbook of Natural Fibres, Woodhead Publishing, 1985, pp. 9–23.

[5]   A.J. East, in: Handbook of Textile Fibre Structure, Elsevier, 2009, pp. 181–231.

[6]   A.M. Grancaric, A. Tarbuk, T. Pusic, Coloration Technology 121 (2005) 221–227.

[7]   A. Calvimontes, A. Synytska, Melliand Textilberichte 1 (2006) 16–18.

[8]   A. Kumar, L. Gilson, F. Henrich, V. Dahl, J. Kleinen, T. Gambaryan-Roisman, J. Venzmer, Journal of Colloid and Interface Science 473 (2016) 152–161.

[9]   P. Maroni, F.J. Montes Ruiz-Cabello, C. Cardoso, A. Tiraferri, Langmuir 31 (2015) 6045–6054.

[10]   L. Mivehi, R. Bordes, K. Holmberg, Colloids and Surfaces A: Physicochemical and Engineering Aspects 419 (2013) 21–27.

[11]   T. John, B. Abel, L.L. Martin, Australian Journal of Chemistry 71 (2018) 543–546.

[12]   S. Llamas, E. Guzmán, F. Ortega, R.G. Rubio, Colloids and Interfaces 4 (2020) 47.

[13]   D. Prashar, International Journal of ChemTech Research 4 (2012) 258–265.

[14]   J. Li, Y.J. Yuan, Langmuir 30 (2014) 9637–9642.

[15]   J. Li, T. Guan, C. Hao, L. Li, Y. Zhang, Journal of Chemistry 2015 (2015).

[16]   H. Wang, S. Chen, L. Li, S. Jiang, Langmuir 21 (2005) 2633–2636.

[17] R.A. Watson, in: Handbook of Detergents, Part D: Formulation, Taylor & Francis Group, 2016, pp. 51–104.

[18] J.B. St. Laurent, F. de Buzzaccarini, K. De Clerck, H. Demeyere, R. Labeque, R. Lodewick, L. van Langenhove, in: I. Johansson, P. Somasundaran (Eds.), Handbook for Cleaning/Decontamination of Surfaces, Elsevier, 2007, pp. 57–102.

[19] E. Smulders, in: Laundry Detergents, Wiley-VCH Verlag GmbH & Co. KGaA, 2013, pp. 38–98.

[20] C. Pulce, J. Descotes, in: Human Toxicology, Elsevier, 1996, pp. 683–702.

[21] A.K. Roy Choudhury, in: Principles of Textile Finishing, Elsevier, 2017, pp. 109–148.

[22] M. Weerawatanakorn, J.C. Wu, M.H. Pan, C.T. Ho, Journal of Food and Drug Analysis 23 (2015) 176–190.

[23] L. He, J. Hu, W. Deng, Polymer Chemistry 9 (2018) 4926–4946.

[24] C. Ye, H. Chi, Materials Science and Engineering C 83 (2018) 233–246.

[25] Y.P. Timilsena, Md.A. Haque, B. Adhikari, Food and Nutrition Sciences 11 (2020) 481–508.

[26] S.Š. Marinković, D. Bezbradica, P. Škundrić, Chemical Industry and Chemical Engineering Quarterly 12 (2006) 58–62.

[27] S. Yang, L. Liu, J. Han, Y. Tang, International Journal of Cosmetic Science 42 (2020) 16–28.

[28] M. Bhatia, in: Encapsulation of Active Molecules and Their Delivery System, Elsevier, 2020, pp. 131–140.

[29] J.L. Reyez-Araiza, J. Pineda-Piñón, J.M. López-Romero, J.R. Gasca-Tirado, M. Arroyo Contreras, J.C. Jáuregui Correa, L.M. Apátiga-Castro, E.M. Rivera-Muñoz, R.R. Velazquez-Castillo, J. de J. Pérez Bueno, A. Manzano-Ramirez, Materials 14 (2021) 1420.

[30] Z. Liao, D. Xue, H. Li, L. Shi, Journal of Applied Polymer Science 133 (2016) 1–7.

[31] I.T. Carvalho, B.N. Estevinho, L. Santos, International Journal of Cosmetic Science 38 (2016) 109–119.

[32] K. Bruyninckx, M. Dusselier, ACS Sustainable Chemistry and Engineering 7 (2019) 8041–8054.

[33] Y. He, S. Yao, J. Hao, H. Wang, L. Zhu, T. Si, Y. Sun, J. Lin, Chinese Journal of Chemical Engineering 27 (2019) 2574–2580.

[34] C.G. Carmona, M.J. Lis Arias, O.G. Carmona, F.M. Bezerra, M.P. Andreu, N. de La, C. Díaz, Journal of Mineral, Metal and Material Engineering 5 (2019) 1–11.

[35] S. Wang, W. Zhang, Y. Chen, S. Zhang, W. Wang, Journal of Nanoscience and Nanotechnology 19 (2019) 4147–4153.

[36] M. Silva, I. Martins, F. Barreiro, M. Dias, A.E. Rodrigues, International Journal of Polymer Analysis and Characterization 22 (2017) 709–724.

[37] B.S. Beşen, Fibers and Polymers 20 (2019) 2587–2593.

[38] F.M. Bezerra, M. Lis, Ó.G. Carmona, C.G. Carmona, M.P. Moisés, G.M. Zanin, F.F. Moraes, Powder Technology 343 (2019) 775–782.

[39] D.R. Perinelli, G.F. Palmieri, M. Cespi, G. Bonacucina, Molecules 25 (2020).

[40] Y. Niu, J. Deng, Z. Xiao, X. Kou, G. Zhu, M. Liu, S. Liu, Journal of Thermal Analysis and Calorimetry 143 (2021) 3775–3781.

[41] Y. Li, L. Ai, W. Yokoyama, C.F. Shoemaker, D. Wei, J. Ma, F. Zhong, Journal of Agricultural and Food Chemistry 61 (2013) 3311–3319.

[42] B. Yingngam, W. Kacha, W. Rungseevijitprapa, P. Sudta, C. Prasitpuriprecha, A. Brantner, Powder Technology 355 (2019) 372–385.

[43] M.A. Busolo, S. Castro, J.M. Lagaron, M.K. Krokida, in: Thermal and Nonthermal Encapsulation Methods, CRC Press, 2017, pp. 115–136.

[44] A. Camerlo, C. Vebert-Nardin, R.M. Rossi, A.M. Popa, European Polymer Journal 49 (2013) 3806–3813.

[45] H. Zhao, X. Fei, L. Cao, B. Zhang, X. Liu, Materials 12 (2019) 393.

[46] S. Chen, S.-X. Cheng, R.-X. Zhuo, Macromolecular Bioscience 11 (2011) 576–589.

[47] A.P. Esser-Kahn, S.A. Odom, N.R. Sottos, S.R. White, J.S. Moore, Macromolecules 44 (2011) 5539–5553.

[48] I. Hofmeister, K. Landfester, A. Taden, Macromolecules 47 (2014) 5768–5773.

[49] M. Wei, X. Song, X. Pan, R. Li, C. Chen, X. Du, J. Li, Applied Sciences 10 (2020) 1–7.

[50] A. Shefer, S. Shefer, Moisture Triggered Release Systems Comprising Aroma Ingredients Providing Fragrance Burst in Response to Moisture, WO2003088933, 2003.

[51] M. Liu, C. Yan, J. Han, Z. Guo, Y. Wu, J. Huang, Z. Xiao, W.-H. Zhu, Green Chemical Engineering 2 (2021) 301–308.

[52] D. Lombardo, M.A. Kiselev, S. Magazù, P. Calandra, Advances in Condensed Matter Physics 2015 (2015).

[53] M. Ghezzi, S. Pescina, C. Padula, P. Santi, E. Del Favero, L. Cantù, S. Nicoli, Journal of Controlled Release 332 (2021) 312–336.

[54] X. Bu, N. Ji, L. Dai, X. Dong, M. Chen, L. Xiong, Q. Sun, Trends in Food Science & Technology 114 (2021) 386–398.

[55] F. Araste, A. Aliabadi, K. Abnous, S.M. Taghdisi, M. Ramezani, M. Alibolandi, Journal of Controlled Release 330 (2021) 502–528.

[56] M. Hasannia, A. Aliabadi, K. Abnous, S.M. Taghdisi, M. Ramezani, M. Alibolandi, Journal of Controlled Release 341 (2022) 95–117.

[57] J. Liu, X. Fan, Y. Xue, Y. Liu, L. Song, R. Wang, H. Zhang, Q. Zhang, New Journal of Chemistry 42 (2018) 6457–6463.

[58] M. Nie, M. Azizi, I. Keresztes, A. Kierulf, A. Abbaspourrad, ACS Applied Polymer Materials 3 (2021) 1415–1425.

[59] V.D. Gordon, X. Chen, J.W. Hutchinson, A.R. Bausch, M. Marquez, D.A. Weitz, J Am Chem Soc 126 (2004) 14117–14122.

[60] F. Shima, B. Schulte, H. Keul, M. Moeller, M. Akashi, Polymer Journal 46 (2014) 184–188.

[61] X. Gao, F. Gao, L. Chen, Y. Yao, T. Chen, S. Lin, Journal of Saudi Chemical Society 22 (2018) 297–305.

[62] A. Bartolini, P. Tempesti, A.F. Ghobadi, D. Berti, J. Smets, Y.G. Aouad, P. Baglioni, Journal of Colloid and Interface Science 556 (2019) 74–82.

[63] H. Hardung, D. Djuric, S. Ali, Drug Delivery Technology 10 (2010) 20–27.

[64] S.-Y. Lin, H.-L. Lin, Y.-T. Chi, Y.-T. Huang, C.-Y. Kao, W.-H. Hsieh, International Journal of Pharmaceutics 496 (2015) 457–465.

[65] J. Djuris, I. Nikolakakis, S. Ibric, Z. Djuric, K. Kachrimanis, European Journal of Pharmaceutics and Biopharmaceutics 84 (2013) 228–237.

[66] BASF, BASF, Pharma Ingredients & Services (2019) 1–14.

[67] S. Tanida, T. Kurokawa, H. Sato, K. Kadota, Y. Tozuka, Chemical and Pharmaceutical Bulletin 64 (2016) 68–72.

[68] L. Dian, E. Yu, X. Chen, X. Wen, Z. Zhang, L. Qin, Q. Wang, G. Li, C. Wu, Nanoscale Research Letters 9 (2014) 684.

[69] X. Jin, B. Zhou, L. Xue, W. San, Biomedicine & Pharmacotherapy 69 (2015) 388–395.

[70] J.F. Alopaeus, E. Hagesæther, I. Tho, Pharmaceuticals 12 (2019) 1–23.

[71] A. Sharkawy, I.P. Fernandes, M.F. Barreiro, A.E. Rodrigues, T. Shoeib, Industrial and Engineering Chemistry Research 56 (2017) 5516–5526.

[72] M. Kert, V. Krkoč, M. Gorjanc, Polymers (Basel) 11 (2019) 1919.

[73] F. Salaün, in: Active Coatings for Smart Textiles, Woodhead Publishing, 2016, pp. 179–220.

[74] U. Capasso Palmiero, J. Ilare, C. Romani, D. Moscatelli, M. Sponchioni, Colloids and Surfaces B: Biointerfaces 190 (2020) 110926.

[75] J. Lopez-Sanchez, M. Alajarin, A. Pastor, J. Berna, The Journal of Organic Chemistry 86 (2021) 15045–15054.

[76] B. Kronberg, K. Holmberg, B. Lindman, in: Surface Chemistry of Surfactants and Polymers, John Wiley & Sons, Ltd, Chichester, UK, 2014, pp. 211–229.

[77] J.O. Dihora, M.A. Brown, US 20160228338 A9 - Shampoo Compositions With Increased Deposition Of Polyacrylate Microcapsules, US 20160228338 A9, 2016.

[78] H. Najafi, H.A. Jerri, V. Valmacco, M.G. Petroff, C. Hansen, D. Benczédi, M.A. Bevan, ACS Applied Materials and Interfaces 12 (2020) 14518–14530.

[79] M.A. Brown, T.A. Hutchins, C.J. Gamsky, M.S. Wagner, S.H. Page, J.M. Marsh, International Journal of Cosmetic Science 32 (2010) 193–203.

[80] J. Venzmer, Chemie in Unserer Zeit 42 (2008) 72–79.

[81] S. Liu, Understanding Molecular Interactions to Enhance Deposition of Perfume Microcapsules on Fabric Surfaces, PhD thesis, University of Birmingham, 2018.

[82] K.A. Günay, D.L. Berthier, H.A. Jerri, D. Benczédi, H.A. Klok, A. Herrmann, ACS Applied Materials and Interfaces 9 (2017) 24238–24249.

[83] G. Dardelle, M. Jacquemond, P. Erni, Advanced Materials 29 (2017) 1–6.

[84] R. Toomey, J. Mays, D.W. Holley, M. Tirrell, Macromolecules 38 (2005) 5137–5143.

[85] Y. Yan, X. Zhou, J. Ji, L. Yan, G. Zhang, The Journal of Physical Chemistry B 110 (2006) 21055–21059.

[86] R. Muppalla, H.H. Rana, S. Devi, S.K. Jewrajka, Applied Surface Science 268 (2013) 355–367.

[87] G. Fontani, R. Gaspari, N.D. Spencer, D. Passerone, R. Crockett, Langmuir 29 (2013) 4760–4771.

[88] B. Peng, X. Chu, Y. Li, D. Li, Y. Chen, J. Zhao, Polymer (Guildf) 54 (2013) 5779–5789.

[89] M. Zhang, J. Soto-Rodríguez, I.-C. Chen, M. Akbulut, Soft Matter 9 (2013) 10155.

[90] Q. Huang, Z. Mei, K. Takata, J. Yang, Cosmetic & Toiletries 128 (2013) 810.

[91] R.G. Berger, Flavours and Fragrances: Chemistry, Bioprocessing and Sustainability, Springer-Verlag Berlin Heidelberg, 2007.

[92] R. Rouseff, K. Goodner, in: K. Goodner, R. Rouseff (Eds.), Practical Analysis of Flavor and Fragrance Materials, Blackwell Publishing Ltd., Chichester, UK, 2011, pp. 45–68.

[93] V. Normand, J. Tang, A. Struillou, Flavour and Fragrance Journal 23 (2008) 49–57.

[94] L. Cabrales, N. Abidi, F. Manciu, Fibers 2 (2014) 285–294.

[95] M. Adnan, J. Jeyakodi Moses, in: A. Majumdar, D. Gupta, S. Gupta (Eds.), Functional Textiles and Clothing, Springer Singapore, Singapore, 2019, pp. 193–202.

[96] Y. Akiyama, Y. Matsue, T. Mori, S. Nishijima, Colloids and Surfaces A 559 (2018) 1–7.

[97] A. V. Svensson, E.S. Johnson, T. Nylander, L. Piculell, ACS Applied Materials and Interfaces 2 (2010) 143–156.

[98] L. Fernández-Peña, E. Guzmán, Cosmetics 7 (2020) 26.

[99] T. Luxbacher, I. Petrinić, T. Pušić, H. Bukšek, in: 8th INTERNATIONAL TEXTILE, CLOTHING & DESIGN CONFERENCE – Magic World of Textiles, Magic World of Textiles, Dubrovnik, CROATIA, 2016, pp. 346–351.

[100] C. Puglisi, D.B. Solarek, EP 2419078 B1 - Deposition of Hydrophobic Active Ingredients from Surfactant Systems, EP 2419078 B1, 2017.

[101] A.A. Kafi, K. Magniez, B.L. Fox, Journal of Adhesion Science and Technology 26 (2012) 175–187.

[102] L. Xiang, J. Zhang, L. Gong, H. Zeng, Soft Matter 16 (2020) 6697–6719.

[103] Q. Chen, S. Xu, Q. Liu, J. Masliyah, Z. Xu, Advances in Colloid and Interface Science 233 (2016) 94–114.

[104] K. Miyoshi, in: Mechanical Tribology - Materials, Characterization and Applications, CRC Press, 2004.

[105] G. Erdoğan, G. Güler, T. Kiliç, D.O. Kiliç, B. Erdoğan, Z. Tosun, H.D. Kivrak, U. Türkan, F. Özcan, M. Gürsoy, M. Karaman, in: Surface Treatments for Biological, Chemical, and Physical Applications, Wiley-VCH Verlag GmbH & Co. KGaA, Weinheim, Germany, 2017, pp. 67–114.

[106] A.M. Baty, P.A. Suci, B.J. Tyler, G.G. Geesey, Journal of Colloid and Interface Science 177 (1996) 307–315.

[107] D. Brune, R. Hellborg, H.J. Whitlow, O. Hunderi, Surface Characterization: A User's Sourcebook, Wiley, 1997.

[108] G. Renaud, R. Lazzari, F. Leroy, Surface Science Reports 64 (2009) 255–380.

[109] M. Buljan, N. Radić, S. Bernstorff, G. Draić, I. Bogdanović-Radović, V. Hol, Acta Crystallographica Section A: Foundations of Crystallography 68 (2012) 124–138.

[110] M. Thommes, K. Kaneko, A. V. Neimark, J.P. Olivier, F. Rodriguez-Reinoso, J. Rouquerol, K.S.W. Sing, Pure and Applied Chemistry 87 (2015) 1051–1069.

[111] T. Luxbacher, KGK Rubberpoint (2010) 74–78.

[112] Malvern Instruments, Zetasizer Nano: User Manual MAN0485, Malvern Instruments Ltd., 2013.

[113] A. Bartolini, P. Tempesti, C. Resta, D. Berti, J. Smets, Y.G. Aouad, P. Baglioni, Physical Chemistry Chemical Physics 19 (2017) 4553–4559.

[114] D. Xia, H. Yu, J. Tao, J. Zeng, Q. Zhu, C. Zhu, Y. Gan, Colloids and Surfaces B: Biointerfaces 141 (2016) 301–310.

[115] I.M. Hodge, Journal of Non-Crystalline Solids 169 (1994) 211–266.

[116] H. Lim, S.W. Hoag, AAPS PharmSciTech 14 (2013) 903–910.

[117] V. Pacáková, J. Virt, in: Encyclopedia of Analytical Science, Elsevier, 2005, pp. 180–187.

[118] Y. Park, J. Ko, T.K. Ahn, S. Choe, Journal of Polymer Science, Part B: Polymer Physics 35 (1997) 807–815.

[119] J.A. Tamboli, S.K. Mohite, International Journal of Applied Pharmaceutics (2020) 126–134.

[120] P. Molyneux, Water-Soluble Synthetic Polymers, CRC Press, 1984.

[121] S. Verheyen, P. Augustijns, R. Kinget, G. van den Mooter, Thermochimica Acta 380 (2001) 153–164.

[122] C.P. Buckley, A.J. Kovacs, Colloid and Polymer Science Kolloid-Zeitschrift & Zeitschrift Für Polymere 254 (1976) 695–715.

[123] D. Fragiadakis, J. Runt, Macromolecules 43 (2010) 1028–1034.

[124] N.A. Cortez-Lemus, A. Licea-Claverie, Progress in Polymer Science 53 (2016) 1–51.

[125] F. Meeussen, E. Nies, H. Berghmans, S. Verbrugghe, E. Goethals, F. du Prez, Polymer (Guildf) 41 (2000) 8597–8602.

[126] S. Alexander, T. Cosgrove, W.M. de Vos, T.C. Castle, S.W. Prescott, Langmuir 30 (2014) 5747–5754.

[127] Y. Mo, G. Liu, Y. Tu, S. Lin, J. Song, J. Hu, F. Liu, Journal of Polymer Science Part A: Polymer Chemistry 55 (2017) 1021–1030.

[128] C. Sofroniou, M. Baglioni, M. Mamusa, C. Resta, J. Doutch, J. Smets, P. Baglioni, ACS Applied Materials & Interfaces 14 (2022) 14791–14804.

[129] J.A. Emerson, D.T.W. Toolan, J.R. Howse, E.M. Furst, T.H. Epps, Macromolecules 46 (2013) 6533–6540.

[130] M. Vayer, A. Vital, C. Sinturel, European Polymer Journal 93 (2017) 132–139.

[131] A.L. Smith, R.B. Mulligan, H.M. Shirazi, Journal of Polymer Science Part B: Polymer Physics 42 (2004) 3893–3906.

[132] A. Rianjanu, S.N. Hidayat, T. Julian, E.A. Suyono, A. Kusumaatmaja, K. Triyana, IOP Conference Series: Materials Science and Engineering 367 (2018).

[133] K. Norrman, A. Ghanbari-Siahkali, N.B. Larsen, Annual Reports Section "C" (Physical Chemistry) 101 (2005) 174.

[134] B.T. Chen, Polymer Engineering and Science 23 (1983) 399–403.

[135] D.E. Bornside, C.W. Macosko, L.E. Scriven, Journal of Applied Physics 66 (1989) 5185–5193.

[136] C.J. Lawrence, Physics of Fluids 31 (1988) 2786.

[137] D.F.S. Petri, J Braz Chem Soc 13 (2002) 695–699.

[138] G. Matsuno, Sensors and Materials 11 (1999) 401–412.

[139] M. Kimura, Y. Liu, R. Sakai, S. Sato, T. Hirai, T. Fukawa, T. Mihara, Sensors and Materials 23 (2011) 359–368.

[140] K.-Y. Law, The Journal of Physical Chemistry Letters 5 (2014) 686–688.

[141] S. Micciulla, D.W. Hayward, Y. Gerelli, A. Panzarella, R. von Klitzing, M. Gradzielski, L. Chiappisi, Communications Chemistry 2 (2019) 61.

[142] L. Kumar, A. Horechyy, E. Bittrich, B. Nandan, P. Uhlmann, A. Fery, Polymers (Basel) 11 (2019) 1882.

[143] Z. Chen, C. He, F. Li, L. Tong, X. Liao, Y. Wang, Langmuir 26 (2010) 8869–8874.

[144] Z. Chen, C. He, F. Li, L. Tong, X. Liao, Y. Wang, Langmuir 26 (2010) 8869–8874.

[145] S. Park, J.-Y. Wang, B. Kim, W. Chen, T.P. Russell, Macromolecules 40 (2007) 9059–9063.

[146] Sigma Aldrich, O. Si, J.C. Love, L.A. Estroff, J.K. Kriebel, R.G. Nuzzo, G.M. Whitesides, F. He, L. Zhang, Anal Sci 105 (2002) 3.

[147] C.D. Bain, E.B. Troughton, Y.T. Tao, J. Evall, G.M. Whitesides, R.G. Nuzzo, J Am Chem Soc 111 (1989) 321–335.

[148] N.A. Lange, in: Handbook of Chemistry, Handbook Publishers, Inc., 1944, p. 86.

[149] E.P. Serjeant, B. Dempsey, in: IUPAC Chemical Data Series, Pergamon Press, 1979, p. 989.

[150] J.A. Jones, L.A. Qin, H. Meyerson, K.K. Il, T. Matsuda, J.M. Anderson, Journal of Biomedical Materials Research - Part A 86 (2008) 261–268.

[151] H.T.M. Phan, S. Bartelt-Hunt, K.B. Rodenhausen, M. Schubert, J.C. Bartz, PLOS ONE 10 (2015) e0141282.

[152] A. Eraghi Kazzaz, P. Fatehi, RSC Advances 10 (2020) 36778–36793.

[153] V. Lebec, J. Landoulsi, S. Boujday, C. Poleunis, C.M. Pradier, A. Delcorte, Journal of Physical Chemistry C 117 (2013) 11569–11577.

[154] M. Liu, Understanding the Mechanical Strength of Microcapsules and Their Adhesion on Fabric Surfaces, PhD thesis, University of Birmingham, 2010.

[155] B. Cappella, in: Springer International Publishing, 2016, pp. 3–66.

[156] B. Cappella, G. Dietler, Surface Science Reports 34 (1999) 1–104.

[157] S.D. Connell, D.A. Smith, Molecular Membrane Biology 23 (2006) 17–28.

[158] J. Schneider, Y.F. Dufrêne, W.R. Barger, G.U. Lee, Biophysical Journal 79 (2000) 1107–1118.

[159] B. Hofs, A. Brzozowska, A. de Keizer, W. Norde, M.A. Cohen Stuart, Journal of Colloid and Interface Science 325 (2008) 309–315.

[160] M. v Voinova, M. Rodahl, M. Jonson, B. Kasemo, Physica Scripta 59 (1999) 391–396.

[161] I. Reviakine, D. Johannsmann, R.P. Richter, Analytical Chemistry 83 (2011) 8838–8848.

[162] S.F. Taveira, A. Varela-Garcia, B. dos Santos Souza, R.N. Marreto, M. Martin-Pastor, A. Concheiro, C. Alvarez-Lorenzo, Carbohydrate Polymers 200 (2018) 278–288.

[163] T. Stora, S. Escher, A. Morris, Chimia (Aarau) 55 (2001) 406–412.

[164] R. Tekin, N. Bac, H. Erdogmus, Macromolecular Symposia 333 (2013) 35–40.

[165] M. Perfetti, Increasing the Deposition Efficiency of Perfume Ingredients in Liquid Detergents, Università degli Studi di Napoli, 2018.

[166] A. Doliška, Improving the Biocompatibility of PET Surfaces by Adsorbing Mannans and Mannan Derivatives, University of Graz, Austria, 2012.

[167] S. Gunnars, L. Wågberg, M.A. Cohen Stuart, Cellulose 9 (2002) 239–249.

APPENDIX I - EXPERIMENTAL DETAILS

Optical microscopy

The gels were assessed with an inverted microscope (Nikon Diaphot 300), using bright-field, phase contrast techniques.

DSC - Differential Scanning Calorimetry

Measurements were carried out using a Differential Scanning Calorimeter DSC 2500 (TA Instruments), in N_2 atmosphere (flow rate 50 mL/min), using Tzero Hermetic Aluminum pans and lids (TA Instruments), following the sequence described hereafter:
- 1st heating: from 25 °C to 80 °C at a 5 °C/min rate
- Cooling: from 80 °C to 10°C at a 5 °C/min rate
- Isothermal for 10 min
- Re-heat: from 10 °C to 80 °C at a 5 °C/min rate

TGA - Thermo Gravimetric Analysis

Measurements were carried out using a Simultaneous Thermal Analyzer instrument SDT 650 (TA Instruments) and aluminum hermetic pans (TA Instruments). Samples were heated up from 25 °C to 250 °C at a 10 °C/min rate.

SAXS - Small Angle X-Rays Scattering

Samples were first sealed at room temperature in a 1 mm-thick gel and powder Kapton sample holder (Xenocs SA). SAXS measurements were then performed in air at 25°C using a Xenocs Xeuss 3.0 X-ray diffractometer, equipped with a GeniX 3D Cu High Flux Very Long Focus (HFVL) X-ray source (λ = 1.54 Å). 2D SAXS images were collected using an Eiger2 R 1M hybrid photon counting detector (Dectris), with a pixel size of 75 × 75 μm^2. The SAXS profiles were obtained by radial averaging the 2D scattering pattern using XSACT software, expressed as the scattering intensity I as a function of the modulus of scattering vector Q = 4π sin(θ)/λ, with 2θ the scattering angle. Data was recorded with the

detector placed at two sample-to-detector distances of 300 mm and 1800 mm, using exposure times of 3600 s and 4800 s, respectively, to cover scattering vectors in a 0.003-0.8 Å^{-1} range. The measured scattering curves were corrected for Kapton scattering using the XSACT software.

AFM - Atomic Force Microscopy

All measurements were performed at ambient temperature in air, using a XE7 Atomic Force Microscope (Park Systems Corp). All images were obtained with a resolution of 512 x 512 pixels. Images were then analyzed using the image processing software XEI (Park Systems Corp).

Thickness of Soluplus® films

AFM was used in the optimization of Soluplus® thin films. Prior to measuring their thickness, it was necessary to scratch the surface in order to remove the material from the glass slide, before creating an image of the scratch. The difference in the z axis between the untouched film and the center of the scratch was then defined as the thickness of the film.

The scratches were performed using a silicon cantilever (Park Systems Corp), scanning a 0.75 x 1.00 μm² image with a 5 Hz frequency, first in contact mode (twice), then in non-contact mode. Finally, the created scratch was scanned over a 6 x 6 μm² area in non-contact mode.

Morphology of Soluplus® films after absorption/desorption of perfume vapors

Topographic images of Soluplus® films were obtained after adsorption and desorption of the perfume vapors, using a silicon tip in non-contact mode (non-contact cantilever PPP-NCHR 10M with a 5 nm diameter, Park Systems Corp). The scanned images were obtained with sizes of 50 x 50, 10 x 10 and 2.5 x 2.5 μm². For the analyses performed after the adsorption of vapors on the polymeric films, droplets of the tested perfume were placed next to the sample to prevent the desorption from taking place during the measurement. The analyses performed at the end of the desorption of the vapors were measured in air. Images were then analyzed using the image processing software XEI.

Characterization of model surfaces

The analyses were performed in non-contact mode using a silicon cantilever. The images were obtained with sizes of 50 x 50, 25 x 25, 5 x 5 and 1 x 1 μm^2. Roughness was measured on the 1 x 1 μm^2 images using the image processing software XEI.

Adhesive force measurement

100 x 100 μm^2 images were acquired by AFM (Park Systems Corp) with a silicon cantilever (non-contact mode Super Sharp Silicon cantilever, 5 nm tip radius, about 330 kHz resonance frequency and 42 N/m spring constant, Park Systems Corp). All images were obtained in non-contact mode with a resolution of 512 x 512 pixels. The measurements were performed at ambient temperature in air.

After obtention of the images, force-distance curves were recorded on different zones of the substrate by approaching to the surface and retracting it in a range of -4 μm < z < 4 μm relative to the sample surface, using a speed of 0.1 $\mu m/s$ and a resolution of 512 data points per trace. The maximum force was set to 788 nN.

Characterization of deposited micelles

The morphology of the adsorbed micelles on the various substrates was obtained in non-contact mode using a silicon cantilever (non-contact mode Super Sharp Silicon cantilever, 5 nm tip radius and 330 kHz resonance frequency, Park Systems Corp). The images were obtained with dimensions of 50 x 50, 25 x 25 and 5 x 5 μm^2.

QCM-D - Quartz-Crystal Microbalance with Dissipation monitoring

All measurements were performed at 25 °C ± 0.1° C using a QSense Explorer QCM-D instrument (Biolin Scientific). Frequency and dissipation changes were recorded using the instrument software QSoft401 (Biolin Scientific) from the 1st to 13th harmonics.

Preparation of Soluplus® films on quartz crystal sensors

SiO_2-coated AT-cut quartz crystal QSX 303 QCM-D sensors (fundamental frequency of 4.95 MHz, Biolin Scientific) were cleaned following the supplier's recommendation, starting with a UV/Ozone treatment for 10

min. They were then immersed in a 2 wt% solution of sodium dodecyl sulfate (SDS) for 30 min, rinsed with Milli-Q water, dried with a stream of nitrogen and exposed again to UV/Ozone for another 10 min. The sensors were then coated with a Soluplus® thin film using a Spin Coater Model P6700 series (Specialty Coating Systems Inc.) and following the protocol developed in section II.1.2.

Absorption of perfume vapors in Soluplus® films

The absorption experiments were performed on the Soluplus®-coated quartz crystals using a protocol readapted from the literature,[138,139] which involves the transport of perfume vapors using nitrogen as a carrier gas to a closed chamber containing the polymeric film. A scheme of the system can be seen on Figure II.8. The differential pressure for the flow of dry nitrogen was set to 0.5 bar at the supply outlet, being the smallest pressure measurable on the gauge. First, a flow of dry nitrogen gas was introduced into the chamber for at least 10 min to create a baseline of the frequency and dissipation shifts. The measurement was restarted to set the baseline value for the frequency and dissipation changes to 0 Hz and 0 ppm, respectively. The perfume vapors were then introduced via bubbling of N_2 gas through the liquid perfume in order to create the gas phase sample. The perfume vapors were passed through the QCM-D cell until a stable frequency signal was monitored for at least 5 min. Finally, the flow of nitrogen was introduced again to obtain a desorption curve until a stable frequency signal was monitored for at least 5 min. The data was normalized by the vapor pressure of each perfume before quantification.

Confirmation of perfume inclusion in Soluplus® micelles

Inclusion of the water-soluble perfumes, namely Eucalyptol and Citronellol, in Soluplus® micelles was investigated by QCM-D using the Soluplus®-coated quartz crystal sensors. First, Milli-Q water was flowed in the cell (flow rate 0.1 mL/min) until the frequency and dissipation changes were stable ($\Delta F < 2$ Hz over 10 min). The measurement was then restarted to set the baseline value for the frequency and dissipation shifts to 0 Hz and 0 ppm, respectively. A solution of Soluplus® micelles (25 mg/L) was introduced into the chamber (flow rate 0.1 mL/min) in

order to obtain a layer of micelles, again until the frequency and dissipation changes became stable (i.e., no more adsorption of polymer micelles occurred). Finally, a solution of Soluplus® + perfume (Eucalyptol or Citronellol) (concentration of 25 mg/L for each component) was passed over the sensor and the changes in frequency and dissipation were monitored over one hour, after which the experiment was stopped.

<u>Adsorption of Soluplus®-perfume micelles on model surfaces</u>

Adsorption of micelles on model surfaces was performed on the gold-coated quartz crystals that had been functionalized with different thiols. Prior to each measurement, the sensors were cleaned with ethanol in an ultrasonic bath for 15 min, rinsed with water and dried with a gentle stream of nitrogen. The measurements were started by flowing Milli-Q water into the chamber using a peristaltic pump with a flow rate of 0.5 mL/min until the obtention of a stable frequency for all harmonics. The flow rate was then decreased to 50 μL/min and the measurement was restarted to set the baseline value for the frequency and dissipation shifts to 0 Hz and 0 ppm, respectively. The micelle solution was then passed into the QCM-D cell for 1 h at 25°C. Finally, to remove the loosely adsorbed materials and simulate rinsing conditions, Milli-Q water was flowed into the chamber for 1 h with a flow rate of 100 μL/min. The acquired data was processed using Dfind software (Biolin Scientific).

XRR - X-Rays Reflectivity

XRR measurements were performed on a Xenocs Xeuss 3.0 X-ray diffractometer, equipped with a GeniX 3D Cu High Flux Very Long Focus (HFVL) X-ray source (λ = 1.54 Å). An Eiger2 R 1M hybrid photon counting detector (Dectris), with a pixel size of 75×75 μm^2, was used to collect the data. A thin, parallel X-ray beam was scanned over incident angles (θ) of $0° < \theta < 1°$ with a step size of 0.005° and a 20 s exposure time. The sample-detector distance was 600 mm.

Contact angle measurements

The wetting behavior of water on the different surfaces was characterized using a static contact angle measurement apparatus (Ramé

Hart Instrument Co). The experiments were performed at room temperature with water droplets (5 µL) in air.

CRM - Confocal Raman Microscopy

Raman spectra and maps were acquired using a Renishaw InvIa Qontor confocal MicroRaman system equipped with a 532 nm (Nd:YAG solid state type, 50 mW, 1800 l/mm grating) lasers, a Renishaw Centrus 1UTR57 detector, a front-illuminated CCD camera (256 x 1024 px, working temperature −70 °C) and a research-grade Leica DM 2700 microscope. The Raman spectra were recorded in the wavenumber range from 100 to 4000 cm-1 using the extended range mode, with three acquisitions of 10 s each. Bidimensional maps were acquired using a long working distance 50x objective in high-confocality and static spectral range modes. Maps were acquired with steps of 0.5 µm along the x-y plane, with acquisition times per point of 1 s. Raw data were processed using Renishaw software WiRE v.5.2 for maps generation.

DLS - Dynamic light scattering

The particle size distribution of Soluplus® micelles loaded with the different perfumes was determined by DLS at 25 °C using a 90Plus Particle Size Analyzer (Brookhaven Instruments Corp.). Samples were illuminated with a He−Ne laser beam (λ = 659.0 nm) and the scattered intensity was collected at a scattering angle of 90°.
Measurements were performed for 1 minute, 4 times per sample. The intensity autocorrelation function of the scattered light was recorded and normalized. The data was fitted to a lognormal distribution to determine the average hydrodynamic diameter D_h and polydispersity index (PDI) of the micelles.

Measurement of kinematic viscosity

Measurements were performed by recording the time to flow 50 mL of solution through a graduated burette. As the experiment was not performed using a standard gravimetric capillary, the flow time values could not be converted into kinematic viscosity values. However, since

those two terms are proportional (kinematic viscosity = flow time x capillary constant), the flow time values could be used as measured to compare the solutions. Values are reported with a variation of ± 15 % to account for manipulation error.

HS-GCMS - Headspace Gas Chromatography coupled with Mass Spectrometry

Components were analyzed using the 7890B Gas Chromatograph coupled with a 5977A Mass Selective Detector (GC-MS) from Agilent Technologies. Samples were placed into 20 mL glass vials and closed with a cap mounted with a perforable silicon septum. Vials were retrieved with a G7039A Multi-Purpose Sampler (Gerstel) and heated to 65 °C for 10 minutes. The headspace above the samples was then extracted using a 100 μm Polydimethylsiloxane (PDMS) Solid Phase Microextraction (SPME) fiber assembly (Supelco) for 5 min. The volatile compounds were desorbed into a CP-Sil 5 CB nonpolar column (15 m x 0.15 mm x 0.15 μm, Agilent Technologies) with a temperature-programmed analysis (from 40 °C for 0.5 min to 280 °C for 1 min with a heating rate of 40 °C/min). Finally, analytes were detected by fast GC-MS in full scan mode. Data was acquired and analyzed with the MassHunter Acquisition Software (Agilent Technologies).

Wash tests

Wash tests were performed in a Washtec launderometer (Roaches) at 25 °C.

APPENDIX II - PHYSICAL CHEMICAL PROPERTIES OF STUDIED FRAGRANCES

Perfume name	Structure	Mol weight (g/mol)	logP (-)	Water solubility (mg/L)	Density (g/cm³) (20 °C)
Eucalyptol (ECL)		154.25	2.74	3500 (21 °C)	0.92
Citronellol (CTN)		156.26	3.1	300 (25 °C)	0.85
Methyl nonyl acetaldehyde (MNA)		184.32	4.9	1.3 (20 °C)	0.83
Methyl anthranilate (MA)		151.16	1.88	2850	1.17
Undecavertol (UDV)		170.29	3.97	63	0.85
Delta-Damascone (DD)		192.2	4.2	46	0.93
Limonene (LMN)		136.23	4.57	13.8	0.84
Alpha-pinene (APN)		136.23	4.83	2.49	0.86
Habanolide (HBN)		238.37	4.91	1.86	0.94
Iso-E Super (IES)		234.38	5.12	1.08	0.96

Perfume name	Vapor pressure (25°C) (Pa)	Boiling Point (°C)	HSP-D (MPa$^{1/2}$)	HSP-H (MPa$^{1/2}$)	HSP-P (MPa$^{1/2}$)	HSP-t (MPa$^{1/2}$)
Eucalyptol (ECL)	120	176-177	16.7	4.6	3.4	17.65
Citronellol (CTN)	10	225	16.49	3.96	7.89	18.70
Methyl nonyl acetaldehyde (MNA)	0.85	242.14	16.07	4.19	3.21	16.91
Methyl anthranilate (MA)	100	256	19.1	8.5	9.2	22.82
Undecavertol (UDV)	1.1	228	16.35	3.38	7.5	18.30
Delta-Damascone (DD)	2.72	246.61	16.89	3.48	2.61	17.44
Limonene (LMN)	264	178	17.2	1.8	4.3	17.82
Alpha-pinene (APN)	633	156	16.4	1.1	2.0	16.53
Habanolide (HBN)	0.02	333	17.01	3.47	3.78	17.77
Iso-E Super (IES)	0.23	290.4	16.9	3.29	2.44	17.39